THE EFFECTS OF PROCESS PARAMETERS ON THE CELL MORPHOLOGY OF THE ALUMINUM FOAM

by

Tolga Uçak

B.S. in M.E., Istanbul Technical University, 2003

Submitted to the Institute for Graduate Studies in
Science and Engineering in partial fulfillment of
the requirements for the degree of
Master of Science

Graduate Program in Mechanical Engineering

Boğaziçi University

2007

Anneme, babama ve kardeşime…

ACKNOWLEDGEMENTS

First of all, I would like to express my gratitude to my thesis supervisor Professor Sabri Altıntaş for his valuable supervision and support throughout this study. Besides, I have also learned from him the academic approach and attitude in the way of searching for the “knowledge” which will guide me through all my life.

I would also like to thank Nazım Mahmutyazıcıoğlu for his intimate friendship, invaluable technical support, encouragements when things went wrong, and jokes that cracked me up even in bad times.

I thank to İbrahim Mutlu for his precise and fine work in machining of various parts of experimental setup used in this study. I am also grateful to Ray Cook, from ALPOCO U.K., for his generous support in supplying the aluminum powders. I also thank to Gökhan Çaylı, from the Chemical Engineering Department, for kindly spending his time for helping me in thermogravimetric analyses.

A special thanks goes to my colleagues at the Mechanical Engineering Department, for their friendships and invisible contributions that made possible to bear the difficulties during the writing of this thesis.

Last, but not least, I thank to my family: my parents, Mehmet Uçak and Şenay Uçak. Especially I am deeply grateful for their efforts to provide me more comfortable conditions during my whole education life and for their patience and unconditional support throughout my graduate study; my brother Uğur Uçak, for his cheerful telephone calls and messages provided that I call or send a message, for being considerate and constructive.

ABSTRACT

THE EFFECT OF PROCESS PARAMETERS ON THE CELL MORPHOLOGY OF THE ALUMINUM FOAM

Aluminum foams have gained a considerable amount of attention in recent years with their very low specific weight, relatively high compression strength among cellular materials combined with good energy absorption. In the present study, powder metallurgy method, which offers flexibility in materials selection and possibilities like near net shaping, was utilized to produce aluminum foams by using pre-alloyed AlMg1SiCu (AA6061) powders as base material and titanium hydride (TiH_2) as blowing agent. First, effects of compaction temperature, pressure and time on precursor quality were investigated. Then optimum foaming parameters were found by foaming trials with various parameters. Heat treatment of TiH_2 powders was conducted and modification of decomposition properties was analyzed by thermogravimetric analysis (TGA). Enhancements of foam morphology by tailoring the decomposition properties of TiH_2 and addition of Al_2O_3 particles were analyzed by scanning electron microscopy (SEM). Aluminum foams were subjected to heat treatments in order to investigate the effects on compression strength. Quasi-static compression tests of heat treated foams were performed and precipitated phases were analyzed by EDAX (Energy Dispersive X-Ray) analyses.

As a conclusion, it was found that compaction of the powder mixture by primarily cold pressing and subsequently hot pressing under 270 MPa at 450 ^{o}C for 30 minutes resulted in sufficient densification which was very close to theoretical density. Optimum foaming temperature for AA6061 was found to be between 750 and 775 ^{o}C. Heat treating the TiH_2 powders was found to shift the decomposition temperature up to 75 ^{o}C. It was observed that addition of Al_2O_3 particles prevented drainage and cell coalescence by mechanically supporting the cell structure. Strength increase about 25 per cent was achieved by solution heat treatment and subsequently ageing of the aluminum foams.

ÖZET

ÜRETİM PARAMETRELERİNİN ALÜMİNYUM KÖPÜKLERİN HÜCRE YAPILARI ÜZERİNE ETKİLERİ

Son yıllarda alüminyum köpükler sahip oldukları düşük özgül ağırlık, yüksek enerji soğurma ile birlikte diğer hücresel metallere göre yüksek olan basma mukavemetleri sayesinde hatırı sayılır derecede bir ilgi toplamaktadır. Bu çalışmada malzeme seçiminde esneklik ve hassas şekillendirme imkanı sunan bir yöntem olan toz metalürjisiyle köpük üretimi kullanılmıştır. Matris malzemesi olarak önceden alaşımlandırılmış toz halindeki AlMg1SiCu (AA6061) alüminyum alaşımı ve köpürtücü malzeme olarak da titanyum hidrür (TiH_2) kullanılmıştır. Öncelikle, sıcaklık, basınç ve zaman gibi sıkıştırma parametrelerinin köpürmeye hazır numunenin yoğunluğu üzerine etkileri incelenmiş, ardından değişik parametrelerle yapılan köpürtme denemeleri sonucunda en uygun köpürtme parametreleri bulunmuştur. TiH_2 tozlarına ısıl işlem uygulanmış, işlemin TiH_2'nin ayrışma özelliklerinde meydana getirdiği değişimler Termal Gravimetrik Analiz (TGA) ile ortaya konmuştur. TiH_2'in ayrışma özelliklerinin değiştirilmesi ve toz karışımına Al_2O_3 eklenmesi ile elde edilen köpük morfolojisindeki iyileştirmeler Tarama Elektron Mikroskopu (SEM) ile analiz edilmiştir. Köpük numunelere ısıl işlem uygulanmış ve basma mukavemeti üzerindeki etkileri incelenmiştir. Bunun için quasi-statik basma testleri yapılmış ve çökelmiş olan fazlar EDAX analizi ile incelenmiştir.

Sonuç olarak, soğuk olarak sıkıştırılmış ve ardından 450 ^oC'de 30 dakika süre ile 270 MPa basınç altında sıkıştırılan numunelerin teorik yoğunluğa çok yaklaştığı tespit edilmiştir. AA6061 alaşımı için en uygun köpürme sıcaklığının 750 ile 775 ^oC arasında olduğu bulunmuştur. TiH_2'ye uygulanan ısıl işlemin ayrışma sıcaklığın 75 ^oC kadar ötelediği termo gravimetrik analiz yardımı ile tespit edilmiştir. Al_2O_3 eklenmesinin, köpük yapısını mekanik olarak destekleyerek drenaj etkisini ve hücre irileşmesini önlediği gözlemlenmiştir.Çökelme sertleştirmesi ve ardından yapılan yaşlandırma ısıl işlemlerinin %25 civarında dayanım artışına neden olduğu tespit edilmiştir.

TABLE OF CONTENTS

LIST OF FIGURES

LIST OF TABLES

LIST OF SYMBOLS/ABBREVIATIONS

p_{at}	Atmosphere pressure
p_o	Gas pressure inside the cell
E^*	Young's Modulus of metal foam
E_s	Young's Modulus of cell wall
ε	Strain
ρ^*	Density of metal foam
ρ_s	Density of cell wall material
ν^*	Poisson ratio
φ	Fraction of solid contained in cell edges
σ_{ys}	Yield stress of the cell wall
σ_{fs}	Fracture strength of the cell wall
AISI	American Iron and Steel Institute
CIP	Cold Isostatic Pressing
DIN	Deutsches Institut für Normung
EDAX	Energy Dispersive X-Ray
GPZ	Guiner-Preston Zones
HRC	Rockwell C Hardness
MMC	Metal Matrix Composite
SEM	Scanning Electron Microscope
SHT	Solution Heat Treatment
SSSS	Supersaturated Solid Solution
TGA	Thermo Gravimetric Analysis

1. INTRODUCTION

The history of metal foams dates back to the 1940s. A large number of patents [1-7] were issued since then and from the late 1950s to the 1970s and many variants of foaming processes were proposed. A second surge of scientific activities starting in the late 1980s led to the re-establishment of some of the old techniques and to a much higher research activity.

There are two fundamental strategies for making metallic foams. Direct foaming methods start from a specially prepared molten metal containing uniformly dispersed non-metallic particles to which gas bubbles are added to create foam. This can be done in various ways: through a capillary or porous frit, by adding a chemical agent which decomposes in the melt or by making use of gas dissolved in the metal which is precipitated into bubbles by temperature or pressure control. Indirect foaming methods start from a solid precursor which consists of a metallic matrix containing uniformly dispersed blowing agent particles, for Al-based alloys mostly titanium or zirconium hydride. Upon matrix melting, this precursor expands and forms a foam [8].

Direct foaming of aluminum melts is done by gas injection (Cymat / Metcomb) [9, 10], with blowing agents (Alporas) [11] or solid-gas eutectic solidification (Gasar/Lotus) [9]. Foaming the melt by gas injection involves addition of particles, such as SiC, Al_2O_3 or Mg_2O, to enhance the viscosity and injecting the gas (air, nitrogen, argon) into the melt using special designed rotating impellers or vibrating nozzles which generate gas bubbles in the melt. Second method involves directly addition of blowing agent to the melt instead of gas injection. The gas evolved from blowing agent creates pores inside the melt and forms a highly porous structure. Third method uses the difference in gas solubility of liquid and solid metals. First the melt is charged with gas under high pressure (up to 50 bar) and then the temperature lowered to below the melting point of the metal which entraps the gas bubbles in the melt resulting a porous structure.

Foaming of powder compacts begins with the mixing of aluminum powders (pure [12, 13] or alloyed [14]) with appropriate blowing agent (generally TiH_2[15] or ZrH_2[13]). In the literature, between 0.6-0.8 wt. % of TiH_2 is commonly used [13, 16] which is considered to be sufficient to achieve a high expansion rate. Matijasevic [16] reports that mixing stage has to be carried out in a clean medium to avoid impurities. These impurities can act as a nucleus for big voids during the foaming stage. Densification of the powder mixtures can be done by cold or hot uniaxial pressing [17], cold isostatic pressing (CIP) [18], extrusion [19, 20] or powder rolling [21]. The aim of this stage is to obtain a fully densed precursor with having a density up to 99 % of theoretical density of the matrix material. Duarte [14] claims that hot pressing temperature is a critical parameter for the foaming behaviour and highest expansions are obtained for hot pressing temperature between 400 and 450 ^oC. As TiH_2 decomposes at about 400 ^oC [13, 22], the decomposition temperature has to be shifted up to higher temperatures in order to close the gap between the onset of decomposition and liquidus temperature of the alloy. Heating the titanium hydride powders at various temperatures between 400 and 520 ^oC [12, 23, 24] was reported to delay the hydrogen releasing temperature. By this way, crack formation inside the precursor during the hot compaction stage and thereby hydrogen loss can be prevented. Heating the precursor above the melting temperature of the alloy results drop in viscosity and thus let the hydrogen pressure overcomes the strength of the matrix and forms cells inside the precursor. In this stage, heating rate has to be over 100 ^oC/min [25] to rapidly pass the gap between the onset of decomposition and solidus temperature of the alloy; otherwise high degree of hydrogen loss will result lower expansion rates.

The 6XXX series of wrought aluminum alloys is widely used in automotive industry as it offers medium strength with good corrosion resistance, reasonable weldability and moderate costs combining with heat treatable characteristic [26]. As aluminum foams offer a flat stress-strain curve called as “plateau region”, they can be utilized whenever high energy absorption is required. Figure 1.1 shows the possible application areas of aluminum foams such as reinforcement in automobile body, flat sandwich products, complex near net shaped parts and decorative applications.

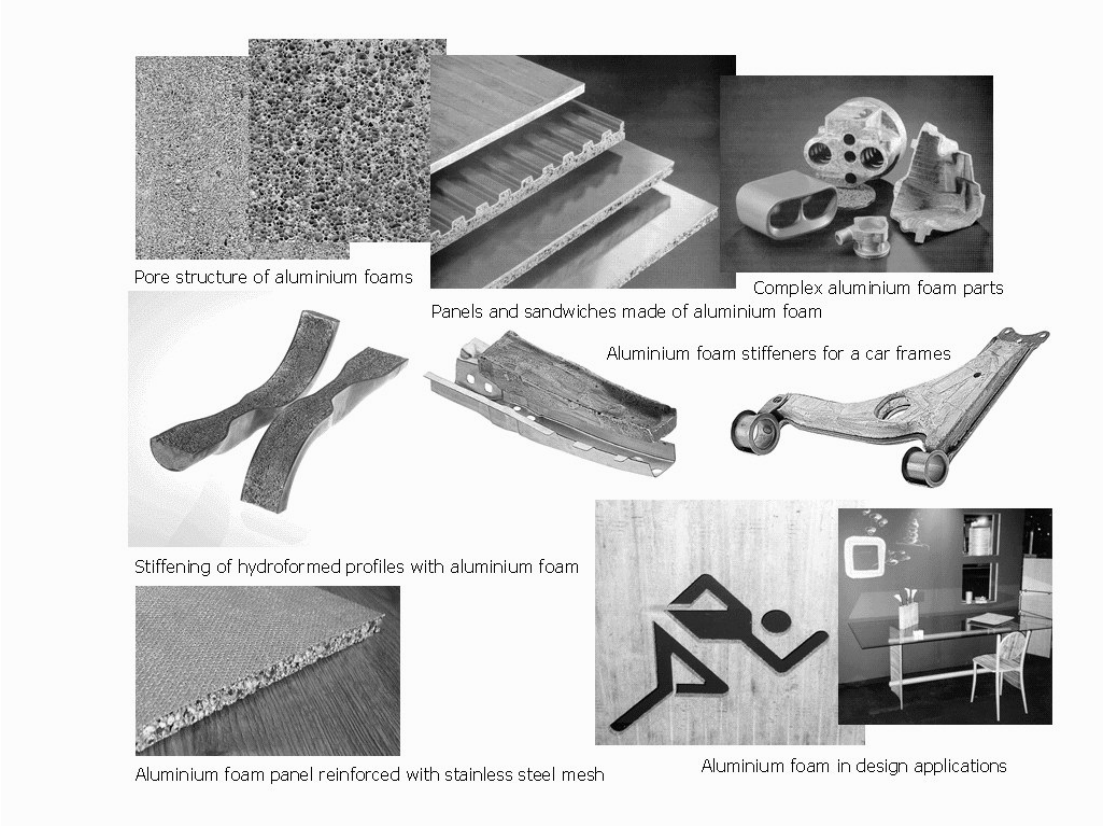

Figure 1.1. Some applications of closed-cell aluminum foams [9]

2. LITERATURE SURVEY

2.1. Manufacturing Methods of Aluminum Foams

Almost any material can be foamed. There are many ways to manufacture cellular metallic materials. Some methods are similar to techniques used for foaming aqueous or polymer liquids, whereas others are specially designed by taking advantage of characteristic properties of metals such as their sintering activity or the fact that they can be electrically deposited [9]. Below, typically used foaming methods and materials used in these methods are seen.

i)Bubbling gas through molten Al–SiC or Al–Al_2O_3 alloys (Al, Mg).

ii)By stirring a foaming agent (typically TiH_2) into a molten alloy (typically an aluminum alloy) and controlling the pressure while cooling (Al).

iii)Consolidation of a metal powder (aluminum alloys are the most common) with a particulate foaming agent (TiH_2 again) followed by heating into the mushy state when the foaming agent releases hydrogen, expanding the material (Al, Zn, Fe, Pb, Au).

iv)Manufacture of a ceramic mold from a wax or polymer-foam precursor, followed by burning-out of the precursor and pressure infiltration with molten metal or metal powder slurry which is then sintered (Al, Mg, Ni–Cr, stainless steel, Cu).

v)Vapor phase deposition or electro deposition of metal onto a polymer foam precursor which is subsequently burned out, leaving cell edges with hollow cores (Ni, Ti).

vi)The trapping of high-pressure inert gas in pores by powder hot isostatic pressing (HIPing), followed by the expansion of the gas at elevated temperature (Ti).

vii)Sintering of hollow spheres, made by a modified atomization process, or from metal-oxide or hydride spheres followed by reduction or dehydridation, or by vapor-deposition of metal onto polymer spheres (Ni, Co, Ni–Cr alloys).

viii)Co-pressing of a metal powder with a leachable powder, or pressure infiltration of a bed of leachable particles by a liquid metal, followed by leaching to leave a metal-foam skeleton (Al, with salt as the leachable powder).

ix)Dissolution of gas (typically, hydrogen) in a liquid metal under pressure, allowing it to be released in a controlled way during subsequent solidification (Cu, Ni, Al).

2.2. Foaming of Aluminum Using Melting Methods

Metallic melts can be foamed by creating gas bubbles in the liquid provided that the melt has been prepared such that the emerging foam is fairly stable during processing. This can be done by adding fine ceramic powders or alloying elements to the melt, which form stabilizing particles, or by other means. Currently, three ways for foaming metallic melts are known: firstly, by injecting gas into the liquid metal, secondly, by causing an in-situ gas release in the liquid by admixing gas-releasing blowing agents to the molten metal, thirdly, by causing the precipitation of gas which was previously dissolved in the liquid.

Pure liquid metals cannot easily be caused to foam by bubbling gas into them. Drainage of liquid down the walls of the bubbles usually occurs too quickly to create a foam that remains stable long enough to solidify. However, 10–30% of small, insoluble, or slowly dissolving particles, such as aluminum oxide or silicon carbide, raises the viscosity of the aluminum melt and impedes drainage in the bubble membrane, stabilizing the foam. Gas-injection processes are easiest to implement with aluminum alloys because they have a low density and do not excessively oxidize when the melt is exposed to air or other gases containing oxygen. There are several variants of the method, one of which is shown in Figure 2.1. Pure aluminum or an aluminum alloy is melted and 5–15 wt.% of the stabilizing ceramic particles are added. These particles, typically 0.5–25 μm in diameter, can be made of alumina, zirconia, silicon carbide, or titanium diboride.

Air is most commonly used but carbon dioxide, oxygen, inert gases, and even water can also be injected into liquid aluminum to create bubbles. Bubbles formed by this process float to the melt surface, drain, and then begin to solidify. The thermal gradient in the foam determines how long the foam remains liquid or semi-solid, and thus the extent of drainage. Low relative density, closed-cell foams can be produced by carefully controlling the gas injection process and the cooling rate of the foam.

2.2.1. Foaming of Aluminum Melts by Gas Injection Method

Cymat Aluminum Corp. in Canada has developed the first commercial way for foaming aluminum and aluminum alloys. In this technique, silicon carbide, aluminum oxide of magnesium oxide particles are used to enhance the viscosity of the melt and to adjust its foaming properties [10]**.** In general, aluminum alloys are used as base metal. The stabilizer particles have a mean particle size from 5 to 20 μm and are typically added to the melt in a volume fraction of from 10 to 20 %. Then the melt is foamed by injecting gases into it, which the gases can be air, nitrogen or argon. Gases are injected to the melt by specially designed rotating impellers or vibrating nozzles as can be seen in Figure 2.1.

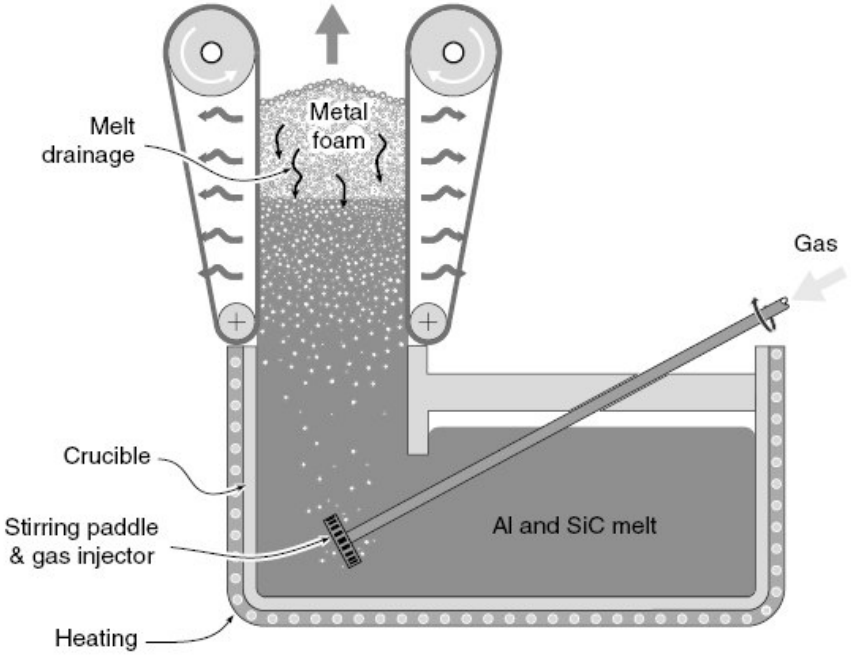

Figure 2.1. A schematic illustration of the manufacture of an aluminum foam by the melt gas injection method (CYMAT) [27]

The resultant viscous mixture of bubbles and metal melt floats up to the surface of the liquid where it turns into a fairly dry liquid foam as the liquid metal drains out [28]. The presence of ceramic particles in the melt makes the foam stable. The instantaneously formed metal foam can be removed from the liquid surface by a conveyor belt.

Banhart [9] indicates that the porosities of aluminum foams produced with this method range from 80 to 98 % corresponding to the densities between 0.069 and 0.54 g/cm3, average pore size from 25 down to 3 mm, and wall thicknesses from 50 to 85 μm. Advantages of the direct foaming process include the large volume of foam which can be continuously produced and the low densities which can be achieved. Metal matrix composite (MMC) foams are therefore probably less expensive compared to other cellular metallic materials.

2.2.1. Foaming of Aluminum Melts by Blowing Agent Addition

An alternative way for foaming a metal melt is to add a blowing agent directly to the melt instead of blowing gas into it [9-11]. At the decomposition temperature, the blowing agent releases its gas which forms a porous structure as can be seen in Figure 2.2.

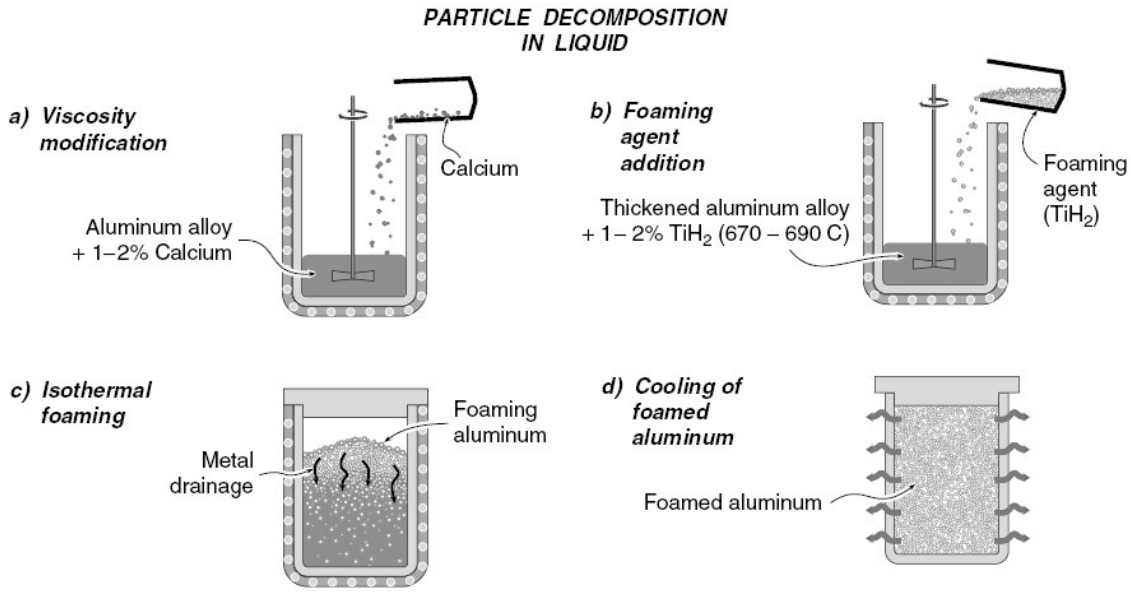

Figure 2.2. Manufacturing process of ALPORAS [27]

This method has been used by Shinko Wire, Japan, company under the registered trade name ALPORAS since 1986 [11] with a high commercial production volume of up to 1000 kg per day. In order to stabilize the melt calcium (Ca) is added at 680 ^{o}C. Then the melt is stirred for a certain of time to increase its viscosity continuously by a factor of up to

five [27]**.** This increase in viscosity comes from the formation of calcium oxide (CaO), calcium-aluminum oxide ($CaAl_2O_4$) or perhaps even Al_4Ca intermetallics [11, 29].

As Ma [30] mentioned that adding Ca into aluminum melt or even stirring the melt in atmosphere can increase the apparent viscosity of the melt. It is because the vortex caused by stirring destroys the oxide film of the melt and introduces oxygen from air into the melt causing the oxidation of aluminum. The reason is that the reaction of Ca with oxygen in air leads to destroy of the oxide film of the aluminum melt surface and promotion the oxidation of aluminum. The more the addition of Ca, the stronger the oxidation is, the more amount of oxide is in the melt, hence the higher the apparent viscosity is. Calcium is usually added by a weight percentage of 1.5-3. After reaching the desired viscosity, TiH_2 is added, generally about 1.6 wt. %, which acts as a hydrogen source in the hot viscous melt. As a consequence of hydrogen decomposition, the melt starts to expand and fills the foaming vessel. The foaming stage takes place at constant pressure. After the foaming stage the vessel is cooled and the solid aluminum foam is taken out of the mould for further processing [11]. The morphology of a foam which is produced by this method is quite homogeneous when compared to other method's products, as can be seen in Figure 2.3.

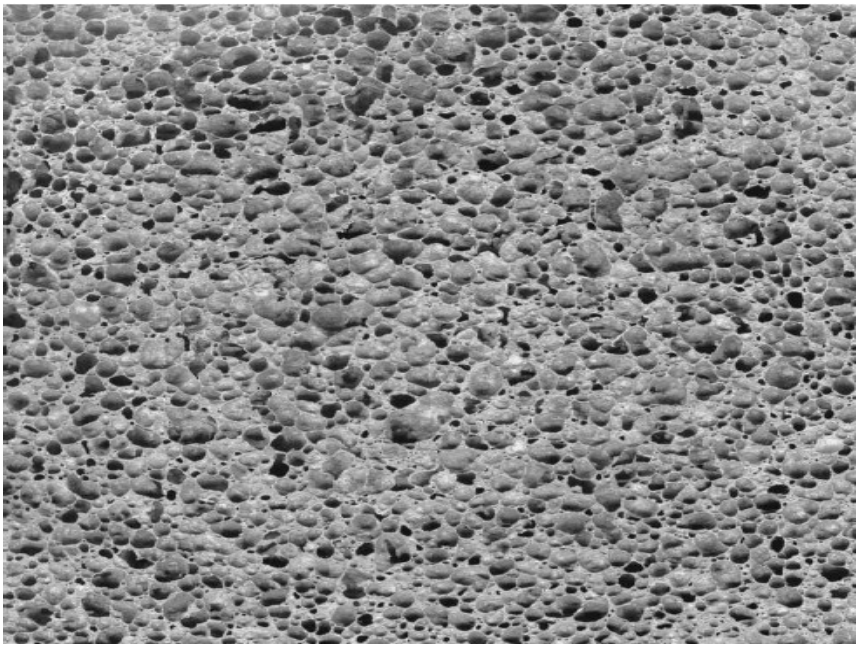

Figure 2.3. Pore structure of aluminum foamed (ALPORAS) by adding TiH_2 [9]

The foamed aluminum is typically produced in batches of 2050x650x450 mm by Shinko Wire [11]. Then the foam block is cut off to the required sizes.

Another method developed about 15 years ago exploits the difference in gas solubility of liquid and solid metals. A melt is first charged with gas under high pressure (up to 50 bar), e.g. with hydrogen or nitrogen. If the temperature is then lowered to below the melting point of the metal the gas will precipitate. Under favourable conditions gas bubbles are entrapped in the metal. The resulting pore morphologies are largely determined by the gas content, the pressure over the melt, by the direction and rate of heat removal and by the chemical composition of the melt. Generally, largely elongated pores oriented in the direction of solidification are formed as seen in Figure 2.4. Pore diameters range from 10 μm to 10 mm, pore lengths from 100 μm to 300 mm, and porosities from 5 to 75 %. The word "gasar" was coined for such materials which means "gas-reinforced" in a Russian acronym. Recently, the method has been adapted in Japan [9] where the material was named “lotus-structured” for its resemblance with lotus roots.

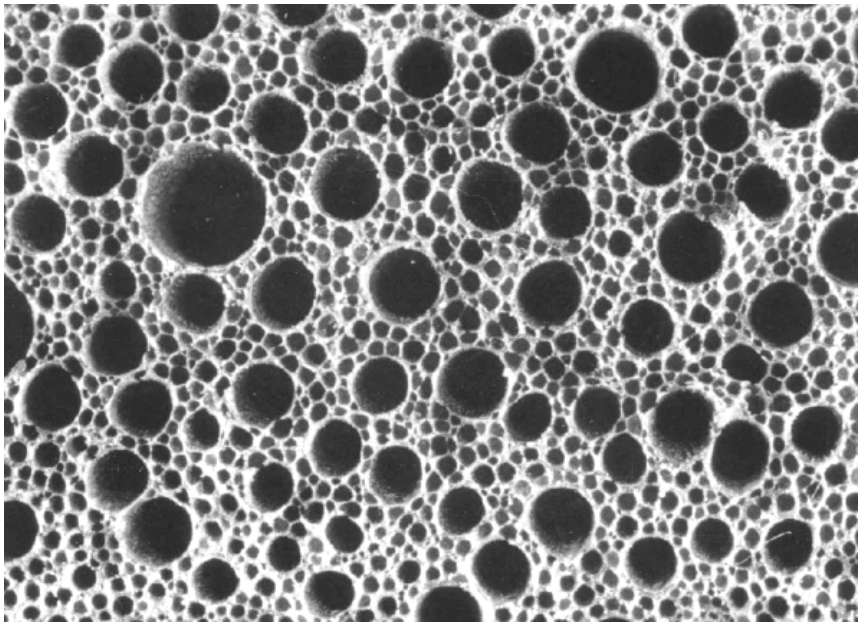

Figure 2.4. Pore structure of a “gasar”, surface normal to direction of pores is shown**[9]**

Open-cell polymer foams with low relative densities and a wide range of cell sizes of great uniformity are available from numerous sources. They can be used as templates to create investment-casting molds into which a variety of metals and their alloys can be cast.

It is thought that the ERG DUOCEL ranges of foams are made in this way. An open-cell polymer foam mold template with the desired cell size and relative density is first selected. This can be coated with a mold casting (ceramic powder) slurry which is then dried and embedded in casting sand. The mold is then baked both to harden the casting material and to decompose (and evaporate) the polymer template, leaving behind a negative image of the foam. This mold is subsequently filled with a metal alloy and allowed to cool. The use of a moderate pressure during melt infiltration can overcome the resistance to flow of some liquid alloys. After directional solidification and cooling, the mold materials are removed leaving behind the metal equivalent of the original polymer foam. Metal powder slurries can also be used instead of liquid metals. These are subsequently sintered. The method gives open-cell foams with pore sizes of 1–5 mm and relative densities as low as 0.05. The process can be used to manufacture foams from almost any metal that can be investment cast [27].

In addition to these methods, another method was proposed by Tzeng et al. [31], which used a modified two-stage foaming technique. In this method minerals that are naturally abundant and less expensive than conventional foaming agents such as TiH_2 or ZrH_2. First, the foaming agent is added to aluminum melts, and a preliminary cell frame is formed when the agent has been distributed thoroughly. For instance, heavy carbonate minerals are deposited in the rock sediment of the earth's crust; marbles contain plenty of mineral calcite, which is natural carbonate crystal, and magnesite, which is a natural magnesium carbonate crystal. Heating the preliminary cell frame forms full bubbles, just as in cakes, which are expanded using yeast to generate a porous structure. This two-stage foaming process can produce a structure of fine pores. A preliminary cell aluminum foams paste can be cast, or even processed into a prefab model, to reduce the cost of subsequent processing. The two foaming agents in this two-stage foaming process are inexpensive and have different thermal decomposition temperatures. The increase in the foaming agents' viscosity and scattering effects facilitates thorough and complete mixing. Casting or preliminarily processing the aluminum paste reduces the cost of subsequent processing. The pores in the products are very small. The products are suitable for being cut into slices that contract uniformly when cooled.

2.3. P/M Technique for Manufacturing Aluminum Foams

Manufacturing of metallic foams from metal powders (typically aluminum and its alloys) and particulate foaming agents (typically TiH_2 and ZrH_2) was patented in 1963 by Allen et al [7]. The schematic view of the process is given in Figure 2.5. The production process begins with the mixing of metal powders - elementary metal powders, alloy powders or metal powder blends - with a blowing agent, after which the mix is compacted to yield a dense, semi-finished product at about 400-480 °C [9, 10, 32, 33] The foaming agent thus becomes uniformly distributed and gas-tightly embedded in the metal matrix. If metal hydrides are used as foaming agents a content of less than 1 % is sufficient in most cases [9, 14, 16, 25, 27]**.**

The compaction can be done by any technique that ensures that the blowing agent is embedded into the metal matrix without any notable residual open porosity. Examples of such compaction methods are uniaxial or isostatic compression, rod extrusion or powder rolling. The manufacture of the precursor has to be carried out very carefully because residual porosity or other defects will lead to poor results during further processing. As Matijasevic and Banhart [16] mentioned use of impure powders or the presence of adsorbed water, dirt or gases entrapped in the precursor during compaction seem to have an adverse effect on foaming, in the sense that these impurities can act as nuclei for big voids in early stages of gas evolution from the blowing agent. The voids are then thought to grow to large pores.

Heating the precursor at temperatures near the melting point of the matrix material is the next step. The blowing agent, which is homogeneously distributed within the dense metallic matrix, decomposes [18, 25, 32, 33] and the released gas forces the melting precursor material to expand, thus forming its highly porous structure. . The time needed for full expansion depends on temperature and the size of the precursor and ranges from a few seconds to several minutes. In Figure 2.6, expansion behaviour of aluminum/TiH_2 precursors foamed at 750 ^{o}C is seen [9].

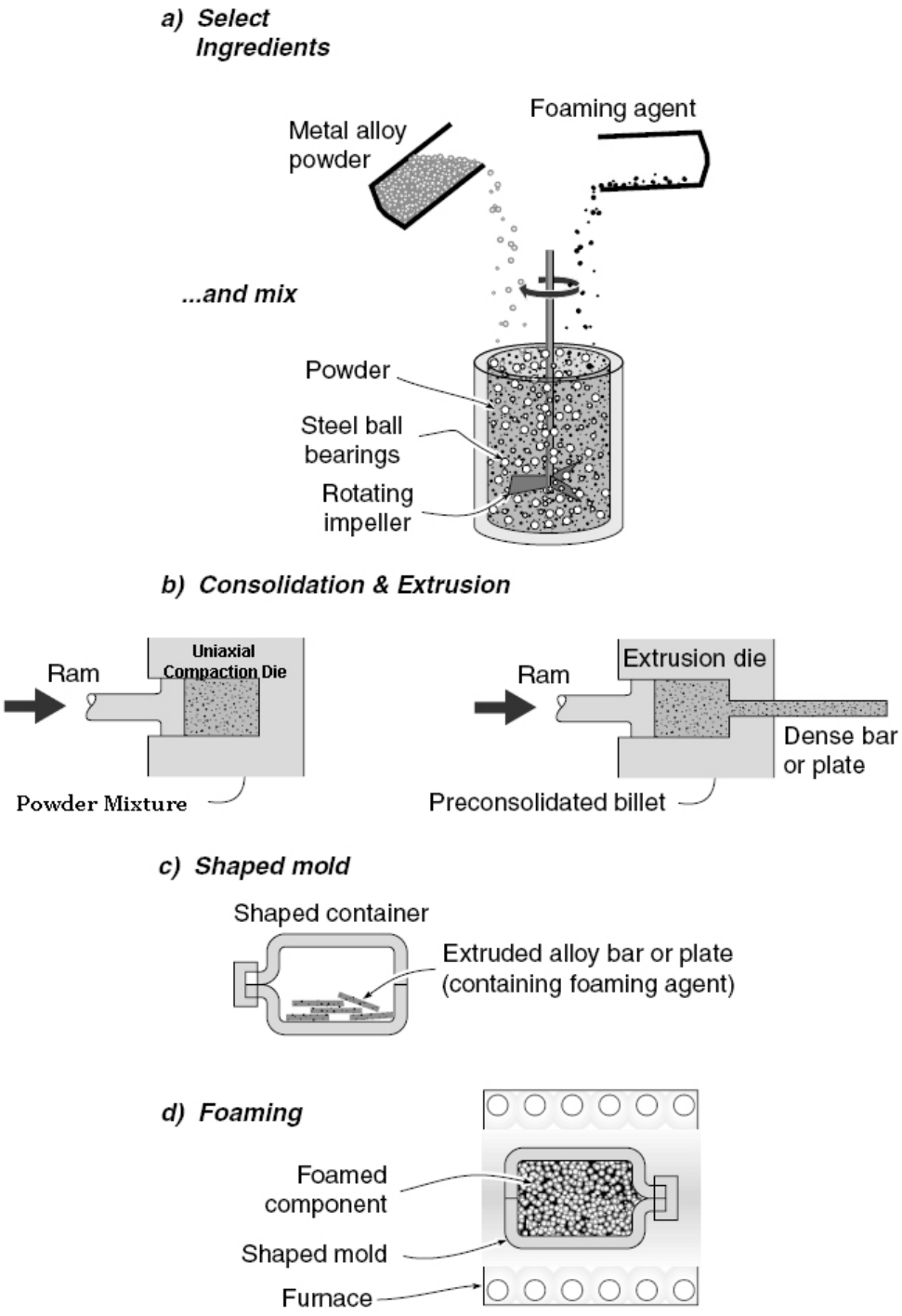

Figure 2.5. The sequence of powder metallurgy steps used to manufacture metal foams by gas-releasing particles in semi-solids [27]

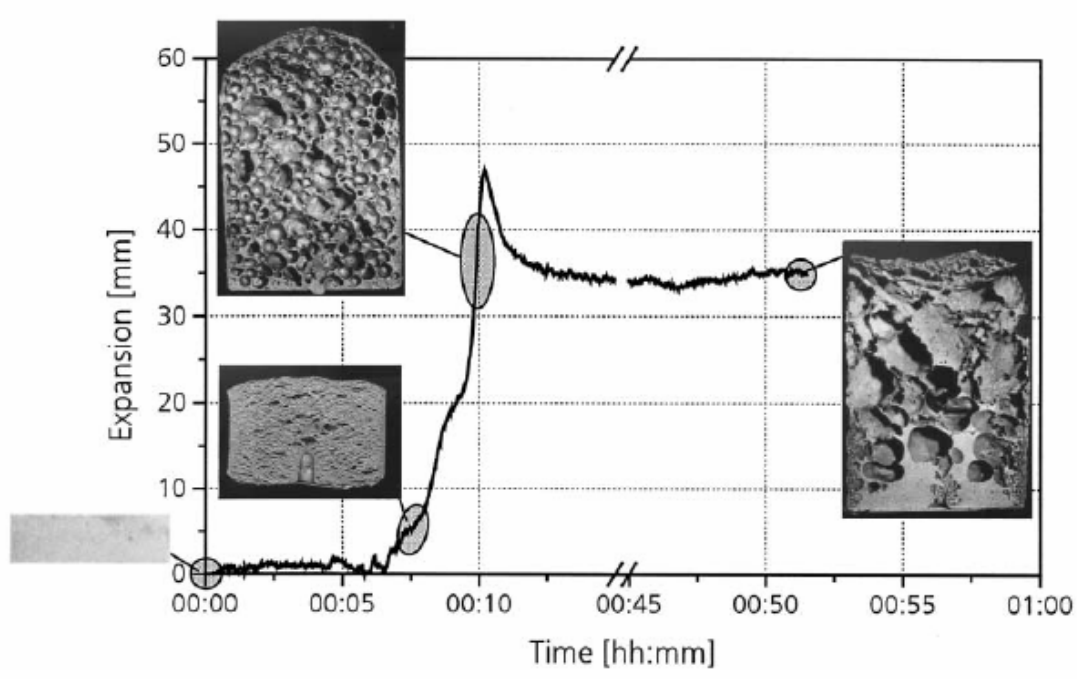

Figure 2.6. Expansion behaviour of aluminum/TiH_2 compacts when foamed at 750 ^oC [9]

Foaming a piece of precursor material in a furnace results in a lump of metal foam with an undefined shape unless the expansion is limited in certain directions. This is done by inserting the precursor material into a hollow mould and expanding it by heating. In this way near-net shaped parts can be obtained.

As described in literature [9, 27]**,** quite complicated parts can be manufactured by injecting the still expanding foam from a reservoir into suitable moulds. As soon as the mold has been filled with foam, it must be cooled to below its melting point to stabilize the foam structure [25, 34, 35]. Banhart [32] indicates that, this method is not restricted to aluminum and its alloys: tin, zinc, brass, lead, gold and some other metals and alloys can also be foamed by choosing appropriate blowing agents and process parameters.

The powder compact melting method is now in the stage of a small-scale commercial exploitation by the German companies Schunk (Gießen) and Honsel (Meschede) and the Austrian companies Mepura (Ranshofen) and Neuman Alufoam (Marktl). The names "Foaminal' and "Alulight" have been patented for these foams.

2.4. Preparation of the Precursors

2.4.1. Selection of Powders

The appropriate selection of the raw powders with respect to purity, particle size and distribution, alloying elements, and other powder properties is essential for successful foaming. Commercial air-atomized aluminum powders proved to be of sufficient quality. However, powders from different manufacturers lead to notable differences in foaming, and empirical criteria have been derived to facilitate the selection of powders [25].

2.4.2. Mixing of Powders

The mixing procedure should yield a homogeneous distribution of alloying elements and the blowing agent to ensure that high-quality foams with uniform pore size distributions are obtained. As Matijasevic [16] reported, mixing media should be adsorbed water and dirt free since these seem to have an adverse effect on foaming. During foaming, these impurities can act like nuclei for big voids. Then the voids are thought to grow to large pores.

2.4.3. Densification of Powders

In literature various ways of consolidation of powders are present. These methods involve cold isostatic pressing (CIP), extrusion and uniaxial compaction of powders. The aim of compaction of powders is to obtain a foamable precursor material with a theoretical density close to 100% theoretical density of aluminum matrix. This means that no residual open porosity inside the precursor is to be remained. Beside, during compaction one has to ensure that the blowing agent is completely embedded into the aluminum matrix so that no residual open porosity remains. Generally, the powder mix is first compacted to cylindrical billets of 70-80% theoretical density by CIP and then these billets are pre-heated to temperatures of 350-400 C and extruded to rectangular bars of various dimensions [34]. Alternatively the powder mixture is compacted uniaxially at room or elevated temperatures to obtain foamable precursors. This method enables one to yield more than 99 % relative density if hot compaction is applied after cold compaction.

Kennedy reported that [36] a minimum compaction density is required to achieve appreciable expansion and this appears to be of the order of 94% of theoretical density. As seen from Figure 2.7 cold compacted precursors produced under lower pressures had lower densities due to poor densification.

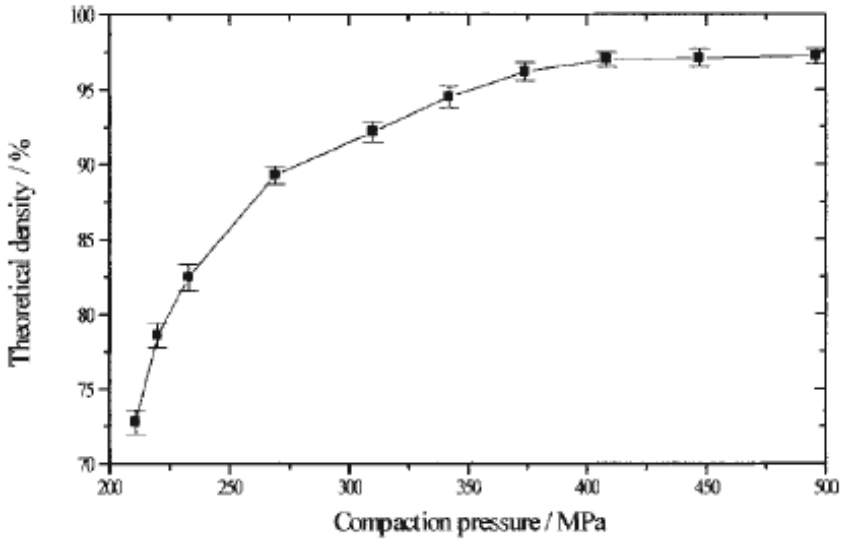

Figure 2.7. Variation in theoretical density with compaction pressure [36]

Although for densities greater than 94% the internal porosity is closed, the foam expansions were observed to increase with precursor density. Increased interparticle shear, associated with higher compaction densities, will result in increased disruption of surface oxide films, enhancing the possibility of cold welding between Al particles. This is likely to produce interparticle channels that are more gas tight at elevated temperature and, on melting, enable the liquid to more readily burst through the oxide layer and envelop the TiH_2 particles. Both these factors will reduce the ease with which gas can escape from the precursor during heating. It is worth noting that since over 75% of the gas evolved during decomposition of the foaming agent does not contribute to expansion, any measures that result in a decrease in gas permeability through the precursor could greatly enhance the foaming response [36].

It is obvious that the hot pressing temperature is a critical parameter for the foaming behaviour. The highest expansions are generally reached for hot pressing temperatures between 400 and 450 ^{o}C. For higher and lower temperatures the maximum expansion is

lower and in the extreme case, for 200 and 550 ^{o}C, virtually no foaming can be observed anymore. The reason for this is that for low compaction temperatures only insufficient densification with a high degree of residual open porosity is achieved, corresponding to a low density of the foamable precursor material. Thus hydrogen gas can escape from the melting precursor through the system of interconnected channels and it does not create and inflate bubbles. About 1% residual porosity appears to be the tolerable limit for this particular alloy system. At the other extreme, too high compaction temperatures also lead to lower maximum expansions because hydrogen is lost already during hot compaction. This loss is almost complete for a compaction temperature of 550 ^{o}C. Thermoanalysis of free TiH_2 powder shows that decomposition begins at 380 ^{o}C and continues up to 570 ^{o}C. However, these results are valid only for free powders and depend also on the heating rates applied in the tests and on the environmental atmosphere. The optimum hot pressing temperature, around 400-450 ^{o}C, is therefore near the initial decomposition temperature of free TiH_2 powder, but this does not harm the TiH_2 embedded in the gas-tight embodiment of the metallic matrix of the foamable precursor material [14]. This confirms that achieving a compacted structure, where the porosity is isolated and the foaming agent is enveloped by the matrix, is vital to successful foaming.

2.5. Foaming of Precursors

In the foaming stage of precursors the gas released by the decomposing blowing agent forms bubbles, and the matrix expands up to a maximum volume. The density and density distribution of the growing foam can be controlled by several parameters. The blowing agent content in the precursor material is obviously important, but furnace temperatures and heating rates also have an influence. The mold material, mold shape, and type of furnace naturally influence the heating rate and, therefore, must also be considered. Careful control of the heating conditions during foaming is essential for obtaining high-quality foams. The difficulty is that the liquid foam is thermodynamically unstable, and conditions change constantly during foaming. There are various intermediate stages: at first, only the mold is heated directly, whereas the foamable material receives heat indirectly via heat conduction through the mold. Initially, there are merely some point contacts between the piece of foamable material in the mold and the mold walls. However, as the temperature increases, the precursor softens and assumes the contour of the mold,

thus increasing the transfer of heat. Moreover, heat transfer via radiation gains importance with rising temperatures. The reflectivity of the mold and precursor surfaces may change during the process and add a further variable. Finally, after foaming begins, the thermal conductivity of the precursor rapidly decreases, thus reducing the heat flow. As soon as the mold has been filled with foam, it must be cooled to below its melting point to stabilize the foam structure. The phenomena during cooling are also quite complex and difficult to describe for reasons similar to those mentioned for the heating phase [25].

In addition to foaming at atmosphere pressure, foaming at various pressures were investigated by several researchers [18, 37]. In order to understand some of the pressure dependencies Garcia-Moreno et al. [38] carried out foaming experiments under pressures between 1-9 bar. Of great interest is the mean pore size diameter as a function of pressure. It decreases for increasing pressure with a more or less linear decay up to 7 bar. The standard deviation is high for low pressures because of the low number of pores in our small samples which do not allow for good statistics. The standard deviation decreases with pressure not only because of the higher number of pores but also because of increasing homogeneity of the foam. They concluded that a maximal foam expansion was found at around 3 – 5 bar and it could be shown that with increasing pressure foam stability increases, while collapse and coalescence phenomena are reduced. It was also claimed that metal foams with a given density and pore size can be produced at the same foaming temperature just by adjusting the surrounding gas pressure.

2.5.1. Evolution of Foam Morphology

Figure 2.8 shows typical expansion curves for the 6061 alloy. The points marked with capital letters A-K indicate the different foaming stages that were prepared. In Figure 2.9 the corresponding micrographs of the various foaming stages are shown (the foamable precursor material is identified by ``P''). As can be seen from the micrographs (a) initiation and evolution of porosity: pores elongated perpendicular to the compaction direction (which was from top to bottom) are formed (phase A); (b) pore growth: the pores are initiated by the evolving hydrogen and are increasingly rounded of as the foam expands (B-G). The initial anisotropy starts to vanish until only a slight asphericity remains. Moreover, initially round pores are deformed to more polyhedral pores as the level of

porosity increases and no more space can be filled by spherical pores; (c) collapse: after maximum expansion no more hydrogen gas is released and the foam begins to decay. This decay leads to foams with large and irregular pores, collapsed and oxidized pores especially at the top of the sample and a solid metal layer at the bottom (see H-K) [14].

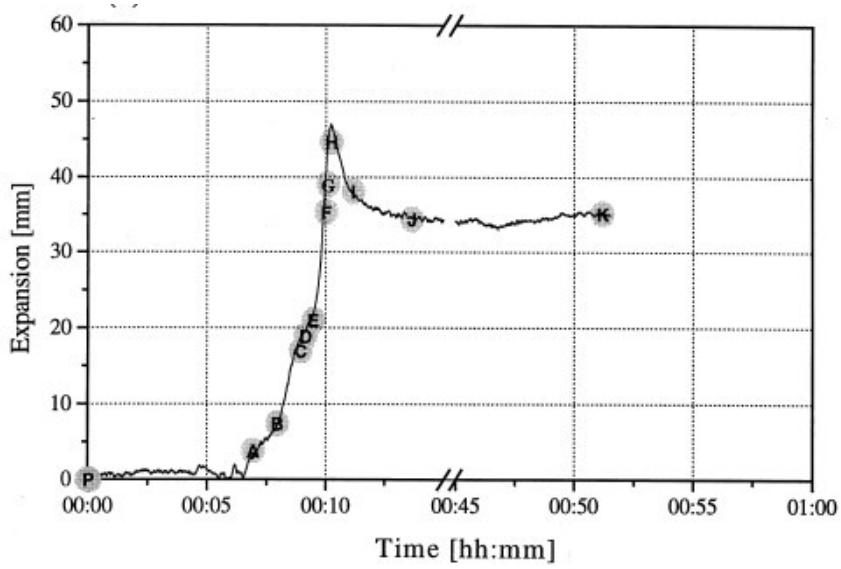

Figure 2.8. Expansion curve for 6061 alloys using a preheated furnace at 800 ^{o}C [14]

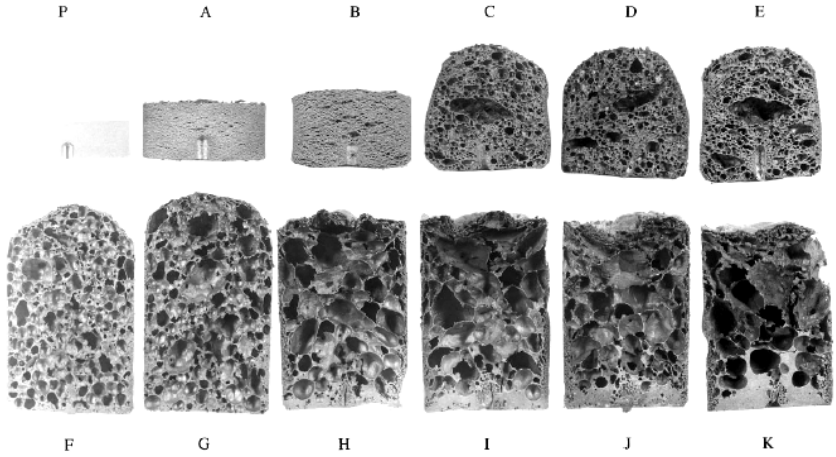

Figure 2.9. Morphology of 6061 foams at different stages [14]

The foams owe their collapse to two mechanisms, drainage and coalescence. Drainage is the flow of molten metal from the cell walls into the cell edges (driven by surface tension) and through cell edges downwards driven by gravity (seen H-K in Figure 2.9). A thick layer of metal at the bottom of the samples is the result of this process.

Coalescence occurs whenever two cells merge to form one large one. It is thought that cell rupture is the reason for such processes but no definite investigations have been carried out yet. It seems that metal membranes are not as stretchable as, e.g., the membranes in soap foams and rupture as soon as their thickness has fallen below a certain critical limit.

2.5.2. Effect of Heating Rate on Foaming

Different furnace temperatures lead to different heating rates and influence the foaming process this way. Clearly, higher heating rates lead to an earlier expansion of the foamable precursor material because the melting temperature is reached at an earlier time [39]. The effect of heating rate on foam expansion can be seen in Figure 2.10. The main possible reasons for the drop in foamability for low heating rates are: (i) gas losses due to the decomposition of titanium hydride during the slow transition through the temperature range from above 500 ^{o}C, where decomposition is rapid and the temperature at which foaming begins; (ii) oxidation which could produce non-metallic layers on the surface of the precursor sample and even inside the sample in regions accessible to air by direct channels. Such oxide layers could contain alumina, magnesia or mixed oxides (6061 alloys contain magnesium), which remain solid throughout the foaming process and therefore mechanically hinder expansion.

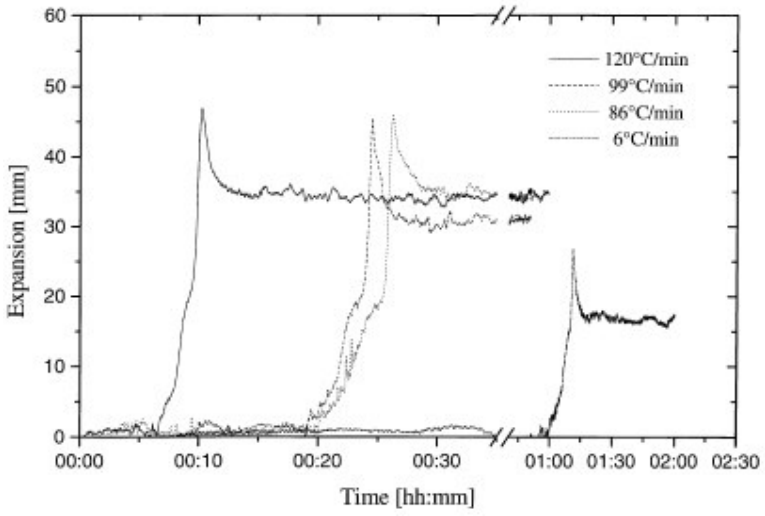

Figure 2.10. Foam expansion curves of 6061 alloys for different heating rates at 800 ^{o}C nominal furnace temperature [14]

2.5.2. Effect of Foaming Temperature on Foaming

It is evident that the foaming process is sensitive to the foaming temperature chosen. If the final sample temperature is below the solidus temperature of the alloy there is not very much more of an effect than a slight solid state expansion. If the final temperature lies in the solidus/liquidus interval foam formation can be observed, but especially for 6061 it is limited to quite low expansions around 100%. The viscosity of the semi-molten material is still quite high at this temperature and surface oxidation leads to an additional resistance towards bubble inflation, counteracting the internal gas pressure built up by the decomposing blowing agent. Increasingly higher temperatures reduce viscosity and promote gas production so that higher and higher volume expansions can be observed. Besides reducing viscosity, high furnace temperatures naturally also lead to high heating rates. This can be advantageous for obtaining high volume expansions [14, 17, 25].

2.6. Tailoring the Decomposition Properties of TiH_2 Powders

2.6.1. Heat Treating the TiH_2 Powders

The melting behaviour of the alloy system and the decomposition characteristics of the blowing agent have to be coordinated. Ideally, gas evolution is surpressed below the solidus temperature of the alloy to avoid formation of cracks before melting. After partial melting the gas released by the blowing agent then leads to the formation of spherical pores provided that the liquid fraction is sufficiently high. As TiH_2 has a very low decomposition temperature when compared to common solidus temperature of commercial aluminum alloys, which is starting at about 400 ^{o}C [13, 24, 40] for untreated hydride, and commercial aluminum alloys have solidus temperatures above 525 ^{o}C, thus there exists an obvious gap [16].

It is obvious that untreated TiH_2 does not fit with the melting range of any of the Al alloys, especially when taking into account that the decomposition of TiH_2 is shifted to even lower temperatures when it is embedded in the aluminum matrix by compaction (probably caused by the fracture of TiO_2- layers covering each TiH_2 particle) [16].

Oxide layers on titanium hydride particles modify their hydrogen desorption behaviour because they form an efficient diffusion barrier: hydrogen not only has to diffuse through the bulk titanium matrix from the inner region of each particle towards the surface but also has to overcome the oxide barrier which is an additional kinetic hindrence. This effect is already known and has been exploited to control hydrogen evolution from TiH_2 in metal foam manufacture. Titanium hydride particles always have a slightly oxidized surface due to handling in air at room temperature which is almost inevitable in the preparation of metal foam precursors. Upon heating under vacuum, however, the oxide layers will be modified. Oxide films tend to disappear after which hydrogen can be desorbed from the hydride particles more easily. This effect starts at 300 ^{o}C and ends at 450 ^{o}C and is caused by oxygen diffusion from the surface of the particle into the bulk. This explains the rather rapid hydrogen losses when powder is heated under vacuum. In addition to this effect one could speculate that differences in thermal expansion coefficients between the hydride core and the oxide shell could create cracks in the oxide layer which would facilitate gas desorption, but there is no direct proof of his effect. If the hydride is exposed to air during heating, the oxygen present will renew the thinning oxide layers on the surface, immediately close eventual gaps in the oxide shell created by thermal stresses and finally create an increasingly thick oxide layer which forms an effective barrier for hydrogen diffusion and further retards desorption [13].

The TGA (Thermo Gravimetric Analysis) curves show that decomposition characteristics of TiH_2 slightly depend on heating rates during treatment. As seen in Figure 2.11, Sandim et al. [41] proved that the lower the heating rates the lower is the onset temperature. The final amount of hydrogen in the transformed powder was found to be also dependent on the applied heating rate, as expected. Lower heating rates enable larger residence times favoring a more pronounced degassing.

As Lehmhus [40] designated that maintaining shifts in decomposition temperature when embedding TiH_2 particles in an aluminum matrix, as happens in production of precursor material for aluminum foam, is only partly possible where these shifts are based primarily on surface layers. Thermal analysis suggests that formation of new surfaces in the TiH_2 particles due to cracking under the mechanical loads exerted during the compaction process reduces the effects of the treatments.

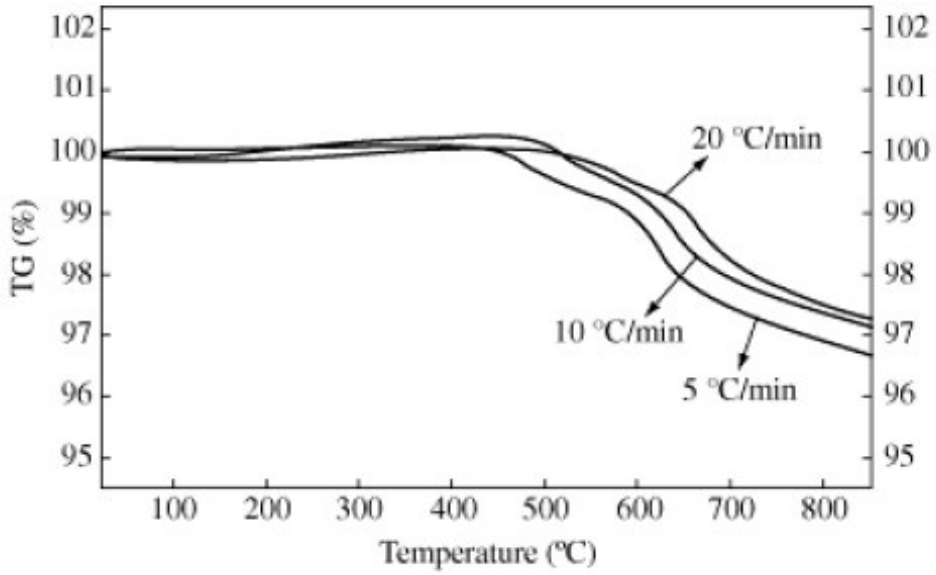

Figure 2.11. TGA curves for TiH_2 powder for heating rates varying 5 to 20 $^oC/min^{-1}$ [41]

2.6.2. Coating of TiH_2 Particles with SiO_2 Layer

In this process TiH_2 powders are pretreated using acetic acid solution (immersing for 10 h), and then washed with distilled water until the solution presented weak acidity (about pH = 6.0). The pretreated TiH_2 particles are added into 500mL distilled water and thus the TiH_2 suspending solution is obtained. The pH of suspending solution is adjusted to about 4.0 using 1.0 mol/L H_2SO_4 solution. The corresponding concentration Na_2SiO_3 solution and 1.0 mol/L H_2SO_4 solution are titrated into the above solution using co-titration methods, whilst continuously being stirring using a magnetic stirrer. The titration process takes about 1 h and is conducted at about 25 ^oC. After titration, the blended solution is aged for about 2 h whilst continuously being stirring, then washed with distilled water, filtered and dried for 2 h at 60 ◦C in air. Finally, the SiO_2 coated TiH_2 particles are obtained after heating at 350 ^oC for 1 h [42]. Schematic representation of coating process can be seen from Figure 2.12.

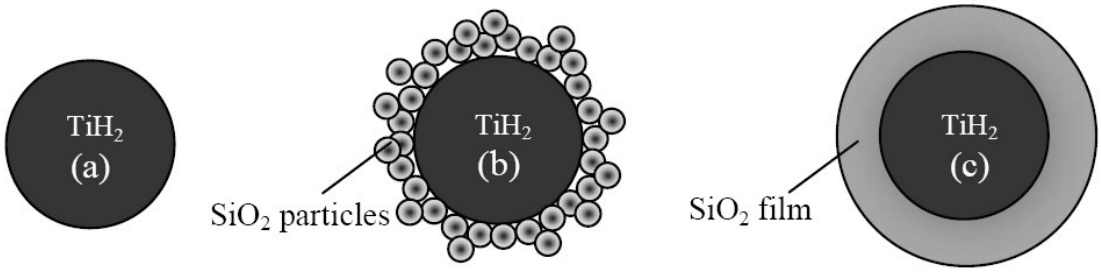

Figure 2.12. Schematic representation of: (a) uncoated TiH_2 particles; (b)SiO_2-coated TiH_2 particles; and (c) SiO_2 gel film-coated TiH_2 particles [42].

The uniformity and densification of coating layers have an important influence on the gas release characteristic of TiH_2 powders. It is assumed that the hydrogen release is dominated by the diffusion of hydrogen in the TiH_2 particles. The density gradient is one of the driving forces for diffusion of hydrogen in TiH_2 particles. When TiH_2 particles are heated at about 700 ^oC, the hydrogen atom quickly diffuses to the surface of TiH_2 particles and then gets rid of matrix. When TiH_2 particles are coated by oxide layers, because the solubility of hydrogen in oxide is small, the diffusion is restricted by the coating layers. The hydrogen accumulates at the interface between TiH_2 and coating layers, thus decreasing the density gradient for hydrogen diffusion and reducing the diffusion driving force. Comparing the particle-coating layers the film-coating layer has a density structure, which is of benefit to restrict the hydrogen diffusion or escape. Therefore, the film-coating layers have an obvious effect for delaying the hydrogen release [42].

2.7. Effects of Ceramic Addition on Foam Morphology

The powder metallurgy route is an attractive method for making Al foam components as it offers the possibilities of near net shaping. The foaming process is very rapid, taking only a few minutes, and the structure and density of the foam changes dramatically with time. The rapid nature of foam expansion and collapse make reproducibility of the pore structure difficult to obtain and is a highly undesirable feature of the metal foaming process. In order to improve the stability of metal foams, ceramic particles are commonly added.

Kennedy [43] claimed that an additional mechanism for improving foam stability is that particles can attach to the gas/liquid interface and modify its curvature, reducing the pressure difference between the plateau border and the cell walls, which also reduces the rate of drainage. In Figure 2.13 micrographs of cell walls of different foams produced by various ceramic additions such as Al_2O_3, SiC and TiB_2. Note that ceramic particles are generally concentrated at cell wall edges which prove a stabilization effect.

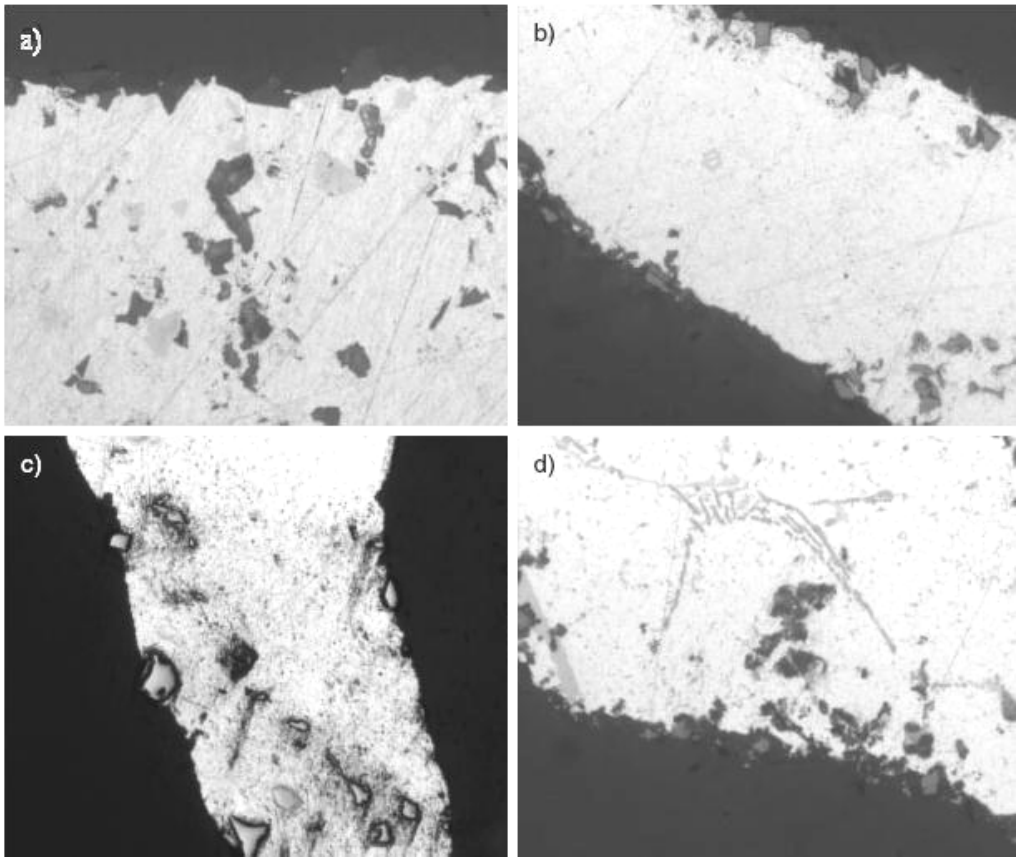

Figure 2.13. Micrographs of foams containing a) Al_2O_3, b)SiC, c)TiB_2 and d) reacted SiC [43]

As Elbir et al. [35] designated, solid particles can increase melt bulk viscosity and they can also significantly contribute to increasing surface viscosity of the cell faces if a significant fraction of particles is located at the gas/melt interface. Both are effective in slowing down capillarity-driven melt flow from cell faces through cell edges. The solid particles may also have a destabilizing effect if an unsuitable particle size is selected for viscosity enhancement, especially when the size of the particles is in the range of cell face

thickness. The higher solid content of the foamed composite compacts is believed to be responsible for the enhanced foaming behaviour. Besides, SiC particles, the solid phases forming as a result of reactions between SiC particles and Al melt may also contribute to enhancement of the Al powder together with SiC_p likely results in detachment of the oxide skin and consequently the retention of relatively small oxide particles.

Banhart [8] designated that a particle attaches to an interface between a liquid and gas if it is partially wetted. Very small particles can become so tightly bound to interfaces that adsorption is irreversible. Depending on the wetting angle the liquid will arrange around the particle. If the film is much thinner than the diameter of the particles, particles can bridge the liquid in the way shown in Figure 2.14. If the particles are wetted (top) they will stabilize a film, if wetting is poor, the film will be destabilized.

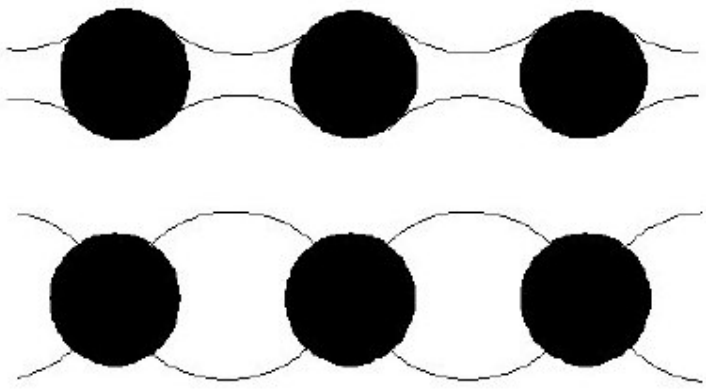

Figure 2.14. Effects of particle wettability on film stability. Top: particles are partially wetted (θ<90°); bottom: particles are poorly wetted (θ>90°)[8]

Another stabilizer mechanism by addition of ceramic is that SiC reacts with molten Al, producing brittle Al_3C_4 and Si-rich Al phases. Microscopic studies on SiC_p/Al composites have shown Al_4C_3 formed around the SiC particles, seen as the dark patches at the interfaces and surfaces of the particles under the microscope and Si simultaneously diffused through the melt, forming a Si-rich band around SiC particles [35].

2.8. Heat Treatment of Aluminum Foams

As Epler [44] mentioned the typical heat treatment of an age-hardening alloys consists of:

1. Solution treating (solutionizing) that results in a homogenous supersatureated solid solution (SSSS)
2. Quenching to a temperature in the two-phase region (generally room temperature) to retain a supersaturated solid solution
3. Ageing at an elevated temperature to control the precipitation of the second phase from the solid solution.

During precipitation hardening, solution heat treatment (SHT) and quenching lead to a supersaturated solid solution of the alloying elements. During aging, precipitates are formed in fine dispersion within the supersaturated regions. Depending on the alloy, these are mainly of Mg_2Si or $MgZn_2$ type. In a critical temperature range between 400 and 290 ^oC, the cooling rate needed to suppress premature formation of such precipitates and achieve maximum strength is said to be in an order of magnitude 100 K s^{-1} for 6061. To achieve such rates, water quenching is obligatory. Lower rates tend to result in a higher fraction of grain boundary precipitates having detrimental effects on toughness, though not in all cases on strength [20].

Al-Mg-Si alloys are an important group of alloys that are widely used in both cast and wrought form. The alloys are age hardenable, and are routinely heat treated to the T6 condition to develop adequate strength. The age-hardening response of the alloys is very significant and hence control of precipitation during heat treatment is critical for attaining optimal alloy performance [45].

Zhen et al. [46] proposed that the precipitation sequence of Al-Mg-Si alloys with high silicon content is believed to be: SSS→independent clusters of silicon and magnesium atoms, co-clusters of silicon and magnesium atoms→GP zones→small precipitates with an unknown structure→ß''→B'→Si precipitates→ß. In addition to that, adding more excess silicon to Al-Mg-Si alloys that already contain silicon in excess of the pseudobinary Al-Mg_2Si composition does not have a pronounced influence on the precipitation of ß'' and ß' phases, but it does promote appreciably the precipitation of silicon precipitates and the small precipitates with an unknown structure. Solute atoms cannot be dissolved completely into the solid solution when Al-Mg-Si alloys are solution heat treated for 2 min.

It is not obvious that the procedures and parameters for heat treating bulk aluminum alloys can be transferred directly to corresponding foamed alloys. Lehmhus [26] explained these reasons as followed:

i)Foams are stable only because the matrix metal contains finely dispersed oxide particles originating from the former surfaces of the powder particles that the foamable precursor material was made of. An oxygen content of 1.1 wt. % was found for the AA6061 powder used and some regions rich in oxides can still be found in fully expanded foams, predominantly near the grain boundaries. This may have an influence on the metallurgical processes during SHT.

ii) The thermal history of a foamed body is different from that of a conventional Al part prior to heat treatment, giving rise to a different microstructure: alloys intended for heat treatment are usually subjected to an annealing treatment to homogenize the distribution of alloying elements and to dissolve or round off grain boundary precipitates of Mg_2Si or AlFeSi. Aluminum foams cannot be treated accordingly, as heating to the temperatures needed for this purpose usually higher than in solution heat treatments, namely up to 575 ^{o}C for alloys of the type examined here might lead to secondary expansion effects. Therefore, the post-foaming microstructure resembles more the solidification structure found in cast aluminum with phases rich in alloying elements at grain boundaries.

iii) The thermal conductivity of aluminum foams is normally more than one order of magnitude lower than that of bulk $Al :\approx 10 W m^{-1} K^{-1}$ in a foam with 0.4 g cm^{-3} density compared to $\approx 150 - 200 W m^{-1} K^{-1}$ for dense alloys. Removal of heat during quenching is therefore expected to be much slower.

iv) Foams are by definition quite heterogeneous structures with struts and membranes of different shapes and cross sections. Quenching is therefore expected to yield different cooling rates for different parts of a sample.

v) Water quenching of foams could be problematic. Firstly, it would induce high thermal stresses changing the structure of the foam, e.g. by creating cracks. Secondly, as

the outer surface of a metal foam as well as the inner cell walls is not free of cracks from the beginning, water can enter the foam after quenching. The pressure drop in gas-filled cells by a factor of almost 3 during transition from 530 to 20 ^{o}C will exacerbate this effect. Intruding and evaporating water could have unpredictable effects both on foam structure and on quenching rates.

vi) The choice of solution heat treatment parameters is limited due to the possibility of unwanted secondary expansion effects.

All these possible problems have to be kept in mind when developing heat treatment procedures for metallic foams.

2.9. Compression Behaviour of Aluminum Foams

The different types of stress-strain curves stem from differences in their failure modes. In samples showing smooth and constantly rising stresses, failure is controlled by bending rather than breaking of cell walls and struts. As strength is density-dependent, a specimen with slightly inhomogeneous density distribution will first be deformed in the section with lowest density ('weakest link'). With this region being simultaneously compressed to higher densities and strain-hardened, a new deformation band will soon develop and take its place. In contrast to this, brittle failure does not necessarily start at a weakest link. Cracks created by thermal stresses induced during production of the foam or heat treatment may become starting points for the failure of the structure as a whole.

Bastawros et al. [47] reported that the early stress/strain response ($\varepsilon_A < 0.05$) of closed cell foam exhibits three stages. As seen in Figure 2.15 stage I represents, at macroscopic axial strains, $\varepsilon_A < \varepsilon_b$, wherein the deformation is nominally linear, but the tangent modulus is lower than the unloading modulus. Stage II, at $\varepsilon_b \le \varepsilon_A \le \varepsilon_0$, characterized by macroscopic non-linearity, yet subject to appreciable strain hardening, with a tangent modulus that decreases rapidly with increase in strain and reaches zero at e_0. Stage III, at $\varepsilon_A \ge \varepsilon_0$, which commences with a stress maximum at e_0, followed by a region

of strain softening, with subsequent stress oscillations about a gradual overall strain hardening.

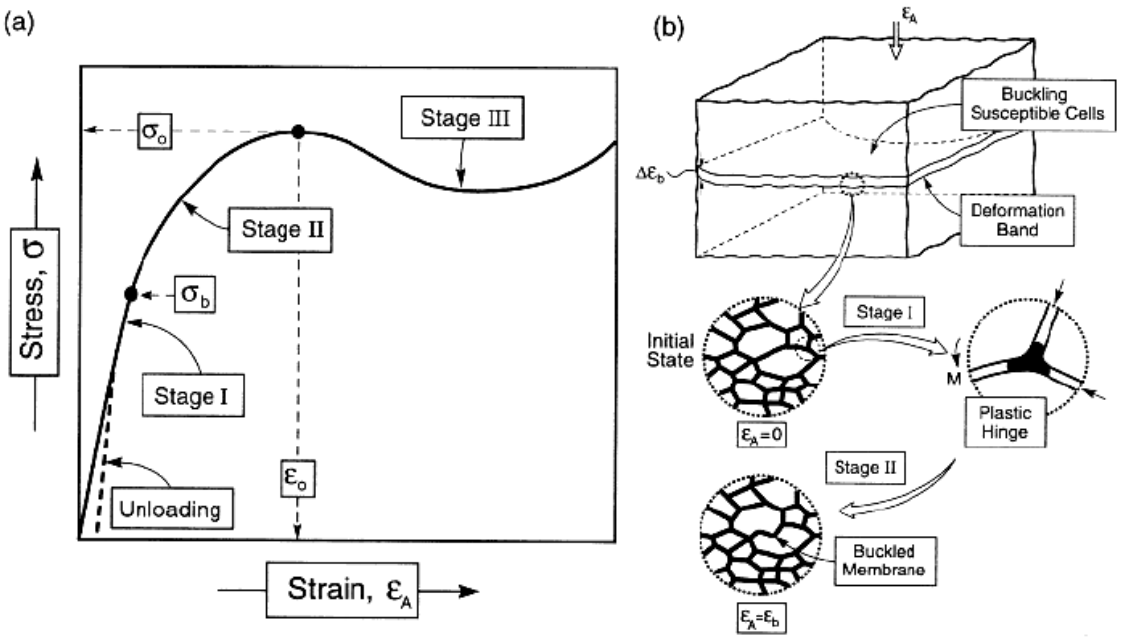

Figure 2.15. A schematic indicating the phenomena that occur during the three stages of plastic deformation in a closed cell Al alloy foam subjected to compression. [47]

Two different types of curves can be distinguished. The first type is typical for ductile alloy foams. These fail with smooth and steadily rising stresses. In contrast, brittle foams show a stress peak if strained beyond the elastic regime and a corresponding drop in stress afterwards. In Figure 2.16 typical stress-strain curves of as foamed, unquenched and quenched samples are seen. Note that, as foamed sample showed ductile characteristic, and the other heat treated samples deformed according to brittle model that included a peak in stress.

Lehmhus and Banhart [26] reported that compression strength is connected to the density of a foam, thus allowing to adjust this property within a certain range. However, because density cannot always be varied freely and in order to gain more control over the properties of metallic foams, adjustment of other variables seems desirable, namely of alloy composition, foam morphology (size and shape of cells) and the metallurgical state of the matrix metal.

The relations for closed cell metal foams, given in the theoretical approach based on the model by Gibson and Ashby, are used for the evaluation of the Young's modulus and the plateau strength during compression loading. In these relations, the basic functions are the relative density ρ^*/ρ_s (where ρ^*= density of metal foam and ρ_s = density of cell wall material) and the fraction φ of the solid contained in the cell edges. The plateau stress σ_{pl}^* is given by the following relation: [48]

$$\sigma_{pl}^*/\sigma_{ys} = 0.3(\varphi\rho^*/\rho_s)^{3/2} + 0.4(1-\varphi)\rho^*/\rho_s + (p_0 - p_{at})/\sigma_{ys} \quad (2.1)$$

where: σ_{ys} = the yield stress of the cell wall; p_o = gas pressure inside the cell and p_{at} = atmospheric pressure. The term $(p_0 - p_{at})/\sigma_{ys}$ is considered to be negligible and relation (2.1) becomes:

$$\sigma_{pl}^*/\sigma_{ys} = 0.3(\varphi\rho^*/\rho_s)^{3/2} + 0.4(1-\varphi)\rho^*/\rho_s \quad (2.2)$$

The Young's modulus E^* is given by the following relation:

$$E^*/E_s = \varphi^2\left(\rho^*/\rho_s\right)^2 + (1-\varphi)\left(\rho^*/\rho_s\right) + p_0(1-2\nu^*)/E_s\left(1-\rho^*/\rho_s\right) \quad (2.3)$$

Where v*=Poisson ratio and E_s=cell wall Young's modulus.

The term $p_0(1-2\nu^*)/E_s\left(1-\rho^*/\rho_s\right)$ is considered to be negligible and relation (2.3) becomes:

$$E^*/E_s = \varphi^2\left(\rho^*/\rho_s\right)^2 + (1-\varphi)\left(\rho^*/\rho_s\right) \quad (2.4)$$

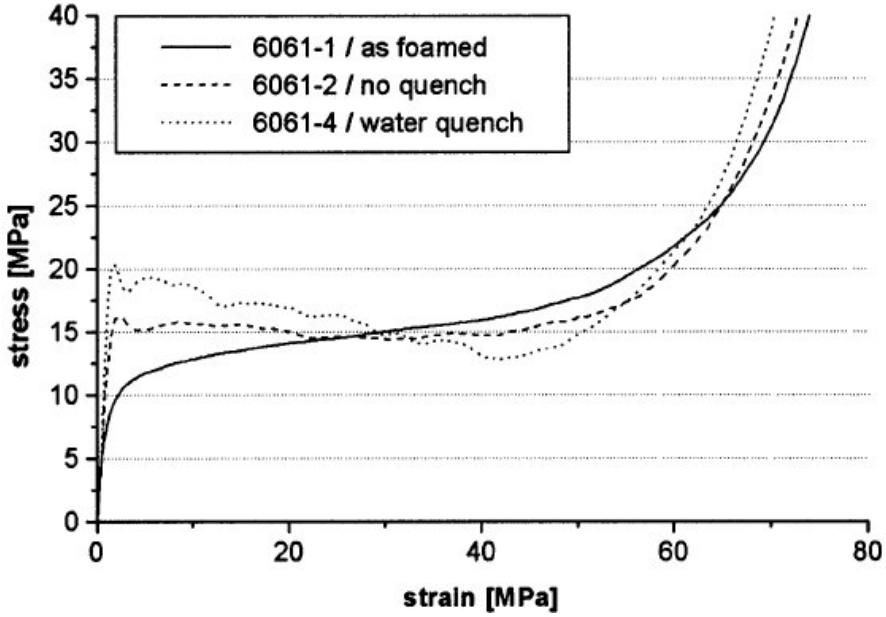

Figure 2.16. Typical stress-strain curves of heat treated AA6061 aluminum foams [20]

The salient structural features of a foam are its relative density, ρ^*/ρ_s, the degree to which the cells are open or closed, and their shape anisotropy ratios R_{12} and R_{13}. The crucial cell wall properties are the solid density, ρ_s, the Young's modulus, E_s, the yield strength, σ_{ys}, the fracture strength, σ_{fs}, and the creep parameters n_s, ε_{os} and σ_{os}. Like those for honeycombs, they show linear elasticity at low stress followed by a long collapse plateau, truncated by a regime of densification in which the stress rises steeply [49].

Linear elasticity is controlled by cell wall bending and, if the cells are closed, by cell face stretching; Young's modulus, E^*, is the initial slope of the stress-strain curve. When loading is compressive the plateau is associated with collapse of the cells – by elastic buckling in elastomeric foams (rubbers, for instance); by the formation of plastic hinges in a foam which yields (such as metal); and by brittle crushing in a brittle foam (such as ceramic). When the cells have almost completely collapsed opposing cell walls touch and further strain compresses the solid itself, giving the final region of rapidly increasing stress [49].

3. EXPERIMENTAL STUDY

3.1. Selection of Powders

Selection of the metal powders and blowing agent by means of purity, particle size and distribution, alloying elements, and other powder properties is vital for successful foaming. Commercial air atomized aluminum powders seem to satisfy these criteria. As Lehmhus and Banhart [26] remark, wrought 6XXX aluminum alloys are chosen when medium strength with good corrosion resistance, reasonable welding and moderate costs are needed. Besides, the sensitivity of 6061 alloys to heat treatment and its well known foaming behaviour were effective in selection of 6061 (AlMg1SiCu) aluminum alloy powders. In this study, argon atomised pre-alloyed 6061 powder (53-150 μm), from ALPOCO (U.K.), is used as the base precursor material.

There are several blowing agents for producing aluminum foams via powder metallurgy process, like TiH_2, ZrH_2, MgH_2 and HfH_2. These all have different decomposition properties and material properties. Among these one has to be chosen with respect to the thermal properties of 6061 aluminum alloy. In this study, TiH_2 (<44 μm, 98% purity), from Sigma-Aldrich (Germany), is used as blowing agent considering the reasons below [40]**:**

- The decomposition interval of TiH_2 is suitable for producing aluminum foam. TiH_2 starts decomposition at about 400 ^oC [12, 16, 24, 50] and the 6061 aluminum alloy has liquidus and solidus temperatures, 582 ^oC and 652 ^oC [51], respectively.
- TiH_2 and its phases that form at high temperatures have no adverse effect on foaming. TiO_2, TiO_3 [24].
- TiH_2 is known to have high capacity of hydrogen storage [52, 53]; hence amount of blowing agent can be lower when compared to other types of blowing agents.
- TiH_2 is easily accessible on the market.

Table 3.1 shows the chemical analysis of the compacted mixture which conforms to the specification for alloy AA6061 in the literature, except for the Ti-content. Since the chemical analysis was carried out with a foamable precursor, this excess Ti-content comes from the addition of 0.6 wt. % titanium hydride.

Table 3.1. Chemical composition of AA6061 and its reference values

Element	Mg	Si	Cu	Fe	Mn	Cr	Ti
Measured	0.983	0.657	0.308	0.152	0.005	0.147	0.388
Reference Values for AA6061							
Min (wt. %)	0.800	0.400	0.150	-	-	0.040	-
Max. (wt. %)	1.200	0.800	0.400	0.700	0.150	0.350	0.150

3.2. Mixing of Powders

Blending the aluminum and titanium hydride powders is the first and a crucial step of the entire foaming process. Speaking of reproducibility, it is important to obtain a homogenous titanium hydride distribution in the aluminum matrix. Otherwise, if there are TiH_2 agglomerations in the matrix, foam morphology will vary from sample to sample causing low reproducibility. Therefore, a tumbling mixer, whose schematic view is seen in Figure 3.1, is utilized, having a rotation of 200 rpm that let metal powders to be mixed in a chaotic way for 1 hour. Alumina balls are also added in order to disturb the mixture. As extended mixing times will result in crumbling of alumina balls, 1 hour of mixing time is found to be sufficient. The reason for choosing alumina balls was that they could not add any other element to the mixture other than aluminum oxide, which already existed in the mixture naturally. In all batches, the alloyed aluminum powders are mixed with 0.6 wt. % titanium hydride powder ($<44\ \mu$m) as such in most applications [14, 20, 25].

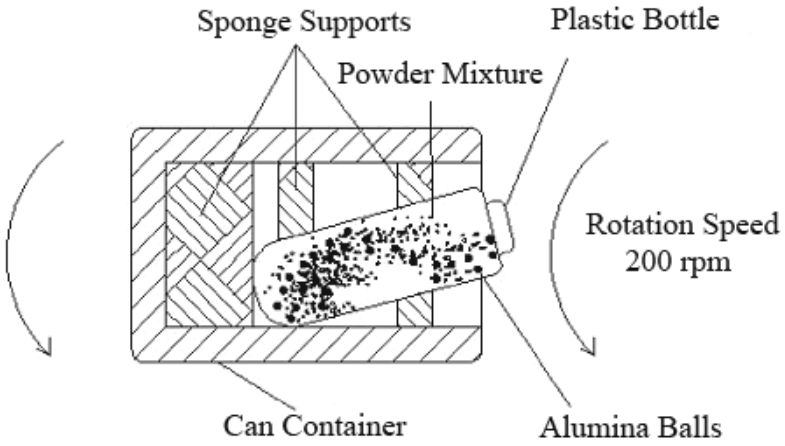

Figure 3.1. Schematic representation of mixing configuration used in this study. (Figure taken from Nazım Mahmutyazıcıoğlu)

Another important point in mixing process is to obtain a clean and homogenous powder mixture in order to carry out a successful foaming. Impure and soiled powders by dirt, water or other particles entrapped in the mixture may have detrimental effect in foaming. Impurities in the mixture will be entrapped inside the precursor during the consolidation process. As Matijasevic and Banhart [16] mentioned, these impurities will act like nuclei of uncontrolled voids during the decomposition of TiH_2, which will form larger pores at the latest stages of foaming.

3.3. Consolidation of Powders

In literature various ways of consolidation of powders are present. These methods involve CIP, extrusion and uniaxial compaction of powders. In this study, uniaxial compaction was employed. For the compaction process, a hydraulic press with a capacity of 280 bar was used. The aim of compaction of powders is to obtain a foamable precursor material with a theoretical density closed to 100% theoretical density of the aluminum matrix. This means that no residual open porosity inside the precursor is to be remained. Therefore, in this study subsequent to the cold compaction powder mixture was also hot compacted at various temperatures, time and pressure, 400-450 ^{o}C, 15-30 min and 270-400 MPa, respectively. After consolidation of powder mixtures densities of the precursors were calculated using Archimedes' method.

Two DIN 1.2344 (AISI H13) hot work tool steel mould were designed with different punch diameters of 27 mm and 22 mm to be utilized in compaction process. The reason for choosing DIN 1.2344 as the mould material was its reliability at high temperatures and high pressures. The moulds had a Rockwell hardness (HRC) value of 53. The compaction moulds and ring heater used in hot compaction stage are seen in Figure 3.2.

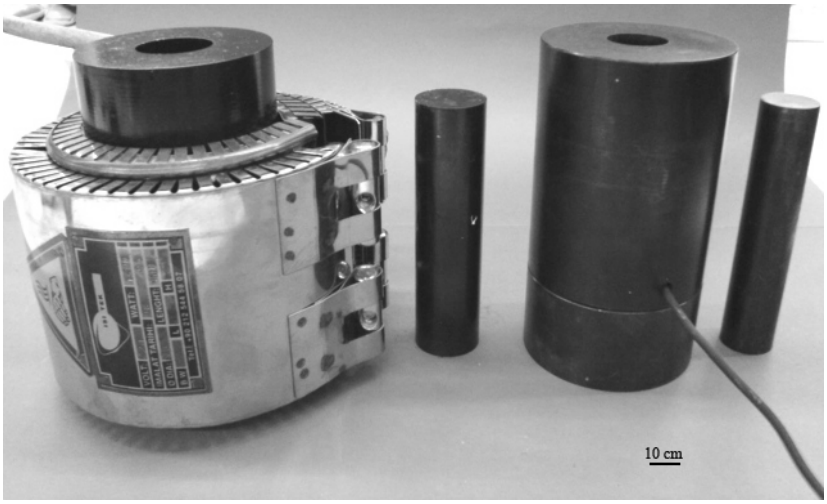

Figure 3.2. Compaction moulds used in densification stage of powder mixtures and ring heater attached to the mould used for hot compaction

First, powder mixture is poured into the mold with 22 mm punch size. Then powders are compacted at room temperature for 10-20 minutes at a pressure of 400 MPa to obtain a precursor for subsequent hot compaction. Cold compaction prior to hot pressing is done since handling of powders at hot compaction temperatures above 400 ^{o}C is very difficult due to the dusty nature of the powders.

An important point about cold compaction is that as Von Zeppelin et al. [13] mentioned, during cold compaction there is a risk of fresh and non-oxidized surface formation due to heavy deformation. Compaction of powders to a dense billet implies heavy deformation of all the individual particles. The newly formed fragments possess fresh and non-oxidized surfaces which are easy to be passed by hydrogen when the compact is heated. Therefore, cold compaction periods must be kept at minimum levels in order not to create non-oxidized surfaces.

For heating the mould to the hot compaction temperatures (400-450 ^{o}C), a ring heater having a capacity of 800W around the mould is utilized. Controlling the temperature is done with two K-type NiCr-Ni thermocouples and two on/off thermo controllers. As seen in Figure 3.3 one thermocouple is penetrated through an opening on the mould. The other thermocouple was used to control the inner heat during the heating of the mould. The ring heater is controlled via the data obtained from the penetrated thermocouple while the other one is employed for reading the inner temperature.

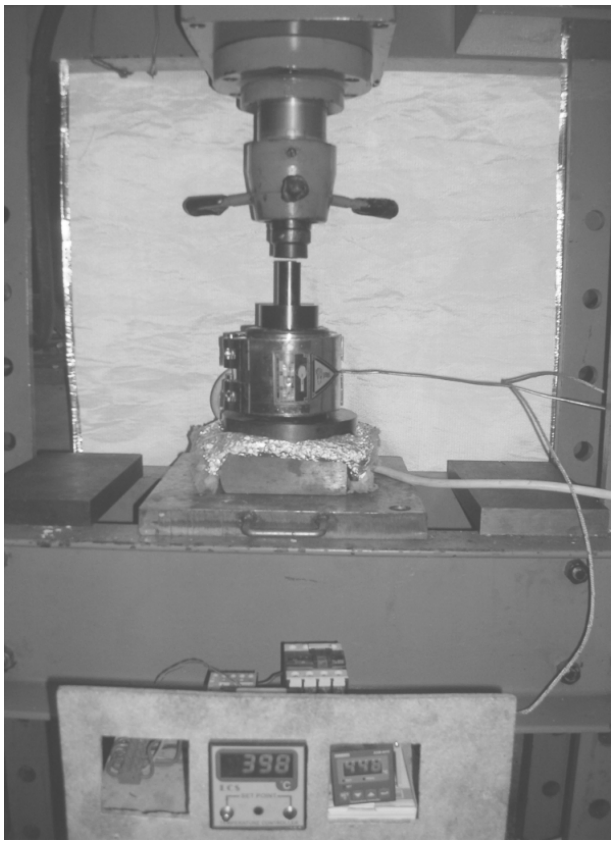

Figure 3.3. Two K-type thermocouples and a ring heater attached on compaction mould

There was a risk of sticking of the precursor on the inner wall of the mould during hot compaction. Ejecting the precursor from the mould and punch took too much time thus retards the overall foaming process. Hence, high temperature paste grease composed of MoS_2 was used to form a film between the precursor and mould wall that prevented adherence.

3.4. Foaming of Precursors

Heating up the precursor, compacted aluminum and TiH_2 powders, above the liquidus temperature of the aluminum matrix (652 ^oC) will yield a highly porous structure. The gas released by TiH_2 forms bubbles inside the viscous melt and expands the matrix. At the early stages of foaming, as the titanium hydride powders are embedded in the aluminum matrix, the initial pressure inside the first pores counteracts the further decomposition and slightly delays the hydrogen release. If the precursor is heated further above the solidus temperature (582 ^oC) of the AA6061 matrix the viscosity of the solid/liquid precursor tends to lower and the inside pressure of the pores begins to exceed the resistance of the matrix and the outside pressure, thus above the liquid temperature pores starts to enlarge. In the present study, the foaming periods and temperatures varied between 3 and 7 minutes and 700-800 ^oC, respectively.

It should be noted that the foaming period varies from a few seconds to several minutes depending on the size of the precursor and the foaming temperature. Therefore, it would be convenient to choose foaming time considering the foaming system (precursor shape, dimension and material) rather than fixing the foaming time. In this study, foaming time varies between 3 to 7 minutes depending on the precursor weight and foaming temperature.

The foaming experiments were carried out in a pre-heated furnace which has a capacity of 2300W as seen in Figure 3.4. In order to optimize the heat flow to the precursor, a foaming mould was designed and used in all the foaming experiments. Throughout the whole foaming stages the outer mould was kept inside the furnace to stabilize the heat flow to the foaming mould. At the beginning of the foaming stage, the foaming mould was placed inside the outer mould to be pre-heated before the precursor put in it. By this way, as Duarte et al. [14] mentioned very high heating rates were enabled to be reached. Temperature of foaming mould was observed via a thermocouple attached to the foaming mould as can be seen from the schematic view of foaming mould system in Figure 3.5.

In order to investigate the effect of ceramic particle addition to the foam morphology, Al_2O_3, a type used in abrasive industry, added precursors were also foamed. Additions were 5 wt. % in all cases and particle sizes were 500 mesh (<32 μm). Meso and microstructure of the various specimens were characterized by cutting out thin slices by diamond cutting saw, seen in Figure 3.7, and then embedding the slices into acrylic solution and polishing. Grinding and polishing were carried out in an order of 240, 400, 600, 1000, 1200 mesh sandpapers and finally with a 1 μm diamond polish paste. One must pay attention to fade away all the scratches at each step of grinding, which means that no scratch belongs to the previous sandpaper has to be remained. As the specimens were produced by powder metallurgy method, there were problems in polishing such as embedding the carbide particles in the aluminum matrix and overabrasions at some points. These problems could be solved by using boron based lubricants.

Figure 3.4. Furnace utilized in foaming experiments

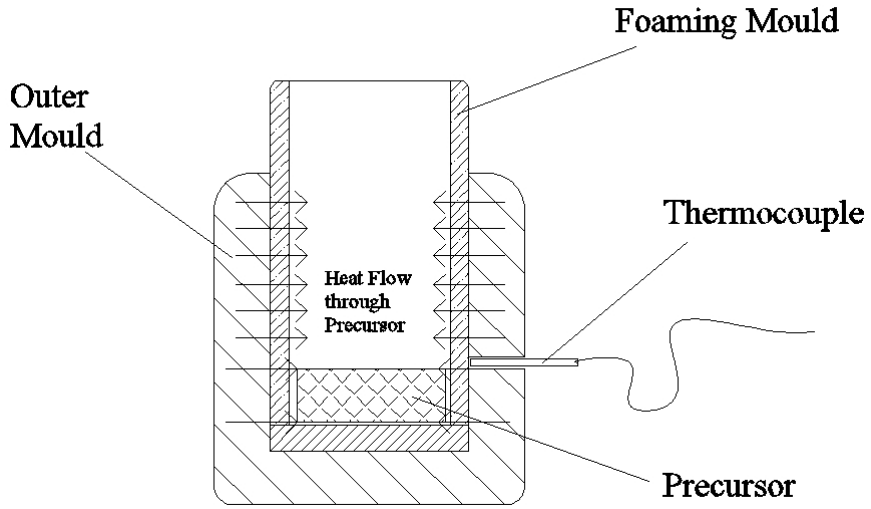

Figure 3.5. Schematic view of foaming moulds with a thermocouple attached

As there is a gap between the decomposition temperature of the titanium hydride powders and the liquidus temperature of the matrix alloy, this interval should be passed as quick as possible. During the early stages of foaming, the hydrogen released from TiH_2 forms cracks inside the solid precursor. These cracks will form larger pores at the latest stages of foaming hence the homogenous distribution of cells would not be obtained. Garcia-Moreno et al. [54] prove that critical heating rates are above 50 $K.min^{-1}$. As the foaming periods and times varied between 3 and 7 minutes and 700-800 ^oC, respectively, so this means that critical heating rates were already exceeded.

The furnace was set to the foaming temperature and the moulds were placed inside. For the initial foaming experiments, after the furnace temperature reached the set temperature, a pause for about an hour was given in order to enable thermal stabilization inside. Then the precursor was dropped in the foaming mould. Both dropping the precursor in the foaming mould and taking the foaming mould out of the furnace after foaming was done in just 10 seconds, hence there was not a considerable temperature fluctuation inside the furnace. The reason for choosing a thick walled outer mould was to enable a homogenous heat flow through the foaming mould by using its thermal inertia.

Both the outer and foaming moulds are made from 310 SS considering its good oxidation resistance at high temperatures such as 800 ^oC in which the foaming experiments were carried out. Two NiCr-Ni type thermocouples were employed to control the furnace

temperature. One was located near to the top of the furnace chamber, and the other was inserted along the outer mould's thickness in order to read the temperature of the foaming mould precisely. According to our foaming experiences, just a slight difference between the two thermocouples' positions had been existed which means that a homogenous heat distribution was obtained inside the furnace.

Stabilizing the foam structure after taking out from the furnace were conducted either cooling in air or in water. Cooling was conducted by either resting in air or blowing air by a fan. Water quenching of foams were done by partially immersing the mould inside the water and moderately moving. Cooling in air by resting the foam inside the mould yields very low cooling rates since interfaces (foam→conduction→mould→convection→air) lowers the heat dissipation. Low cooling rates have an adverse effect on foam structure that due to gravity force liquid material flows down to the bottom and thus thickens the bottom profile. This effect is known as "drainage" [37] which leads to a density gradient between the top and bottom of the foam. Therefore, cooling the mould after taking out from the furnace was conducted by blowing air with a fan.

3.5. Heat Treatment of Titanium Hydride Powders

Heat treatments of TiH_2 powders were performed in order to shift the decomposition temperature to higher temperatures. The objective was to compare the characteristics of gas release under different conditions. As Matijasevic et al. [55] proved that during the heat treatment of TiH_2, oxidation of surface occurs and the oxide compounds of titanium covers the particles. This oxide film acts as a barrier and hinders the decomposition of hydrogen. In literature, heat treatments are performed with loose TiH_2 powders [16, 24] as well as powder compacts [13] of foaming agents. In present study, pre-treatments and thermal gravimetric analysis (TGA) of TiH_2 powders were carried out with loose TiH_2 powders. As-received titanium hydride powders are heat treated in a PID controlled furnace, seen in Figure 3.6, at atmosphere pressure.

Figure 3.6. Furnace used in heat treatments of TiH_2

As TiH_2 starts to decompose at about 400 ^oC and in accordance with the literature [12, 13, 16, 24, 47], powders are heat treated in air at 400,480 and 530 ^oC for 30 and 180 minutes. Heat treatment of TiH_2 powder results a considerable hydrogen loss, however as Baumgartner et al. [25] mentioned only 25% of total TiH_2 in a precursor attend forming bubbles. It is interesting that 60-75 % of the total hydrogen contained in the TiH_2 is already released at the temperatures below 700 ^oC, as revealed by TGA results. Heat treatment of blowing agent can be interpreted as it lowers the efficiency, however as Baumgartner et al. [25] calculated, very low levels of hydrogen gas is sufficient to create a highly porous structure. Assuming that if a precursor contains 0.6 wt. % TiH_2, 1 cm^3 of the precursor contains 0.016 g of TiH_2 which means that the precursor contains 0.65 mg of hydrogen or 0.32 mmol of H_2. At 660 ^oC this corresponds to a volume of 23 cm^3 [25]. Considering that foaming the precursor results a volume expansion factor of 4 and 5, as a conclusion only 25% of the total hydrogen is used to form bubbles, whereas the rest is lost during foaming.

Various amounts of TiH_2 are used for each heat treatment. Slight agglomeration of the powders occurred as a result of the heat treatment and thus agglomerations were broken up before TGA.

The decomposition temperatures at which H_2 is decomposed from both as-received and heat treated loose TiH_2 powders were measured using thermo gravimetric analysis (TGA) on a TA Instruments TGA Q50. This instrument gives the data about at which temperature a weight change occurs by heating the sample with requested heating rates. In this study, a heating rate of 20 $^oC.min^{-1}$ was used. As Sandim et al. [41] mentioned high heating rates will give high onset of decomposition, so in order to yield correct values the heating rate was kept lower. The temperature range was chosen as 20-700 ^oC in order to simulate the behaviour of TiH_2 during the foaming stage. Heating was performed in nitrogen, air and argon atmospheres. At first, flow rate was selected as 60 $ml.min^{-1}$, however this amount of gas flow through the heating room was not enough to purge the oxygen inside, hence instead of a decreasing tendency in weight, an increase in weight was observed due to oxidation of TiH_2. Therefore, flow rate was increased to 240 $ml.min^{-1}$ and this amount was used for all the TGA analysis. Nitrogen and argon atmospheres were chosen thinking that the TiH_2 particles are embedded in aluminum matrix and excluded from oxygen during the foaming stage. The TGA results were adjusted as if all the powder masses were the same.

3.6. Heat Treatment of Aluminum Foams

Heat treatment of aluminum alloys is based on altering their mechanical properties by using particular response of the alloying systems to the heat treatment parameters. One has to make a decision between ductility and strength which are obtained by annealing and precipitation hardening, respectively. Precipitation hardening involves solution heat treatment (SHT) and quenching which leads to supersaturated solid solution of the alloying elements. Subsequently applied aging creates precipitations in fine dispersion within these supersaturated regions. Aging produces precipitates suitable for increasing strength considerably. Besides, annealing homogenize the distribution of alloying elements and dissolve grain boundary precipitates of Mg_2Si or AlFeSi. In the present study, both conditions were investigated. The parameters, seen in Table 3.2, for solution heat treatment, aging and annealing were selected in consistence with relevant literature [20, 26] about aluminum foams as well as equivalent bulk aluminum alloy system [20, 45, 56].

Table 3.2. Heat treatment parameters applied to the aluminum foams

Heat Treatment		SHT	Aging	Annealing
	fHT1	530 ^{o}C for 100 minutes, water quenched	165 ^{o}C for 10 hrs	n/a
	fHT2	n/a	n/a	420 ^{o}C for 1 hr, 230 ^{o}C for 2 hrs
	As foamed	n/a	n/a	n/a

The aluminum foams used for heat treatment were produced from the precursors, weight approximately 15 g, containing heat treated (480 ^{o}C for 180 minutes) 0.6 wt. % titanium hydride. First, the powder mixtures were compacted by using uniaxial cold compaction at a pressure of 400 MPa for 10 min and subsequently compacted at 450 ^{o}C under a pressure of 270 MPa for 30 minutes. The foams were grouped considering their densities into three groups and each group consisted of five samples. First group included the untreated foams which were used as reference samples, while second and third groups included SHT+aging and annealing states, respectively. For the alloying system 6061, Lehmhus et al. [20] designated a critical cooling rate during SHT quenching for about 100 $K.s^{-1}$ at the temperature range between 400 and 290 ^{o}C. By this means, premature formation of precipitates, Mg_2Si for AA6061, can be restrained and achieving higher strengths can be possible. In order to ensure such cooling rates, quenching has to be done in cold water.

Heat treatments of aluminum foams were carried out in the furnace used in the heat treatment of titanium hydride powders. For the solution heat treatment, the samples were kept at 530 ^{o}C for 100 minutes and then the samples were quenched in water one by one. It should be noted that the water reserve has to be big enough to avoid boiling of water. After water quenching, samples were aged at 165 ^{o}C for 10 hours. For the annealed state, two steps were followed. First, the samples were kept at 420 ^{o}C for 1 hour and then cooled in furnace to 230 ^{o}C. Finally, samples were kept at 230 ^{o}C for 2 hours and cooled in air.

3.7. Investigation of Compression Behaviour of Aluminum Foams

In order to minimize the cell damage a rotating diamond saw with a thickness of 0.6 mm is utilized, as seen from Figure 3.7, to prepare the specimens for the compression tests. This cutting method can easily provide a smooth undeformed surface that will not have an adverse effect on compression results.

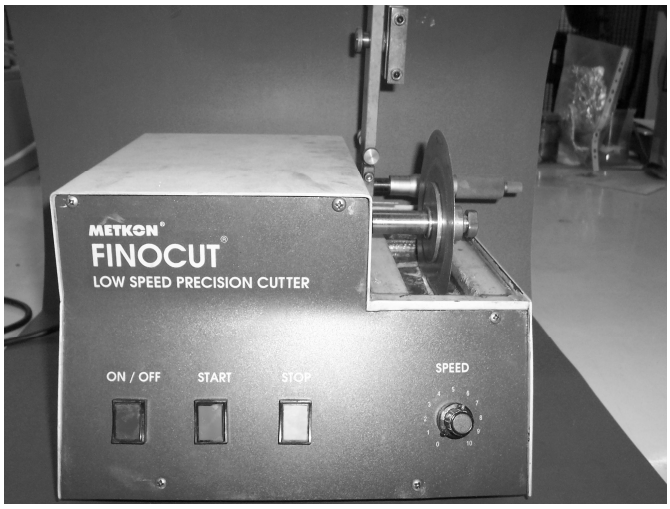

Figure 3.7. Diamond saw used for preparation of the compression test specimens

The ratio of the specimen size to the cell size can affect the measured mechanical properties of foams. It should be noted that, as Ashby et al. [27] reported that the minimum dimension of the specimen should be at least seven times the cell size to avoid size effects. As there are no standards for compression testing of aluminum foams, specimen sizes were selected, according to Ashby's suggestion, as 30 mm in height and 30 mm in diameter.

Quasi-static compression tests were performed on an Instron machine, shown in Figure 3.8, at a crosshead speed of 5 mm/s. Compression of the specimens were aborted whether if 80% strain or 60 kN force was reached. Since the stiffness of the testing machine was much higher than that of the foam samples, the displacement of the cross-head was used to determine the overall compressive displacement. The accuracy of the cross-head displacement measurement was 0.001 mm. Data from the test machine were transferred to the computer via data acquisition interface using MATLAB software. For each three groups five specimens were tested, however the worst two out of five were

neglected in order to minimize the adverse effects due to heterogeneities inside the specimens.

Figure 3.8. Instron test machine used in compression tests of aluminum foams

4. RESULTS AND DISCUSSION

4.1. Mixing of Powders

Figure 4.1 shows the SEM image of wrought aluminum 6061 alloy powders (53-150 μm), from ALPOCO (U.K), used in this study. As seen from the SEM image, particles have globular shape. In all the experiments, 0.6 wt. % of TiH_2, seen in Figure 4.2, (<44 μm, 98% purity) Sigma-Aldrich (Germany), was used as blowing agent. Beside, some trials were performed in order to investigate the effect of weight percentage of TiH_2 to the foam morphology. It was found that 0.6 wt. % was fairly sufficient to obtain high porous structure. Since TiH_2 is a relatively expensive material, as a commercial point of view this is also important to enable cost reduction.

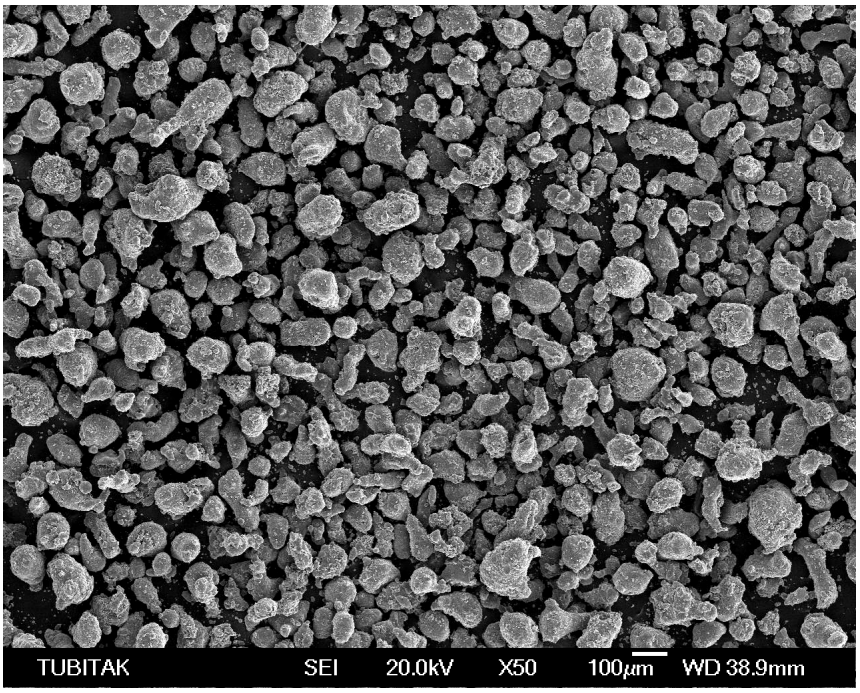

Figure 4.1. SEM image of AA6061 powders used in this study

The mixing of powders, batch of 150 g, was conducted via a tumbling mixer with a rotation speed of 200 rpm for 1 hour. In order to disturb the mixture alumina balls with a

diameter size of 10 mm were added in each batch. Although mixing of powders depends on the amount of powder mixture to be mixed, extended mixing times should be avoided to

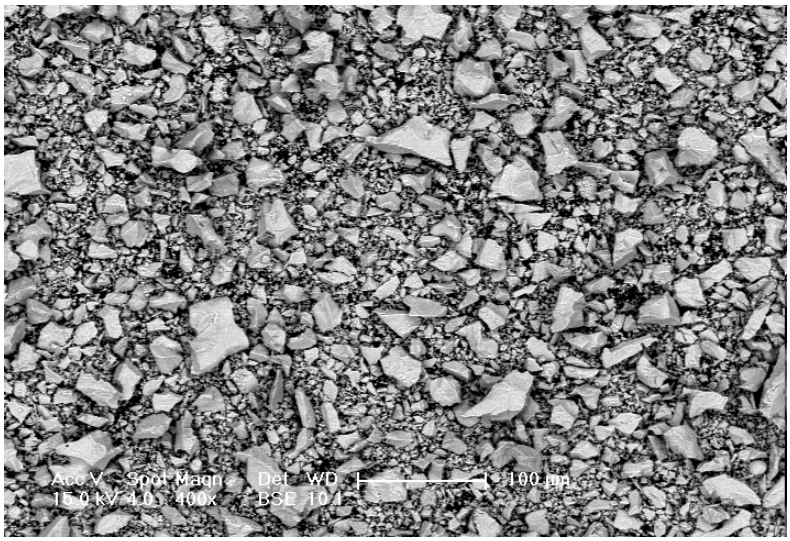

Figure 4.2. SEM image of TiH_2 powders used in this study

prevent milling of the powders. As seen in Figure 4.3, TiH_2 particles were distributed evenly in the aluminum matrix. As a conclusion, this type of mixing method was found to be suitable to utilize in such experimental.

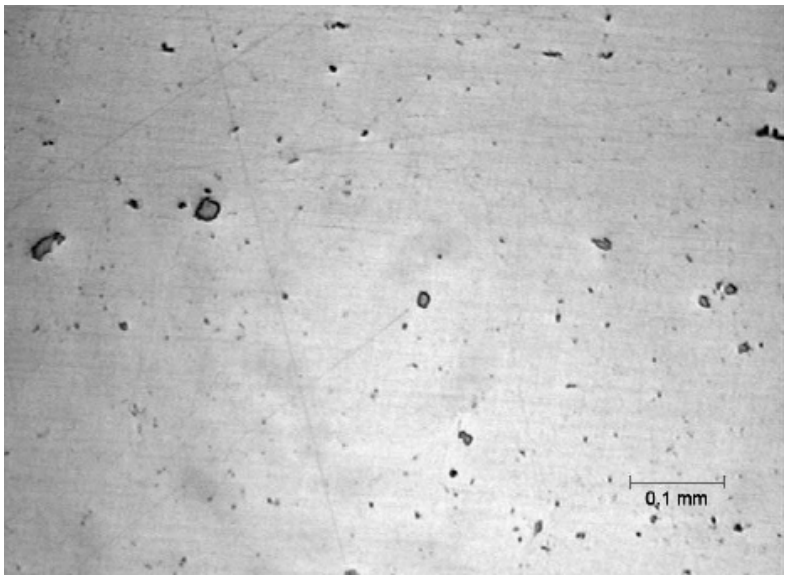

Figure 4.3. Optical image of TiH_2 particle distribution in aluminum matrix

4.2. Production of Foamable Precursors

Compaction of powder mixtures were conducted uniaxial compaction. Producing precursors were done either by hot compaction or combination of cold and hot compaction stages. The reason for carrying out cold compaction before hot compaction was not only obtaining a fully densed precursor but also handling of a solid material in hot compaction stage was easy rather than powders. It was seen that a pre-pressing operation should be done before hot compaction, since due to their dusty nature; powders tend to adhere on the mould walls which adversely affected densification. Trials were also carried out with just cold compaction method to produce foamable precursors. However it was concluded that, due to the poor compaction at room temperature, even at high pressures such as 540 MPa, it was observed that there were pores left inside the aluminum matrix. In Figure 4.4 cross-sections of two precursors are seen which explains this effect. The one at left was produced by cold compaction at room temperature at a pressure of 400 MPa for 20 minutes; the one at right was produced by first cold compaction with the same parameters and subsequently hot compacted at 450 ^{o}C under a pressure of 400 MPa for 20 minutes.

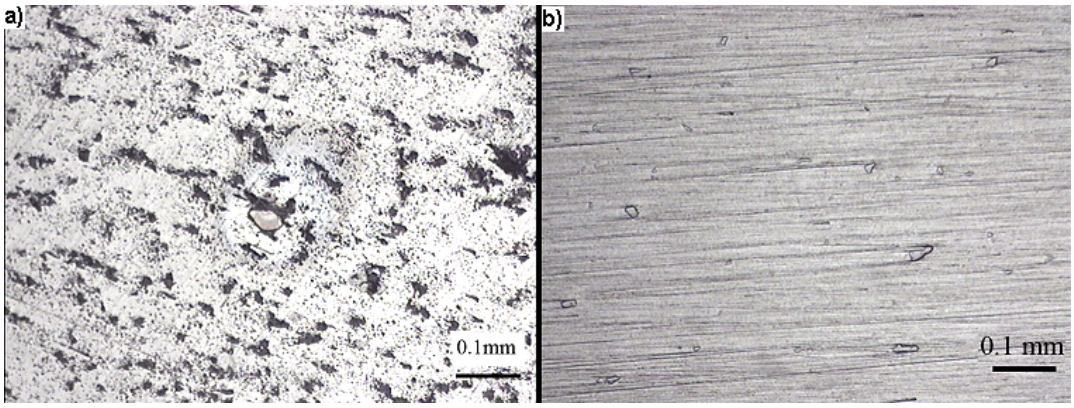

Figure 4.4. Cross-sections of two precursors;
a) Cold compacted (20 ^{o}C, 400 MPa, 20min) b) Cold compacted (20 ^{o}C, 400 MPa, 20min) and hot compacted (450 ^{o}C, 400 MPa, 20min)

Note that the cold compacted precursor has highly concentrated pores inside the matrix that prove a poor consolidation; whilst after hot compaction pores were eliminated and TiH_2 particles were completely embedded into the matrix. One has to avoid such voids inside the precursor because during early stages of foaming, hydrogen evolved from TiH_2

escaped through these pores which would yield a very low expansion rate as seen in Figure 4.5. The sample was foamed at 750 ^{o}C.

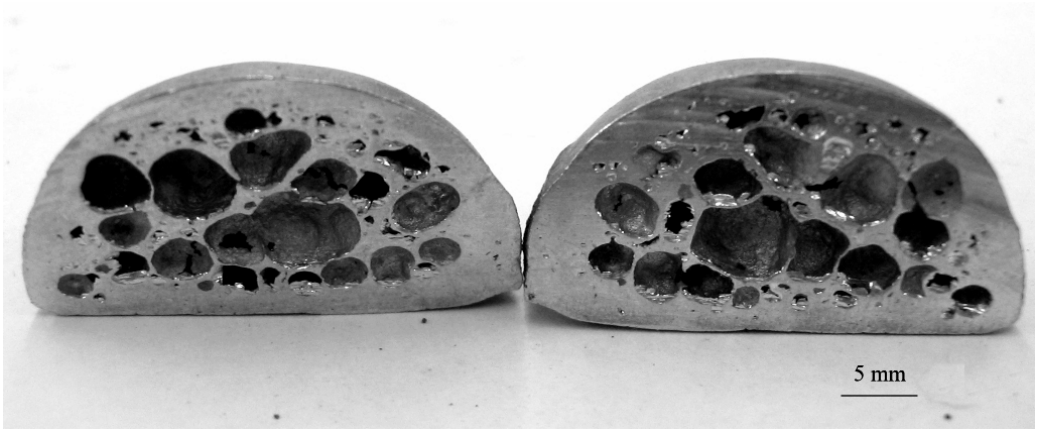

Figure 4.5. Cross-section of a foam which was produced from a cold compacted precursor

Besides, as seen in Table 4.1 and Figure 4.6, densities of the precursors produced with just cold compaction are far away from theoretical density of aluminum matrix (2.7 g.cm^{-3}). Note that the precursors having minimum densities were produced by cold compaction. This is due to the pores inside the matrix.

Table 4.1. Effect of compaction parameters on precursor density

Precursor No.	Compaction Method	Pressure (MPa)	Compaction Time (min.)	Density (g/cm^3)
1	Cold compaction (20 ^{o}C)	400	30	2.09
2	Hot Compaction (450 ^{o}C)	270	15	2.68
3	Cold compaction (20 ^{o}C)	400	15	2.07
4	Hot Compaction (450 ^{o}C)	270	15	2.68
5	Cold compaction (20 ^{o}C)	400	30	2.09
6	Hot Compaction (450 ^{o}C)	270	15	2.69
7	Hot Compaction (450 ^{o}C)	270	15	2.64
8	Hot Compaction (450 ^{o}C)	400	30	2.66
9	Hot Compaction (450 ^{o}C)	270	15	2.66

As a conclusion, it is easy to see that compaction is a very important stage for obtaining high-quality foams. First cold compaction of the powders at a pressure of 400 MPa and then hot compaction at 450 ^{o}C at a pressure of 270-400 MPa for 20-30 minutes are found to be the optimum parameters for densification of powder mixtures.

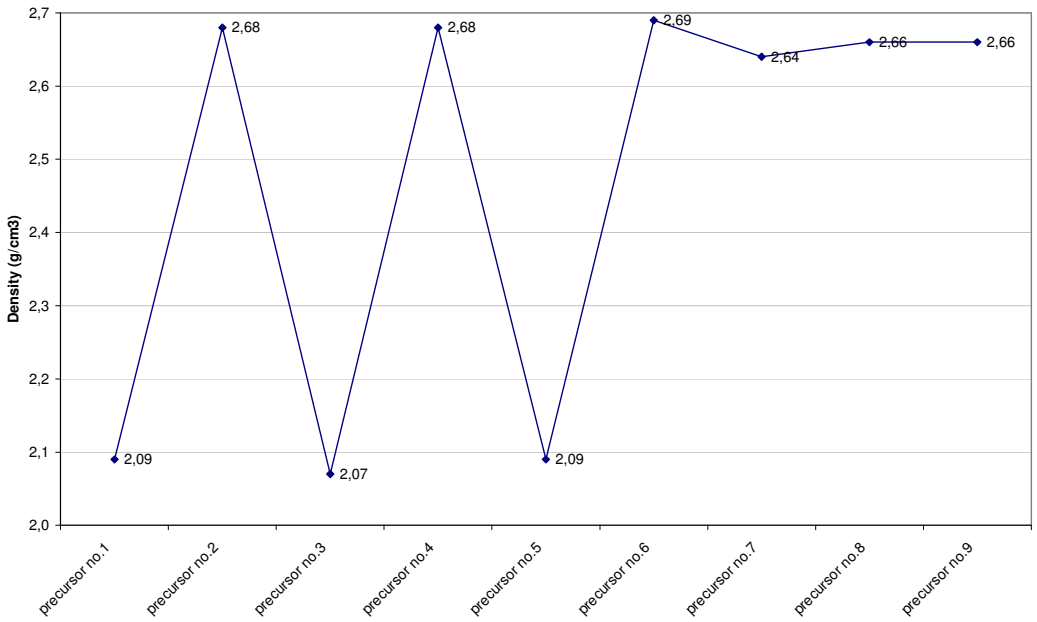

Figure 4.6. Effect of compaction parameters on precursor densities.

4.3. Foaming of the Precursors

Foaming experiments were carried out at temperatures between 700 and 800 ^{o}C. According to the foaming experiences, by pre-heating the furnace heating rates could easily exceed the suggested heating rates [14, 25] and it is thought that average heating rate was about 120 ^{o}C.min^{-1} during the foaming experiments. Throughout the early studies, foaming was carried out as free foaming which means no foaming mould was used. In Figure 4.7 a foam produced by this way is seen. As there were no horizontal constrain, liquid material lost its form and due to gravity high amounts of drainage was seen. Later, foaming experiments were done by using a foaming mould that let the precursor expanded vertically. It is also observed that mould had a mechanically supportive effect to the liquid material especially after taking the foam out of the furnace.

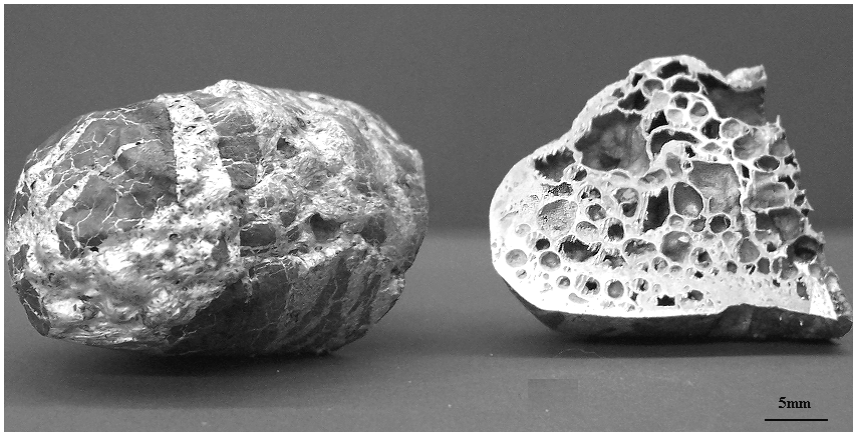

Figure 4.7. Foam produced by free-foaming

Foaming can be divided into three stages: Pore formation, cell growth and fully expansion. The initial stage includes a local increase in partial hydrogen pressure as the precursor heated above decomposition temperature of the blowing agent and formation of pore nuclei as can be seen in Figure 4.8. Note that the initial pores are crack-like which lie perpendicular to the compaction direction. This is due to high matrix strength at relatively lower temperatures. As the precursor is further heated, the matrix loses its strength and pores become more rounded shape. In this stage, internal hydrogen pressure overcomes both the resistance of the material and ambient pressure. At the final stage, corresponding to the temperatures above the liquidus temperature of the matrix, the foam structure is clearly visible and cells are easily distinguished.

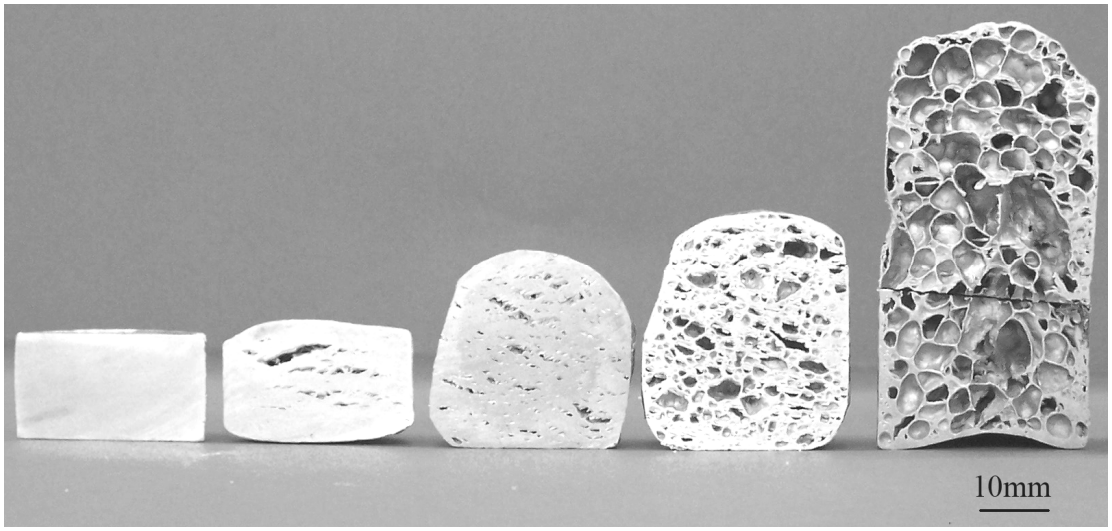

Figure 4.8. Evolution of foam morphologies during different foaming stages

Optimum foaming temperature was found to be 750-775 ^{o}C for the precursors without ceramic particle addition. Below this temperature range, especially at temperatures close to 700 ^{o}C, it is believed that the melt viscosity and surface tension are too high to form bubbles inside the melt and lower heating rate increases the hydrogen loss. Above this range, close to 800 ^{o}C, this time melt viscosity becomes so low that rapid cell coalescence is seen by the rupture of cell walls. Two examples can be seen in Figure 4.9 which explains this effect. The sample in Figure 4.9(a) was foamed at 800 ^{o}C in about 6 min. Note that there are larger cells that were formed by cell coalescence, and slightly drainage occurred at the bottom. During foaming, due to difference between the inner pressure of two adjacent cells small cells and larger ones merged together and very large cells were formed as seen from the figure. Besides, due to gravity the material at the top of the foam flow through the bottom that made top cell walls thinner and the bottom cell walls thicker. Opposite to this, the sample foamed at 700 ^{o}C, seen in Figure 4.8 (b), had highly concentrated drainage at the bottom depending on lower heating rate. This is because at lower temperatures one has to wait for longer to obtain a fully expanded foam.

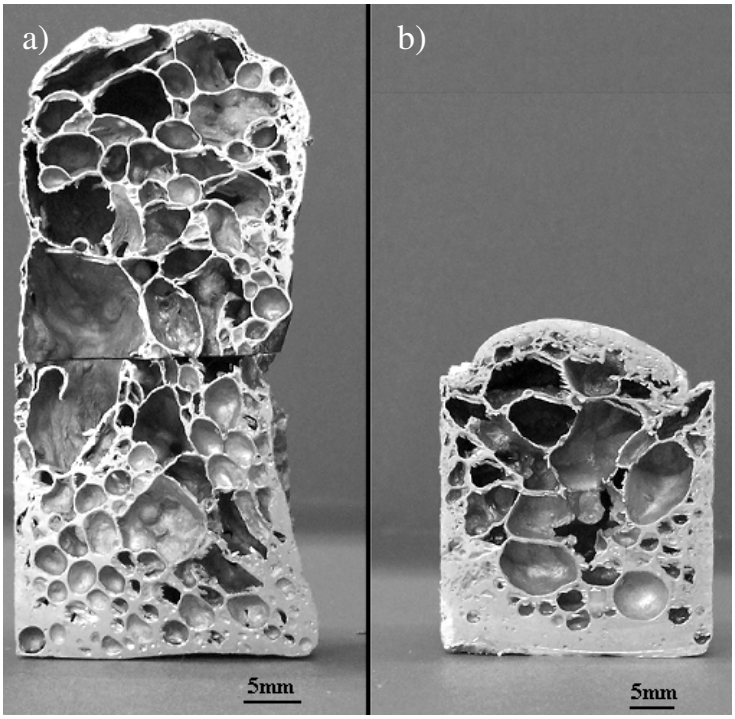

Figure 4.9. Cross-sections of foams produced at a) 800 ^{o}C, b) 700 ^{o}C, note that other parameters were all the same.

The longer foaming time the more cell collapse occurs, so the melt flow through the bottom will yield a thick solid layer. Besides, at 700 ^{o}C due to high melt viscosity than that of 800 ^{o}C, the pressure inside the cells can not easily overcome the strength of the melt, hence especially the cells at the bottom can not grow when compared to the upper ones.

Another important point in stabilizing the foam structure is cooling the foam after taking out from the furnace. While quenching in water was conducted the mould did not completely immersed in water, because the foam after taken out from the furnace was still in liquid phase and unstable. At this high temperature there exists a very high temperature gradient between the water and melted material which results very rapid shrinkage. The foam structure starts to shrink from the top and water penetrates through the gap between the foam and the mould wall. Then an immediate vaporization occurs and relatively high steam vapour breaks up the still ductile foam walls as seen in Figure 4.10.

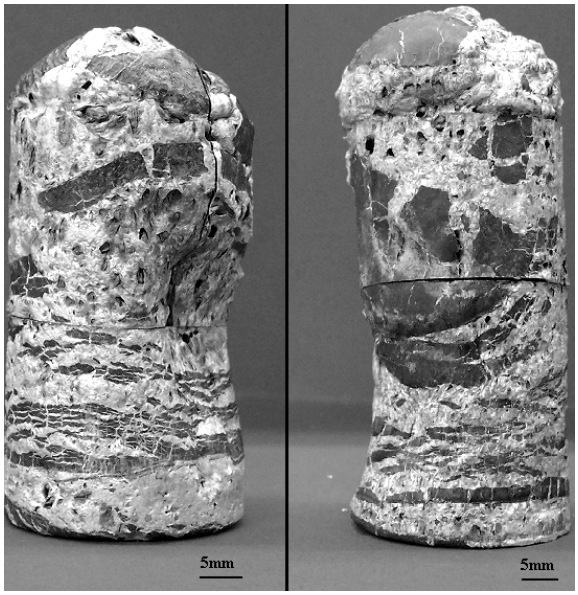

Figure 4.10. Form disorder of water quenched foams

In Figure 4.11 a cell wall of a foam cooled by blowing air is shown. It should be noted that no adverse effect due to cooling such as rupture of the cell wall or discontinuity is seen. Consequently, it can be said that cooling the foam by blowing air was found to be appropriate way in order to prevent adverse effects on foam structure.

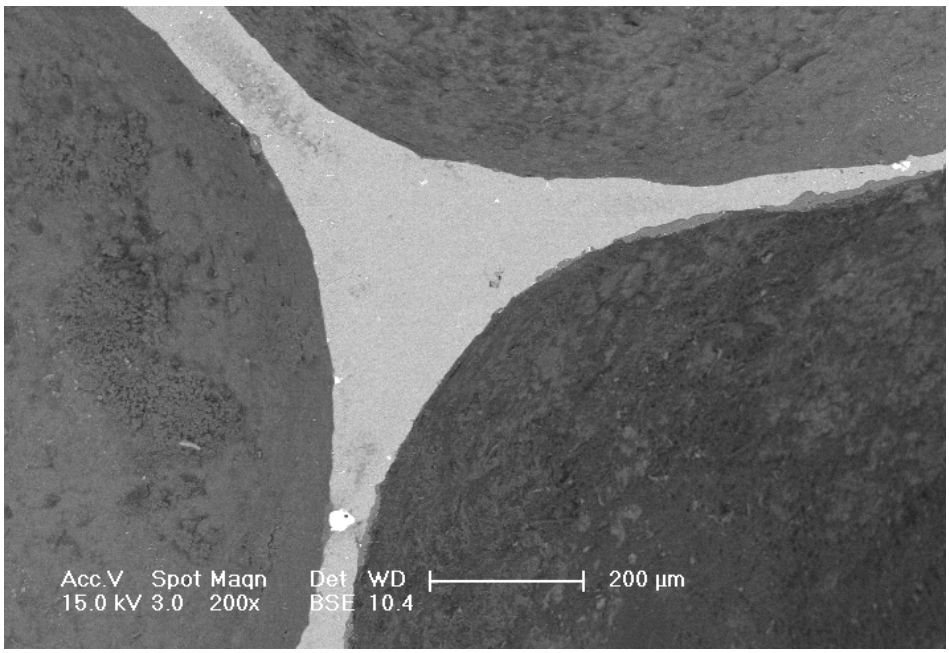

Figure 4.11. SEM image of intersection of three cell walls (Plateau Region) of a foam cooled by blown air

4.4. Enhancement of Foam Morphology

4.4.1. Modification of Decomposition Properties of TiH_2

Treating the TiH_2 powders in argon atmosphere by the parameters seen in Table 4.2 produced a broad desorption range, starting to decompose slightly above 400 ^oC and reaching a maximum value slightly below 500 ^oC. Even at the maximum temperature reached in the experiments, 700 ^oC in this study, hydrogen evolution was still being continued.

Table 4.2. Heat treatment parameters of TiH_2 powders

		Treatment Parameters	
		Temperature (^oC)	Time (min)
	(As-received)	n/a	n/a
Heat Treatments	HT1	400	30
	HT2	400	180
	HT3	480	30
	HT4	480	180
	HT5	530	30

The colouration of the powders due to the heat treatment can be seen in Figure 4.12. According to this, the initially grey powder turned olive green during HT1, dark blue during HT2, blue during HT3, turquoise blue during HT4 and HT5 heat treatment conditions. This colouration proves that highest oxidation was occurred during HT4 and HT5 according to Kennedy [12]. Besides, the same colouration of HT4 and HT5 verifies the results of TGA by means of identical decomposition properties.

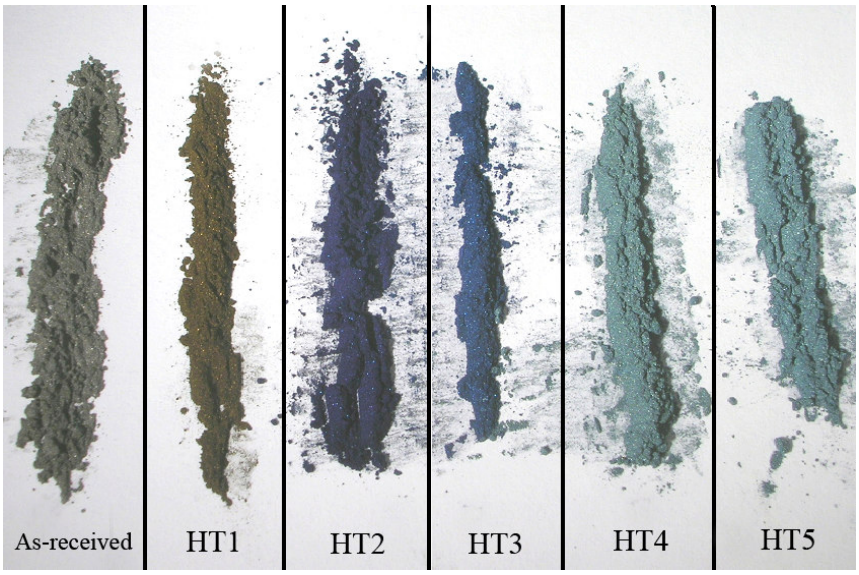

Figure 4.12. Colouration of TiH_2 powders due to heat treatment

As seen in Figure 4.13 the decomposition of the untreated state (as-received) of TiH_2 starts at 400.90 ^{o}C. This result is in good agreement with the relevant studies [12, 13, 57] in the literature. Maximum hydrogen decomposition was occurred at 433.3 ^{o}C and continued distinctively to 529.41 ^{o}C. There was a weight loss of 2.997 % equivalent to 0.4186 mg. Considering that 16 mg of TiH_2 contains 0.65 mg of hydrogen, as-received powders contained 0.5675 mg of hydrogen, and 73% of this hydrogen content was lost when reached to 530 ^{o}C. This means that only 25% of the total TiH_2 attends in cell formation. This result is in consistent with the result of Baumgartner et al. [25].

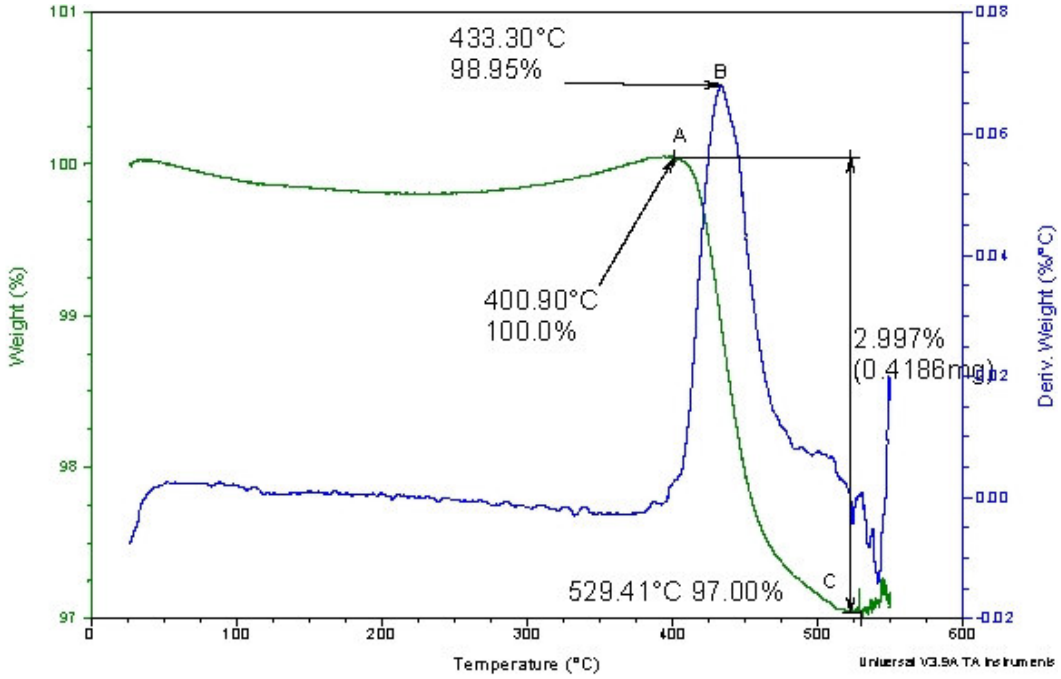

Figure 4.13. TGA curve of as-received (untreated) loose TiH_2 powders.

Considering that the solidus/liquidus interval (582-652 ^oC) of the matrix alloy, it can be said that the decomposition started too early to obtain fully expanded foam. In Figure 4.14 sections of a foam, produced with untreated TiH_2, parallel to (left) and perpendicular to (right) foaming direction powders are seen. At the left a cross-section from the bottom shows that inhomogeneous cell sizes and distribution was obtained. Cell dimensions varied between 1-10 mm which is unacceptable for a high-quality foam. At the left a cross-section from the middle of the foam perpendicular to foaming direction is seen which proves heterogeneous cell distribution and cell coarsening. The sample at the left proves that cells lie along the foaming direction and as a result of using untreated TiH_2 cells having angular forms were formed due to the formation of cracks during the early stages of foaming. Cell coalescence can be seen clearly in the left sample. Since the smaller cells have higher inner gas pressures, during the latest stage of foaming, cells coalesce because of the cell wall rupture. This can be prevented by shifting up the decomposition temperature.

In the heat treatment state HT1, seen in Figure 4.15, the decomposition started at 379.62 ^oC which is a contradiction to the as-received state. This can be due to thermal fluctuation during the analysis or some non-oxidized surface that was left even after heat

treatment. Maximum decomposition occurred at 439.75 ^{o}C which was a little higher than that of untreated state.

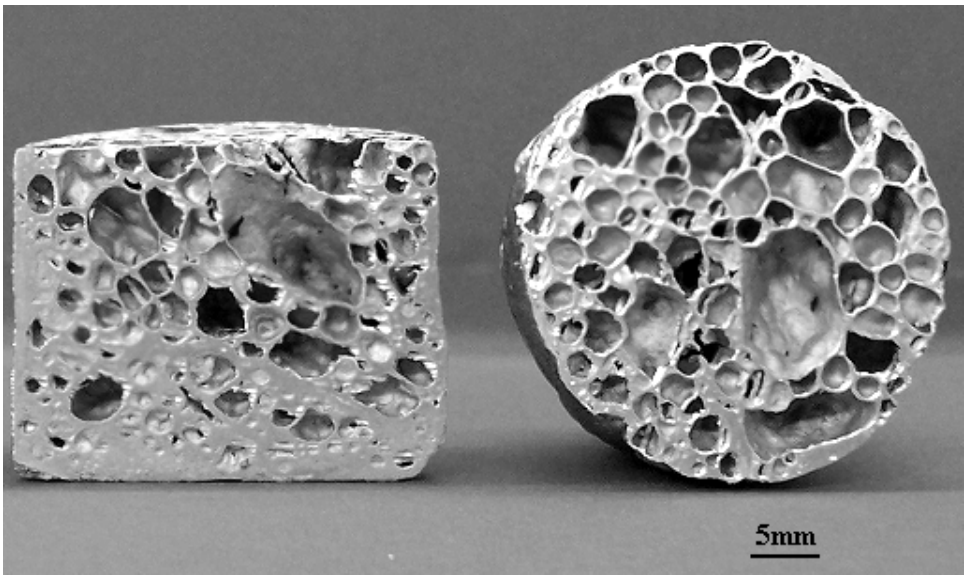

Figure 4.14. Foam morphology of a sample produced with untreated TiH_2 (0.6 wt. %); cross-sections from parallel (left) and perpendicular (right) to foaming direction

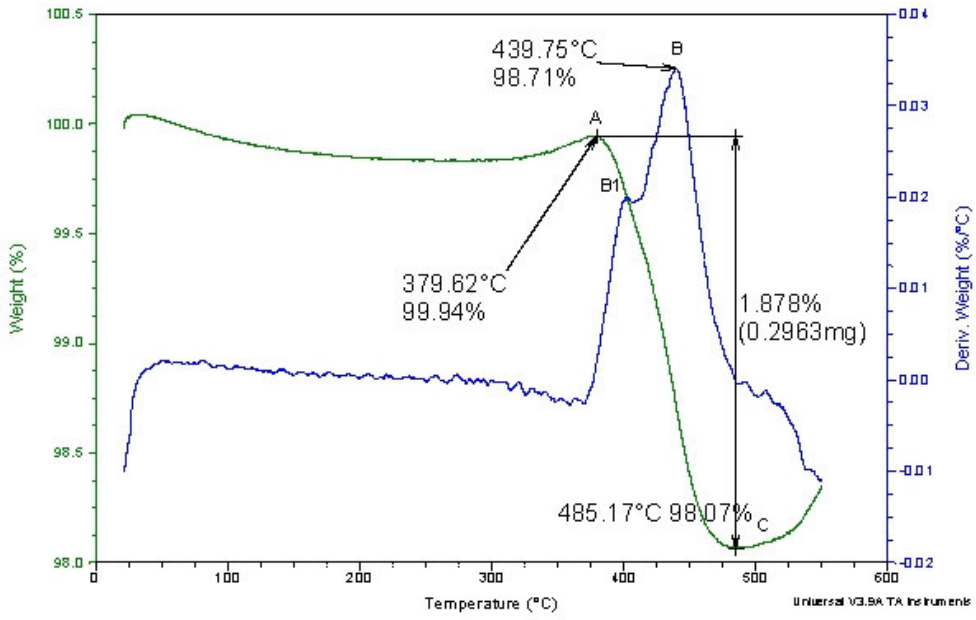

Figure 4.15. TGA of loose TiH_2 powders heat treated at 400 ^{o}C for 30 min. (HT1)

In the heat treatment state HT2, seen in Figure 4.16, decomposition started at 402.31 ^{o}C and maximum decomposition occurred at 444.79 ^{o}C. In HT1 and HT2 decomposition extensively continued to lower temperatures when compared to the untreated state. The two graph shows that the heat treatment at 400 ^{o}C for 30 and 180 minutes have a slight effect on the decomposition characteristics of TiH_2. Considering the hydrogen loss during the treatment, it can be concluded that there is no need to treat the powders at this temperature. As seen from Figure 4.17, HT3 state had a slight effect on the onset of decomposition temperature, however decomposition continued extensively to a higher temperature than HT1 and HT2 treatment states. There is a clear increase in maximum decomposition temperature instead of the onset of decomposition temperature. This can be due to insufficient oxidation of TiH_2 powders.

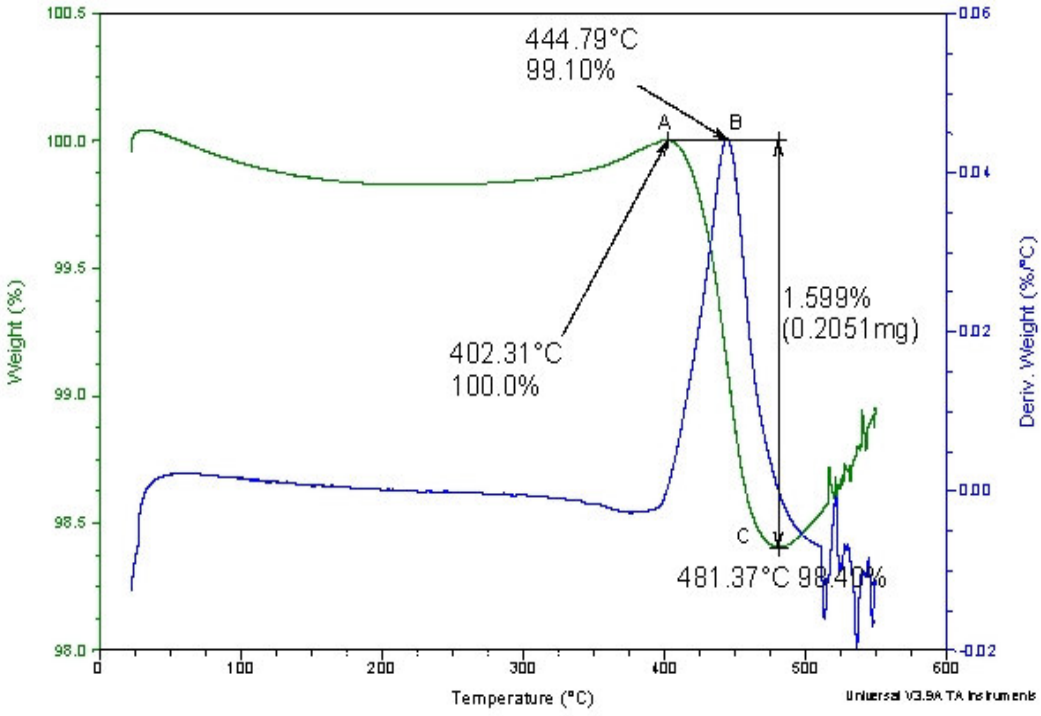

Figure 4.16. TGA of loose TiH_2 powders heat treated at 400 ^{o}C for 180 min. (HT2)

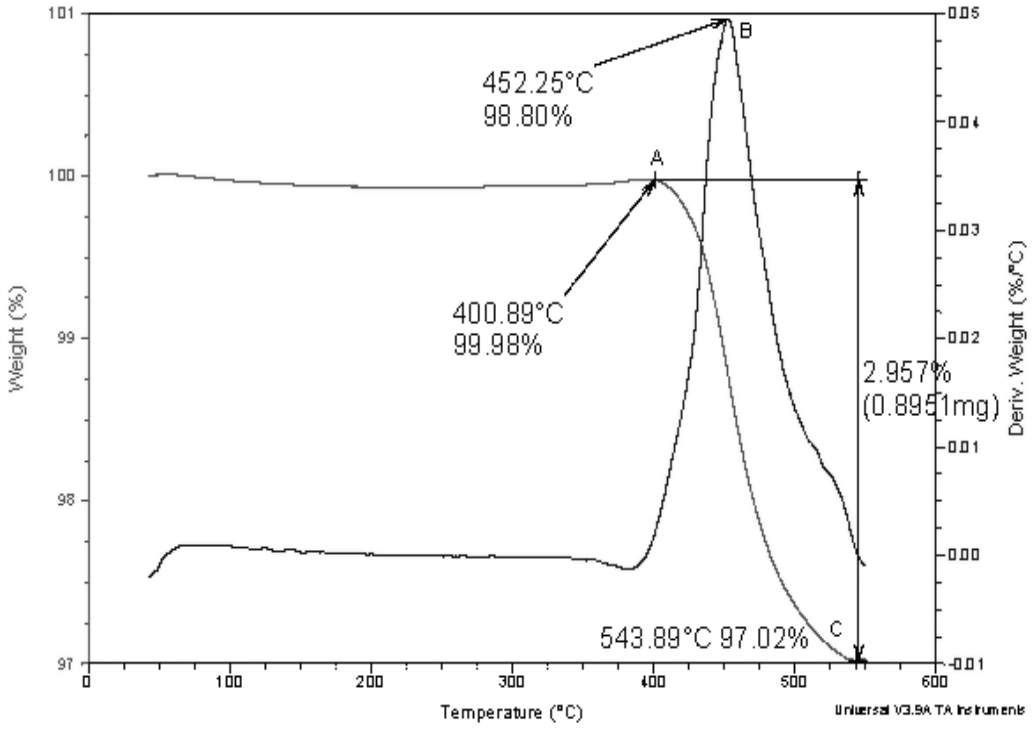

Figure 4.17. TGA of loose TiH_2 powders heat treated at 480 ^oC for 30 min. (HT3)

As seen from the Figure 4.18, it is obvious that both heat treatments at 480 ^oC for 180 minutes and at 530 ^oC for 30 minutes have a great effect on the onset of hydrogen decomposition. In HT4 state, decomposition started at 473.53 ^oC and at 494.66 ^oC maximum decomposition was occurred. The decomposition temperature of the HT5 state was shifted to 466.96 ^oC and maximum gas evolution was seen at 489.04 ^oC. Considering that for optimum densification hot compaction experiments were carried out at 450 ^oC, HT4 and HT5 heat treatments easily satisfied this condition. Thereby hydrogen loss during hot compaction process could be prevented.

As a conclusion, heating the TiH_2 powders at various temperatures shifts not only the onset of decomposition but also the maximum decomposition temperature for about 90 ^oC. Table 4.3 shows that HT1, HT2 and HT3 forms a group while HT4 and HT5 forms another. According to this table, while wt. % weight change decreases, onset of decomposition and maximum decomposition temperature increases from left to right.

Table 4.3. Weight change and decomposition temperatures of different heat treatment states

	As-received	HT2	HT3	HT4	HT5	HT6
Weight Change(wt.%)	2.997 %	1.878 %	1.599 %	2.975 %	1.193 %	1.130 %
Onset of Decomposition (^{o}C)	***400.90***	379.62	402.31	400.89	***473.53***	***466.96***
Maximum Decomposition Temperature	***433.43***	439.86	444.04	452.41	***494.59***	***488.92***

The maximum shift was obtained from the second group, while HT1, HT2 and HT3 treatments do not have any effect on decomposition characteristics; therefore there is no need to carry out these treatments. The delay in hydrogen desorption is beneficial for pore formation since the fraction of liquid present when gas being evolved is higher and corresponding more rounded pores. As untreated powder leads to early decomposition already in solid state, this results in less uniform foam morphology.

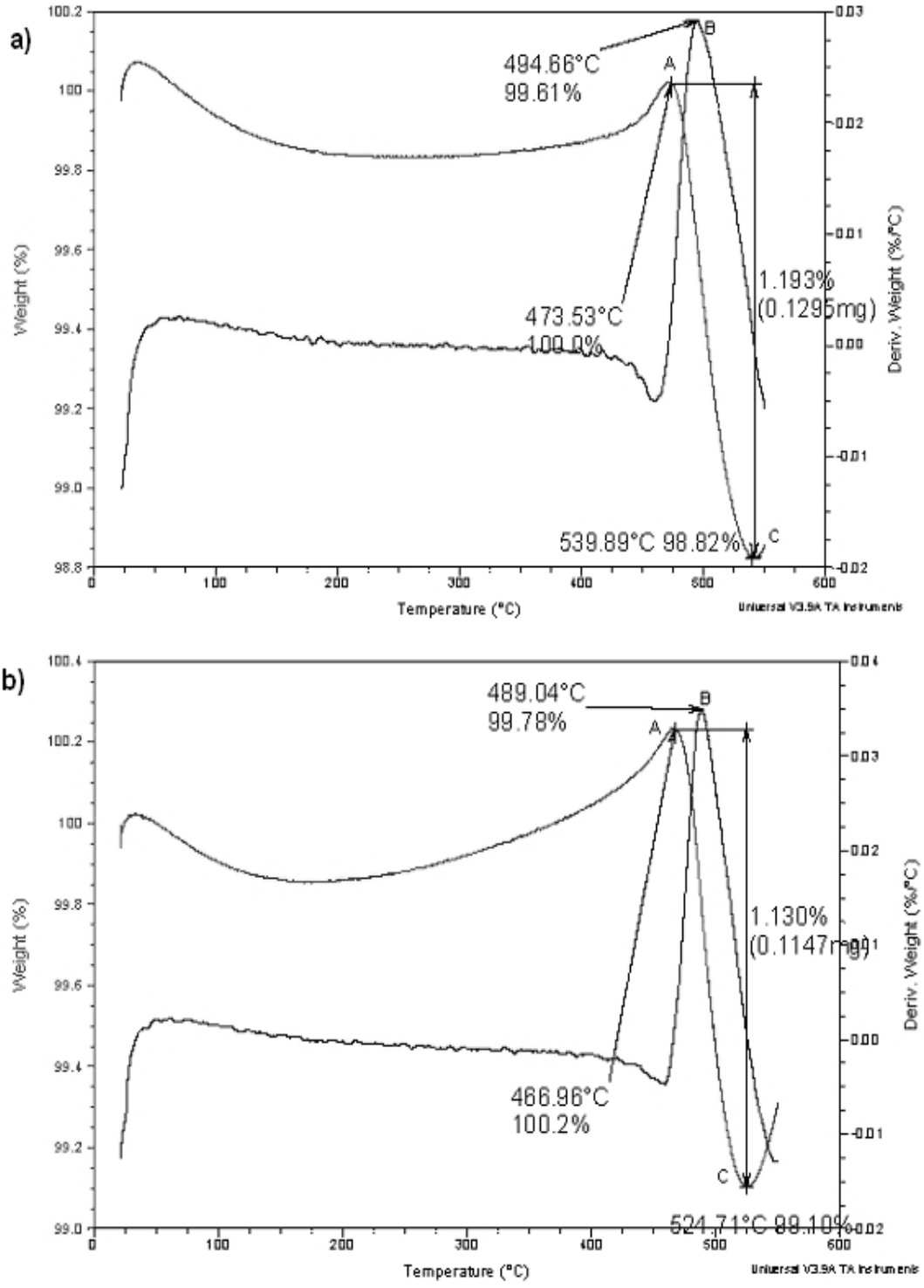

Figure 4.18. TGA of loose TiH_2 powders heat treated; a) at 480 ^oC for 180 min. (HT4) b) at 530 ^oC for 30 min. (HT5)

It should be noted that pores are jagged and more irregular than for the foam blown with TiH_2 powder under HT4 and HT5 conditions. It is clearly seen from Figure. 4.19. that heat treatment of TiH_2 results a shift in decomposition temperature and thereby more rounded cells and homogenous cell distribution can be obtained.

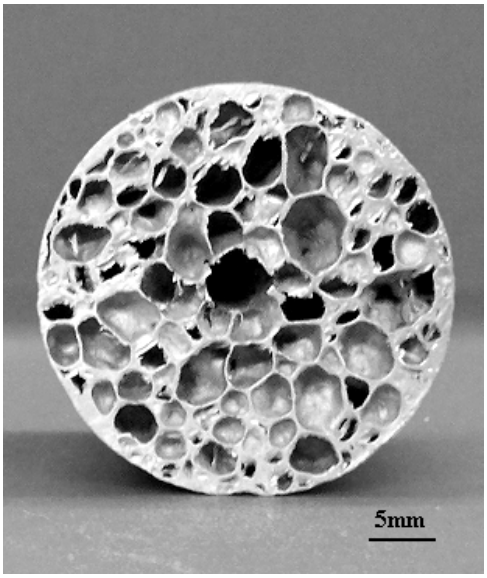

Figure 4.19. Cross-section of a foam produced with heat treated TiH_2 (HT4); foaming temperature was 750 ^{o}C.

In Figure 4.20 a comparison between the samples produced with as-received (a), heat treated at 480 ^{o}C for 30 min (b) and heat treated at 480 ^{o}C for 180 min (c) TiH_2 is seen. All the samples were foamed at 750 ^{o}C for approximately 260 s. It is clear to see that (a) has angular shaped cells due to early decomposition of TiH_2. From the TGA results it can be said that gas evolution started about 400 ^{o}C which resulted cracks inside the precursor. The sample in (b) has more rounded cells than that of (a). This is the result of delay in maximum decomposition temperature which means that the fraction of liquid present when gas starts to evolve is higher and hence molten metallic matrix can accommodate rounded bubbles. In contrast, the sample made using TiH_2 having HT4 conditions exhibit more rounded cells and smooth, non-ruptured and regular cell walls.

As a consequence, different morphologies can be seen between the foams produced with different TiH_2 powders when subjected to various heat treatments. Besides, it was observed that HT4 and HT5 increased the expansion factor of foams. This result can be

seen as a contradiction, since the total amount of hydrogen is reduced by heat treatment. Explanation of this result is that TiH_2 still provides hydrogen in the later stages of foaming.

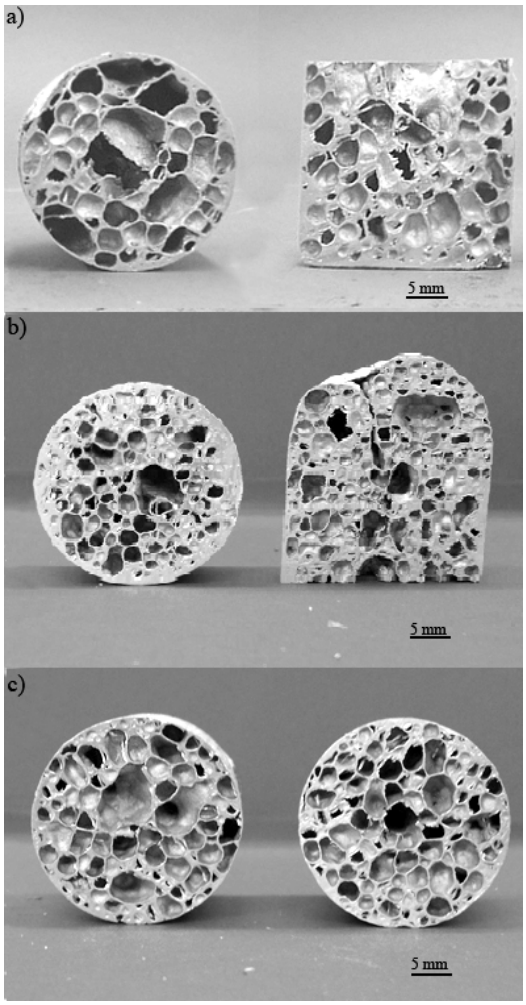

Figure 4.20. Foams produced with (a)as-received TiH_2 (b)heat-treated at 480 ^oC for 30 min. (c)heat-treated at 480 ^oC for 180 min.

In addition to argon atmosphere, thermogravimetric analyses were also conducted in air and nitrogen atmospheres. Figure 4.21 shows the result of thermogravimetric analysis carried out in air. As TiH_2 is very sensible to presence of oxygen, it is obvious that there was a weight gain because of oxidation. Besides, the graph shown in Figure 4.22 represents the analysis conducted in nitrogen atmosphere with a flow rate of 240 ml/min which shows similar behaviour like that of in air. As a conclusion thermogravimetric analysis should not be done in air or nitrogen atmospheres due to oxidation.

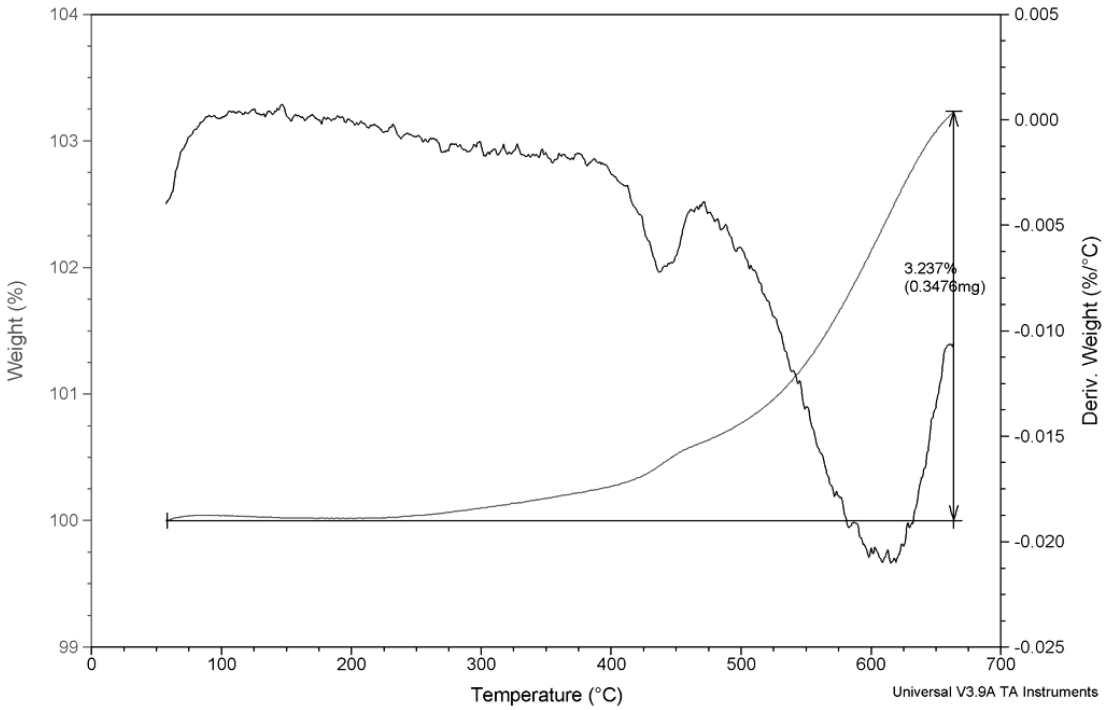

Figure 4.21. Thermogravimetric analysis of TiH_2 conducted in air

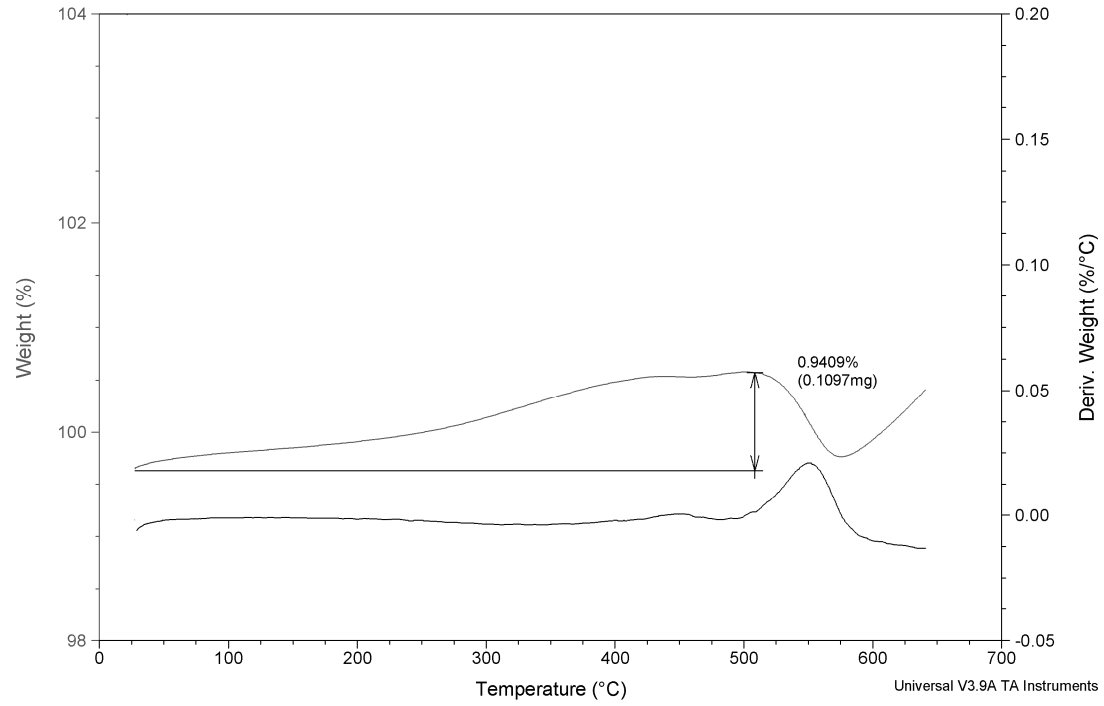

Figure 4.22. Thermogravimetric analysis of TiH_2 conducted in nitrogen with a flow rate of 240 ml/min.

4.4.2. Effect of Al_2O_3 Particles Addition on Foam Morphology

It is thought that the addition of Al_2O_3 particles enhances foam expansion through a reduction in the critical cell wall thickness before rupture of the cell walls. The presence of oxide in the molten powder system tends to prevent good wetting and the ceramic phase is usually located at the cell walls, protruding into the cells. The wetting behaviour prevents drainage of liquid through the cell structure. The wetting effect can be seen from Figure 4.23 that shows a fracture surface of a cell wall of a foam that produced by addition 5 wt.% Al_2O_3. It should be noted that ceramic particles are agglomerated at the cell wall face and embedded into the aluminum matrix which shows a fair wetting of the particles. It is good to have agglomerations on the cell wall face rather than in the cell wall, since if alumina particles were embedded in the cell wall there would be discontinuities that would result low mechanical strength as Kennedy [43] have mentioned.

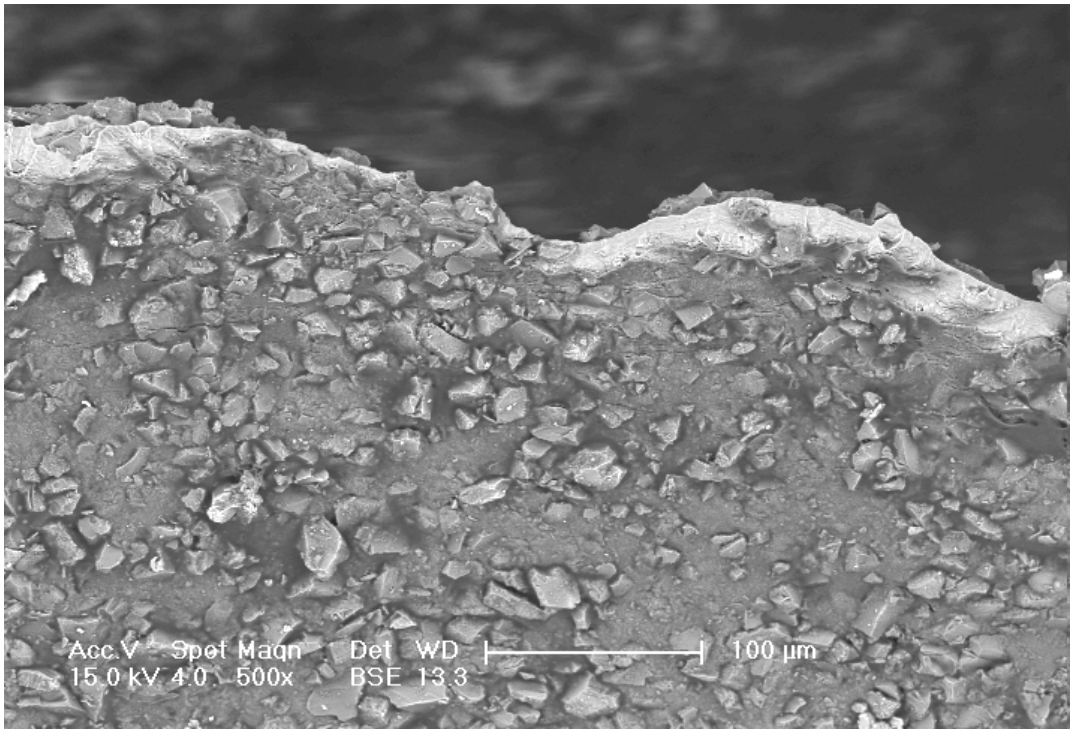

Figure 4.23. SEM image of a fracture of cell wall showing the wetting behaviour of Al_2O_3 particles

Figure 4.24 shows SEM image of a cell wall of a foam produced by Al_2O_3 addition. Note that ceramic particles, dark grey coloured, are embedded into the aluminum matrix,

light grey areas. White particles are oxide compounds of titanium remained from TiH_2. As can be seen in Figure 4.23 for thin walled cells such as to approximately 50-60 μm, while alumina particles are agglomerated on the cell wall faces, for thicker cell walls this situation is changed. In thick cell walls such as approximately 400 μm, alumina particles agglomerate in the cell wall matrix as well as on the cell wall face. This effect provides a structural support to the melted matrix that prevents drainage of the liquid through the plateau regions. By preventing the liquid flow more material is preserved and rupture of the cell wall can be avoided.

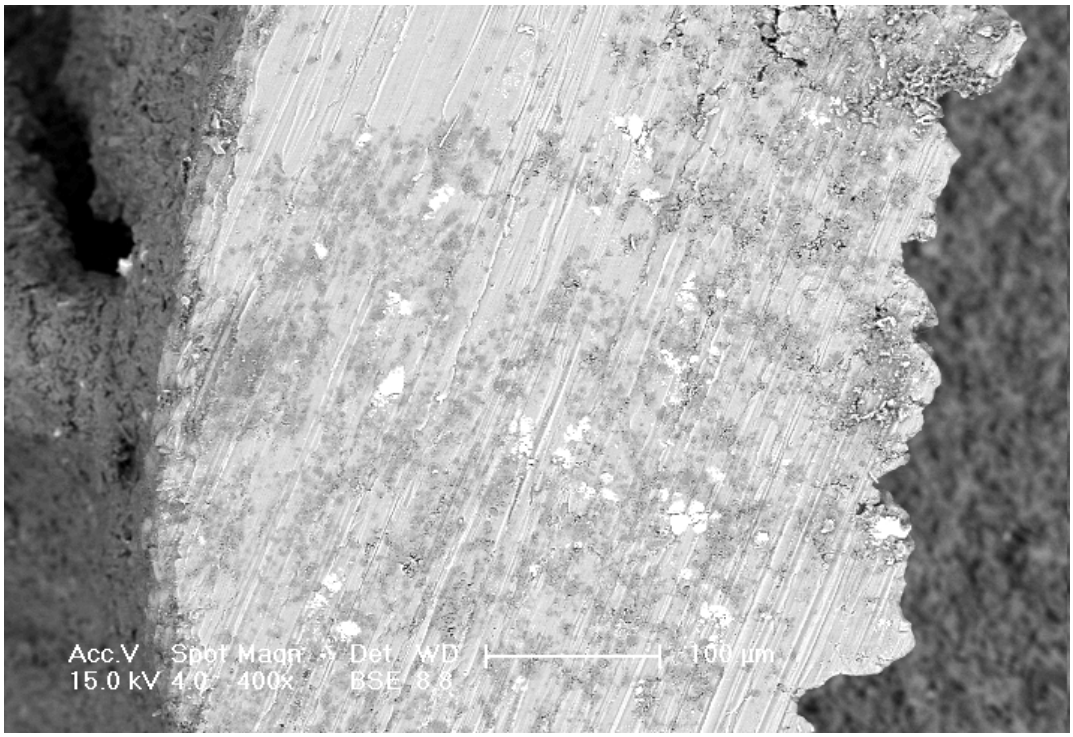

Figure 4.24. Al_2O_3 (<32 μm) particles embedded in a cell wall

In Figure 4.25 two samples produced with and without ceramic addition are seen. Foaming temperature and time was 750 ^oC and 240 s. for both two samples. It is obvious that addition of Al_2O_3 particles lowers the drainage at the bottom and enhances the homogeneity of cell distribution. The sample at left has jagged cells and cell sizes change between approximately 1 and 5 mm. Slight drainage is seen and there are cell coalescences especially at the bottom. These drawbacks were eliminated by alumina addition as seen from the sample at right. Cell size distribution is fairly homogenous with dimensions between 3-4 mm and no cell coalescence or drainage is seen at the bottom of the sample. It

is thought that mechanical support of alumina particles plays role in this enhancement as explained via SEM observations.

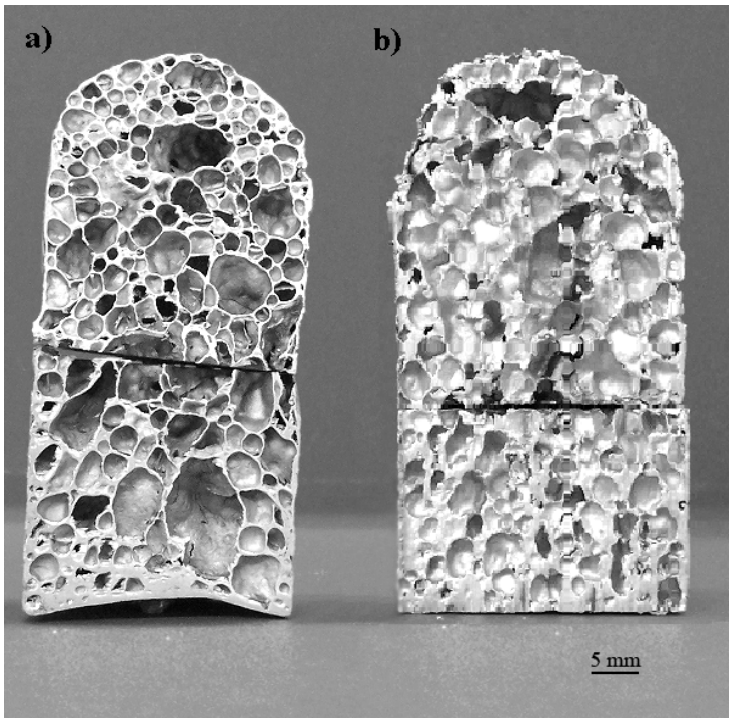

Figure 4.25. Morphology of foams produced without (a) and with (b) Al_2O_3 addition. (foaming temperature: 750 ^oC, foaming time: 240 s.)

On the other hand, it was observed that addition of ceramic particles (Al_2O_3) lowered the optimum foaming temperature. By addition of 5 wt. % Al_2O_3 particles ($<32\,\mu m$) optimum foaming temperature decreased about 10 to 30 ^oC. In Figure 4.26(a) a foam produced without Al_2O_3 addition at 775 ^oC is seen, and in Figure 4.26(b) a foam produced with Al_2O_3 addition at 750 ^oC is seen. Note that, almost the same homogenous morphology was obtained. Besides, it was observed that ceramic addition decreased tendency of drainage. It is believed that, due to partial wetting of ceramic particles by the matrix, particles mechanically support cell walls and plateau region. As a consequence of decreased drainage, more material could be reserved for the top of the foam and thus higher foaming expansion were obtained when compared to ones produced without alumina addition. Also ceramic addition prevents cell collapse especially after taking the foam out of the furnace. It is observed that without particle addition top of the foams tend

to collapse since liquid melt flows down due to gravity. Ceramic addition is thought to prevent this effect which stabilize the foam structure and enable a good foam structure.

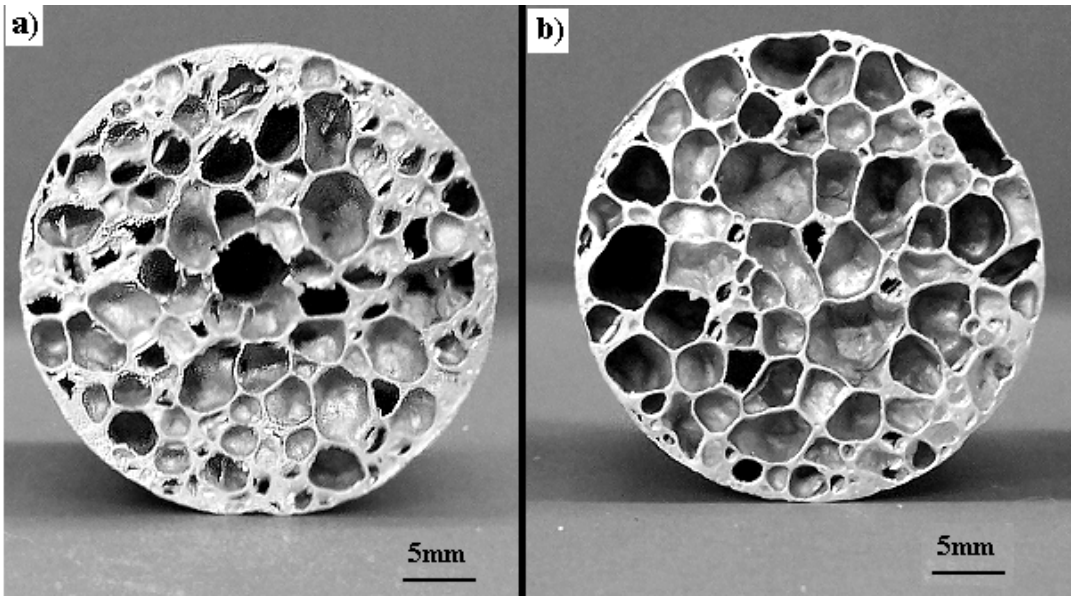

Figure 4.26. Foam produced with heat treated 0.6 wt.% TiH_2 (HT4) with (a), and without (b) alumina addition; foaming temperatures for (a) 750 ^oC, for (b) 775 ^oC.

4.5. Compression Behaviour of Aluminum Foams

In all the compression tests, plastic collapse of the foam cells initiated from the middle of the samples, and as the compression continued the deformation and collapse of the foam cells propagated layer by layer in the direction of compression. Two different types of failure modes exist for aluminum foams, which are brittle and ductile modes. In brittle mode, after elastic region a drop in stress occurs followed by densification and increase in stress. On the other hand, ductile mode assumes a smooth and steadily rising stress [20]. It was observed that untreated and SHT/aged foams failed according to brittle mode while annealed foams failed according to ductile mode. It was observed that the change in lateral thickness of the samples at small deformation was negligible, so the assumption that the Poisson's ratio was nearly zero [49] was confirmed by the compression tests.

In Figures 4.27-29 focused views of load-displacement curves at 5 mm displacement are seen. Figure 4.27 shows load-displacement curve of untreated foams at 5mm displacement. Load increased up to 3.85 kN with the increasing compression until the elastic region and then a drop in load was seen while the displacement was being continued. After the drop, as the displacement increased load kept on increasing and formed a plateau region in which the slope was lower than that of elastic region. Therefore, the curve in Figure 4.28 represents typically a brittle foam failure.

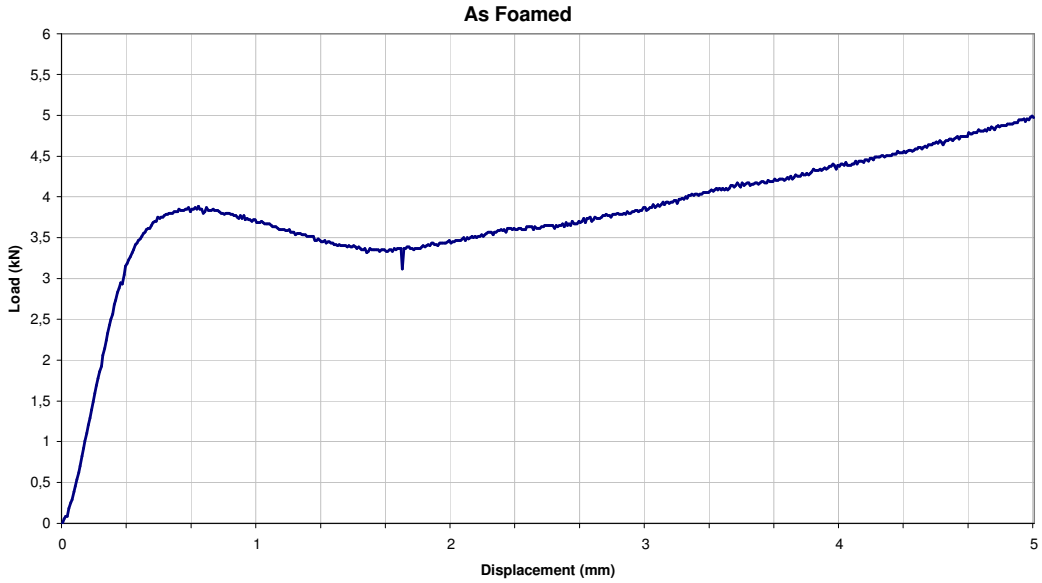

Figure 4.27. Average load-displacement curve of as-foamed specimens at 5mm.

In contrast to As-foamed and SHT/Aged foams, annealed foams showed ductile behaviour as shown in Figure 4.29. There was no peak after elastic region which generally followed by a drop in load. It is thought that in annealed foams failure was controlled by bending rather than braking of cell walls and struts, since the foam did not fragment into pieces during the compression tests, while both as foamed and SHT/aged foams broke up into fragments during the tests. In Figure 4.30 compressed samples up to 80% strain are seen. The way of compression of the samples verify the failure modes that as-foamed and SHT/aged samples failed according to brittle model, while annealed failed according to ductile mode.

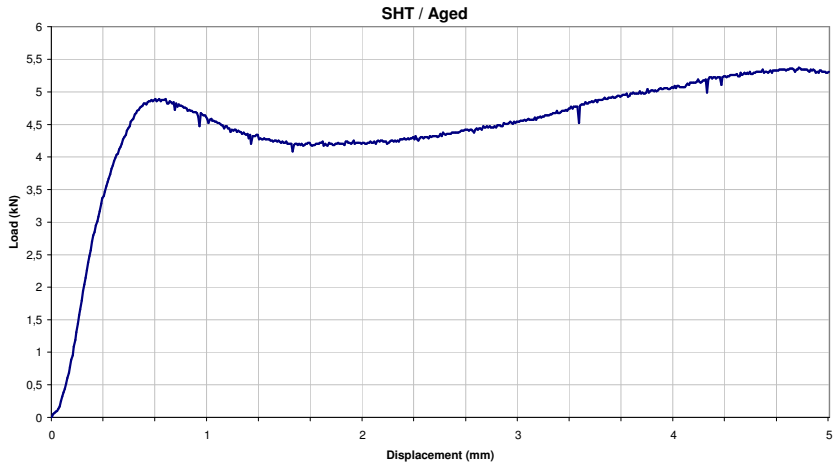

Figure 4.28. Average load-displacement curve of SHT and aged specimens at 5mm.

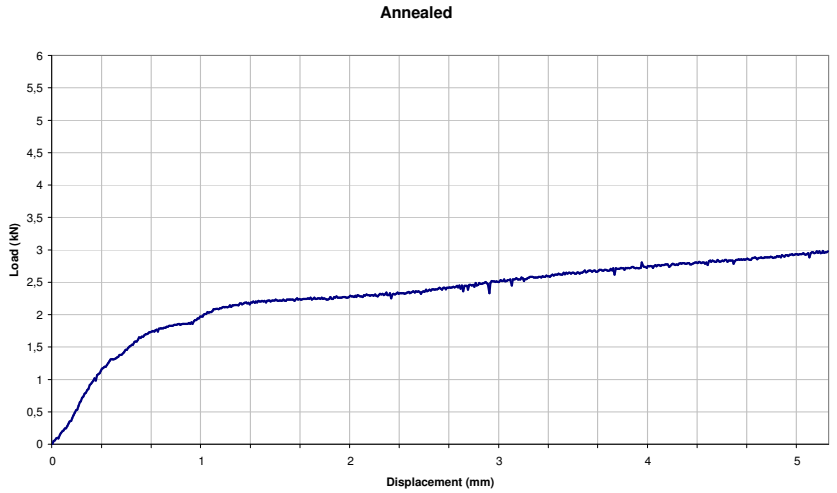

Figure 4.29. Average load-displacement curve of annealed specimens at 5mm.

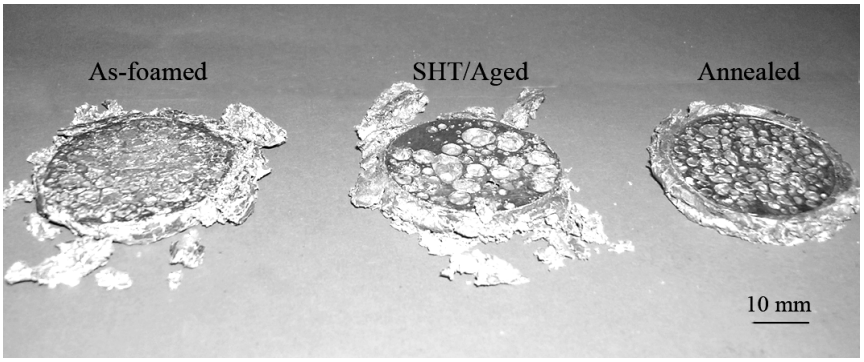

Figure 4.30. Failure behaviour of samples compressed at 80% strain

Densifications of the cells occurred at this stage and then load increases that would form the region called as “plateau region” which can be seen clearly in Figures 4.31-33. The stress value at 20 mm displacement was accepted as the densification stress. Stress values were calculated as engineering stresses since the Poisson’s ratio for foams is nearly zero. This compression behaviour is typical for metallic foams. Beyond the plateau region, at larger strains cell walls consolidate with each other and the foam densifies revealed by an exponential increase in stress.

The average yield stresses of the untreated, SHT/Aged and annealed foams were found to be 5.46, 6.91 and 3.05 MPa, respectively. This result confirms the effect of heat treatments on the compressive behaviour of aluminum foams. Solution heat treatment and ageing provided a gain of 27% in strength when compared to untreated state. On the other hand, as expected annealed foams showed ductile behaviour and therefore low strength values. As can be seen from Figures 4.31-33, the area under the curve, which represents the energy absorption capacity, is highest for that of SHT and aged foams, and lowest for the annealed foams. As the reason for utilizing aluminum foams in energy dissipating systems is the large area under their load-displacement curve, it can be concluded that energy absorption capacity of the AA6061 foams can be increased via solution heat treatment and ageing. Yield stress and plateau stresses for as foamed foams were found to be 5.46 MPa and 12.16 MPa respectively. Densification, which represented collapse of cells and end of the plateau region, started at 27.08 MPa.

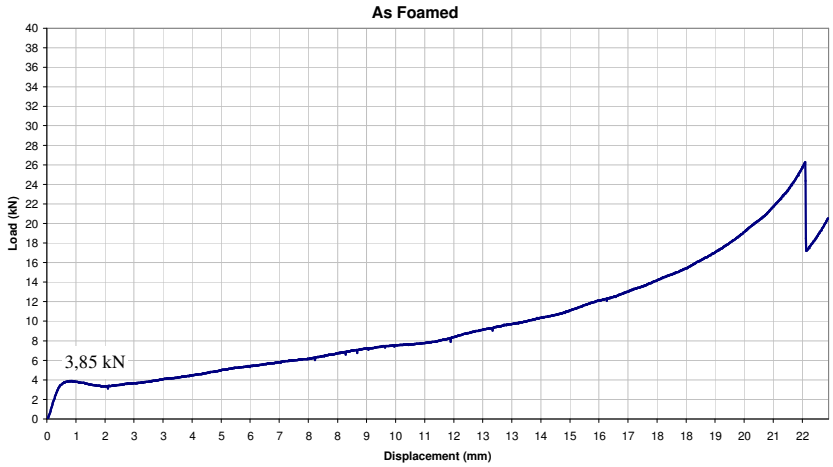

Figure 4.31. Average load-displacement curve of untreated foams.

For the SHT/Aged foams yield and plateau stresses were found to be 6.91 and 13.42 MPa, respectively. In contrast to this, annealed foams exhibited lower values as 3.05 and 7.27 MPa respectively. Densification strengths were 21.22 and 16.38 MPa for SHT and annealed foams.

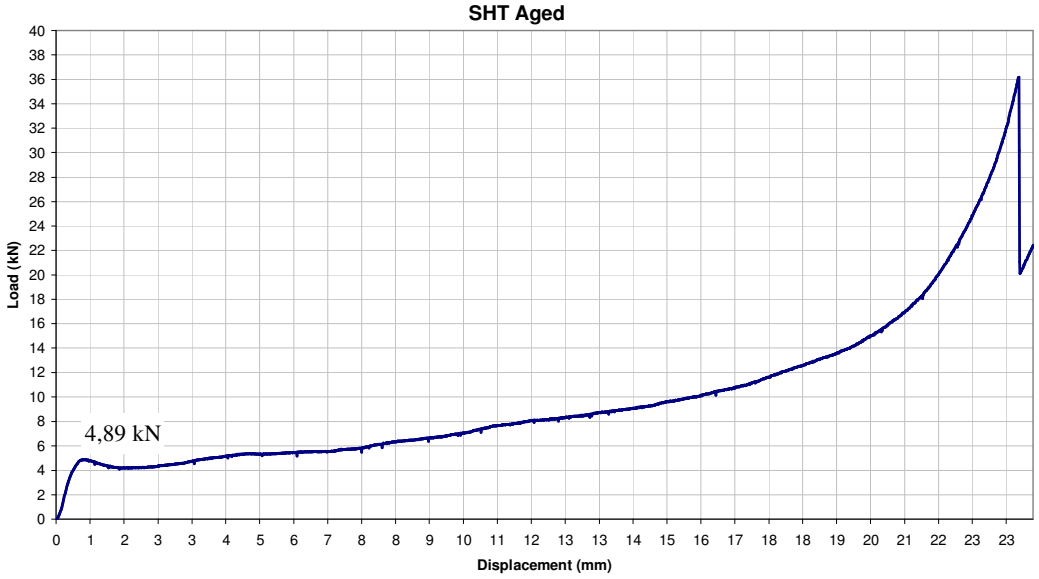

Figure 4.32. Average load-displacement curve of SHT/aged foams.

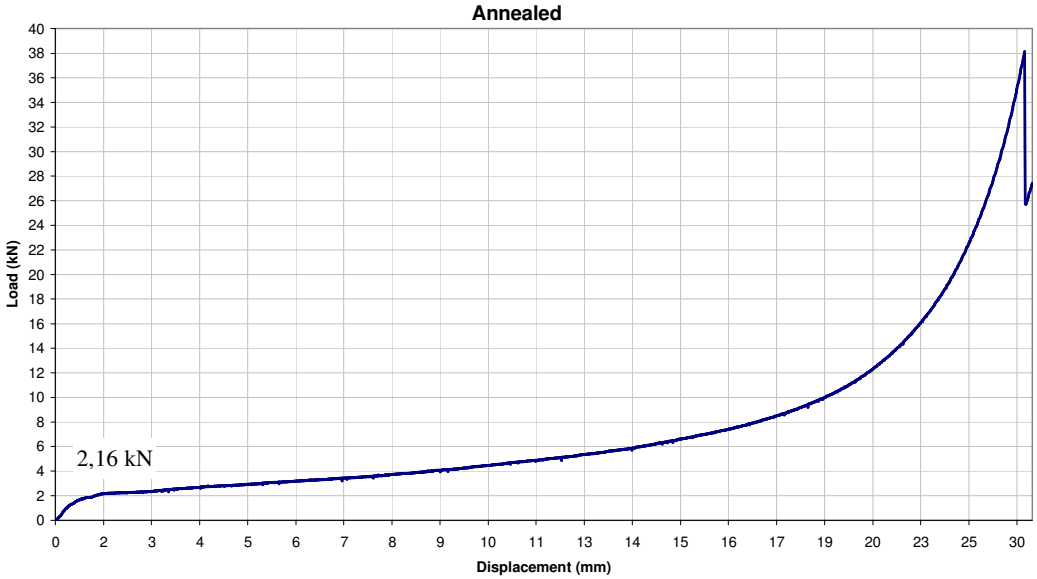

Figure 4.33. Average load-displacement curve of annealed foams.

Table 4.4. Comparison of effect of heat treatments on strength values

	As Foamed	SHT/Aged	Annealed
Yield Stress (MPa)	5.46	6.91	3.05
Plateau Stress (MPa)	12.16	13.42	7.27
Densification Stress (MPa)	27.08	21.22	16.38

4.6. SEM Observations of Precipitated Phases

The differences between the heat treated and as-foamed samples comes from precipitation of phases. In Figure 4.34 a SEM image of grain boundaries of an untreated foam is shown. The image was obtained from inner section of the sample which means a lower cooling rate was occurred in this area. As in consistence with the literature, the sample without any heat treatment is dominated by precipitates in which, by means of EDAX analysis, AlFeSi phases could be identified. White areas represent the precipitations of AlFeSi phases, which are confirmed by EDAX analysis shown in Table 4.5. It was observed that the concentration of precipitations was strong than that of at the cell edge, since the cooling rate was much higher at the cell edge than in the inner sections of the foam. Strong precipitations at the inner section of the foam are thought to be the reason of lower strength values when compared to SHT and aged foams.

Table 4.5. EDAX analysis of precipitated elements at the grain boundaries of the untreated sample

Element	Wt%	Z	A	F
AlK	73,0000	1,0152	0,8214	1,0015
SiK	7,6400	1,0444	0,4938	1,0002
FeK	19,3600	0,9113	0,9943	1,0000
Total	100,0000			

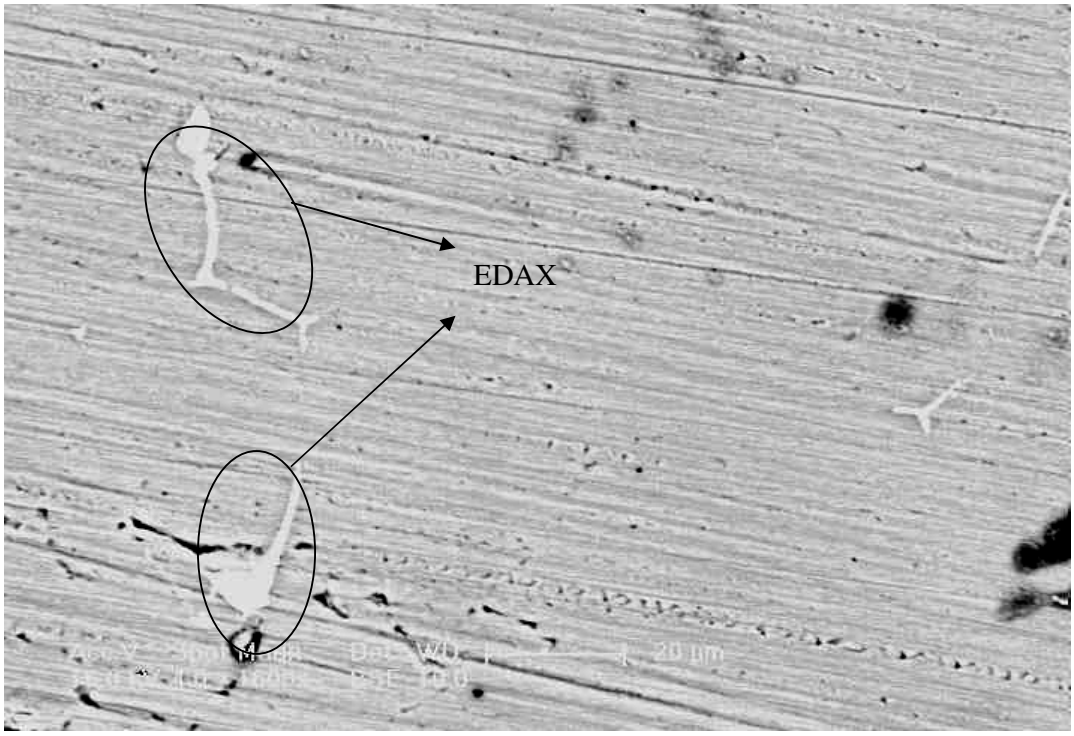

Figure 4.34. SEM image of precipitations at the grain boundaries of an untreated foam.

In Figure 4.35 a SEM image of a cell wall edge is seen. Note that higher concentration of precipitations is observed when compared to the one in Figure 4.34 above. According to the EDAX analysis AlFeSi phases, seen as white areas, were formed at the grain boundaries. Note that at the very edge of the sample, due to higher cooling rates no precipitation was observed. This effect can easily be seen from Figure 4.36. The SEM image was taken from the outer region of the foam, in which the highest cooling rates was seen. No precipitation was observed at the grain boundaries and the black areas could be precipitation free zones as Epler [44] mentioned which could be due to lack of silicon.

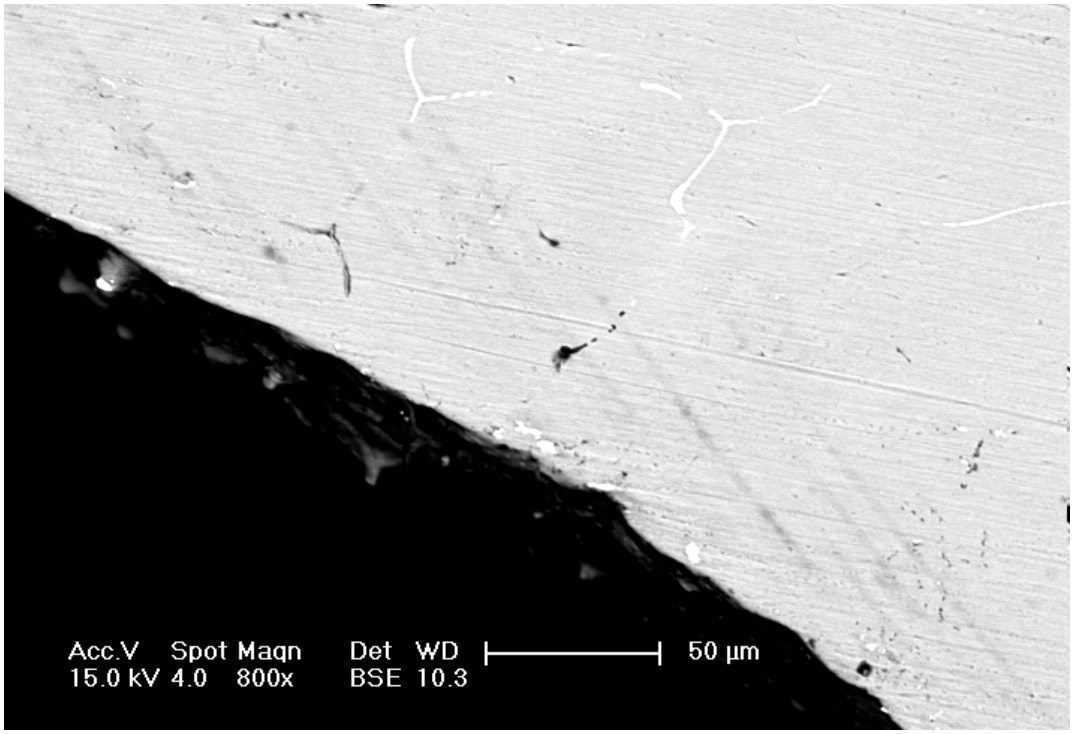

Figure 4.35. SEM image of precipitations at the grain boundaries of an untreated foam.

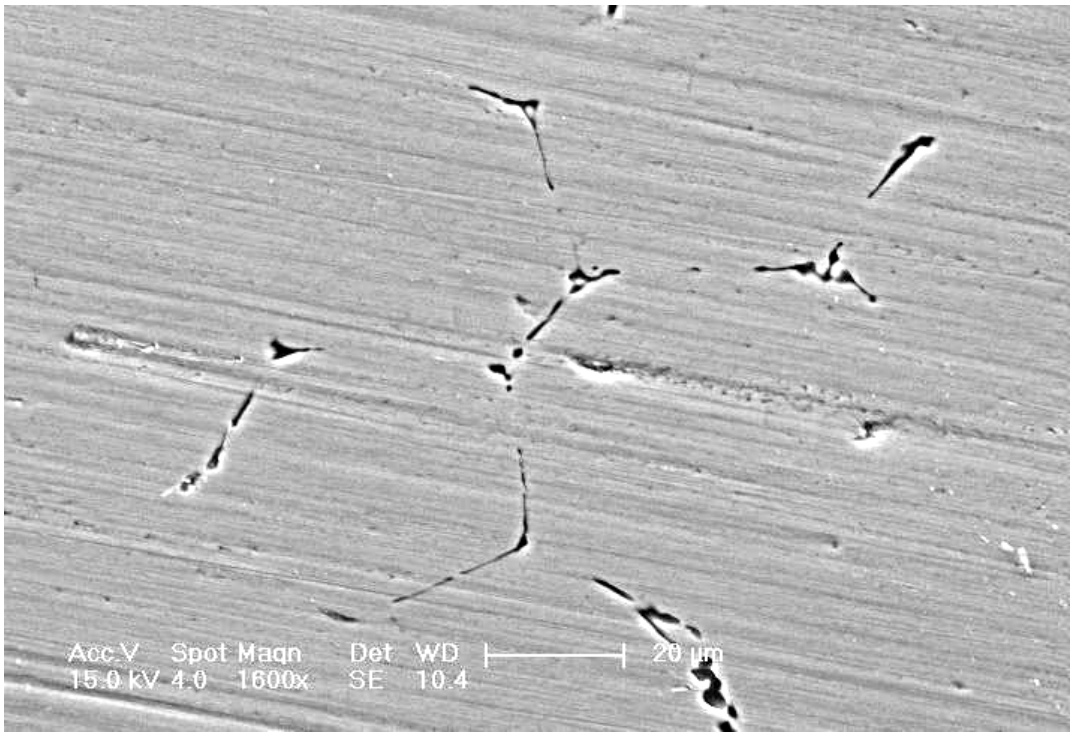

Figure 4.36. SEM image of grain boundaries at the outer region of the foam

As seen from Figures 4.37-38, the solution heat treated and aged foams have a lower precipitate density and grain boundaries can not be visible. The result of EDAX analysis, seen in Table 4.6, proves lower precipitations when compared to untreated and annealed foams. The phases found in the grain boundaries are similar to those found in the untreated (as foamed) state that shows a complete solution of Mg_2Si phases was not achieved during solution heat treatment. This may depend on low quenching rates. However, as the concentration of these precipitates is lower compared to the untreated samples, it can be assumed that a part of the alloying elements could have formed strength increasing GP-zones.

Table 4.6. EDAX analysis of precipitations at the grain boundaries of the SHT and aged foam

Element	Wt%	Z	A	F
MgK	1,6400	1,0305	0,9506	1,0521
AlK	97,7400	0,9993	0,9798	1,0001

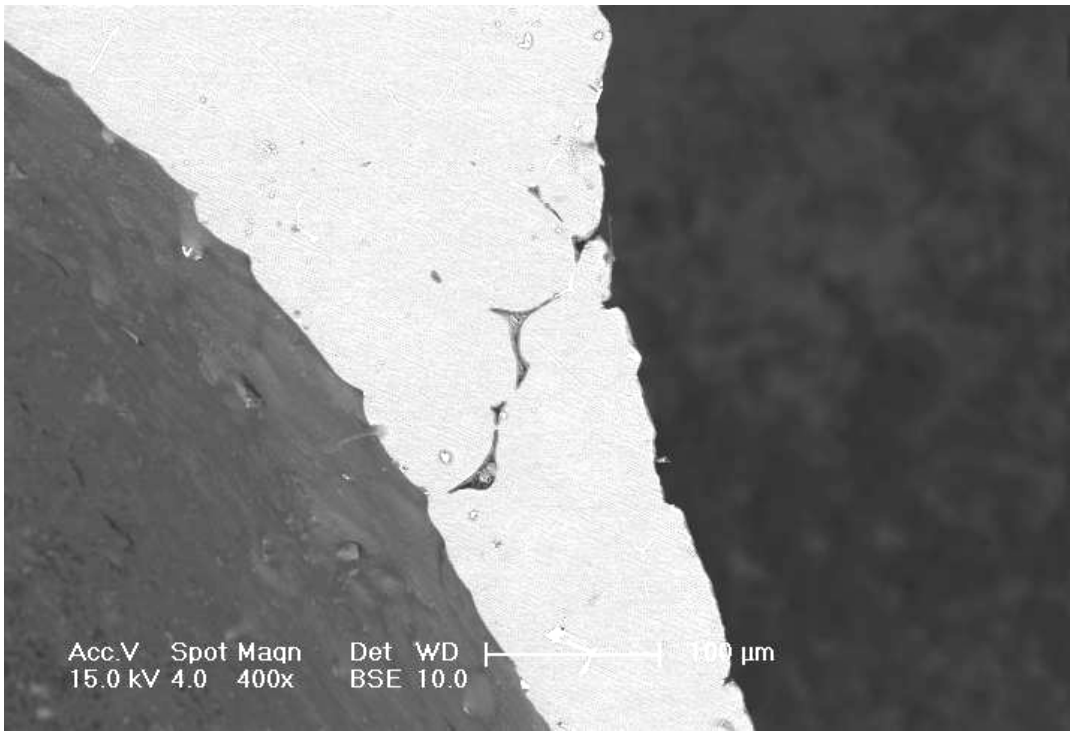

Figure 4.37. A cell wall image of an SHT/Aged foam.

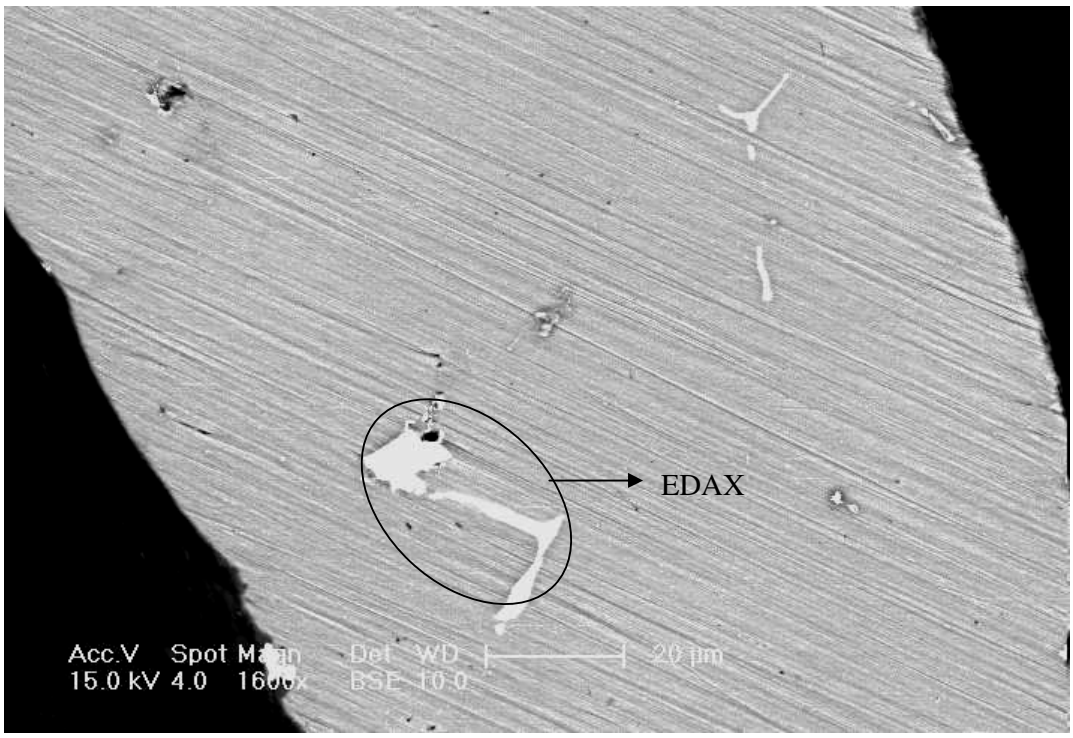

Figure 4.38. SEM image of precipitations of an SHT/Aged foam.

In contrast to SHT and aged samples, annealed foams have different microstructure in which Mg_2Si equilibrium precipitates increased in size and volume fraction. EDAX analysis of the grain boundary precipitations confirms this result as seen from Table 4.7 and Table 4.8. The decreased matrix strength can be associated to formation of Mg_2Si along the grain boundaries.

Table 4.7. EDAX analysis of grain boundary precipitations in annealed foam

Element	Wt%	Z	A	F
MgK	3,3900	1,0340	0,8604	1,0323
AlK	85,3400	1,0032	0,8971	1,0009
SiK	4,8500	1,0306	0,4721	1,0000
FeK	6,4200	0,8991	0,9938	1,0000
Total	100,0000			

In Figure 4.39, at the grain boundaries, seen as light grey areas, AlFeSi intermetallics were formed. Besides, at the needle shaped areas precipitation of Mg and Al elements

confirmed by EDAX analysis seen from Table 4.8. The needle-shaped precipitations were located at or near the grain boundaries. This needle like precipitation areas are thought to be the reason of relatively low strength.

Table 4.8. EDAX analysis of needle shaped precipitations in annealed foam

Element	Wt%	Z	A	F
MgK	3,2100	1,0302	0,9519	1,0485
AlK	96,7900	0,9990	0,9615	1,0000
Total	100,0000			

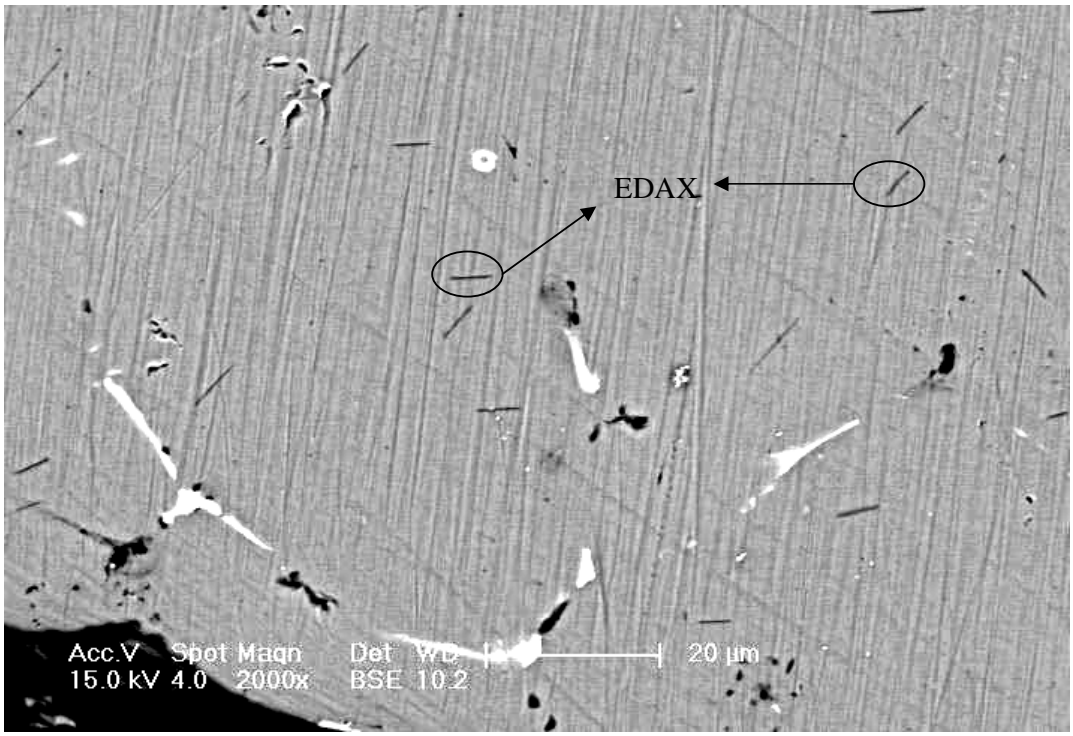

Figure 4.39. SEM image of the needle-shaped precipitations of annealed foam[45]

5. CONCLUSIONS

Aluminum foams have gained a considerable amount of attention in recent years with their very low specific weight, relatively high compression strength among cellular metals combined with good energy absorption. In the course of this thesis, effects of process parameters on foam morphology were investigated. First of all, it was obvious to see that during the mixing stage agglomerations of powders should be avoided in order to obtain a homogenous mixture. Foaming experiments showed that 0.6 wt.% of TiH_2 was fairly sufficient to obtain highly porous structure. This is important as a commercial point of view, since TiH_2 is a relatively expensive material.

The aim of compaction of powder mixture was to obtain foamable precursor with a density close to theoretical density of aluminum matrix. Compaction experiments were done at various temperatures, time and pressure, 400-450 ^oC, 15-30 min and 270-400 MPa, respectively. It was found that compaction of the powder mixture by primarily cold pressing and subsequently hot pressing under 270 MPa at 450 ^oC for 30 minutes resulted in optimum densification. In this way, production of precursors having no residual open porosity was achieved.

Foaming trials of the precursors were carried out in a foaming mould at temperatures between 700 and 800 ^oC. It was found that for AA6061 used in this study, foaming temperature should be between 750 and 775 ^oC. As TiH_2 starts hydrogen decomposition at about 400 ^oC, it was seen that high heating rates are necessary in order not to let hydrogen escape during the early stages of foaming. In the foaming experiments it is thought that heating rates close to 100 ^oC/min were reached which were fairly sufficient as Baumgartner et al. [25] claimed.

Enhancements of foam morphology were investigated by means of modifying the decomposition properties of TiH_2 powders and addition of 5 wt.% Al_2O_3 with a size of 500 mesh ($<32\,\mu m$). In order to shift the decomposition temperature, heat treatments of TiH_2 were performed between 400 and 530 ^oC for 30 and 180 minutes. The results of TGA showed that with a heat treatment of 480 ^oC for 180 minutes it was possible to retard the

onset of decomposition temperature by 75 ^{o}C, which was about 400 ^{o}C for the as-received TiH_2 powders. Besides, maximum decomposition temperature was shifted to 495 ^{o}C which was 430 ^{o}C for as-received TiH_2. It can be concluded that foams with more rounded and uniform cells could be produced by using heat treated TiH_2. In addition to that, addition of 5 wt.% Al_2O_3 was found to lower the optimum foaming temperature about 25 ^{o}C and prevented drainage and cell coarsening by stabilizing the foam structure. SEM observations showed that Al_2O_3 particles were wetted partially by the aluminum matrix and intensively concentrated on the cell walls which proved the mechanical support by the ceramic particles.

As AA6061 is an heat treatable alloy, where strengthening can be increased by precipitation hardening, aluminum foams were subjected to heat treatments by means of SHT followed by ageing and annealing. The result of compression tests at a speed of 5 mm/min. showed that as-foamed and SHT/Aged aluminum foams failed according to brittle manner while annealed foams failed in a ductile manner. The yield strength and plateau stress values were 5.46-12.16 MPa for as-foamed, 6.91-13.42 MPa for SHT/Aged and 3.05-7.27 MPa for annealed specimens, respectively. These results showed that SHT/Aged foams could be used in energy absorption applications rather than annealed foams.

6. FUTURE WORK

As a further study, effect of SiC and other ceramic particles addition on cell morphology and wetting behaviour of these particles can be investigated. TGA can be carried out at higher temperatures such as 800 ^{o}C and evolved hydrogen before, during and after the solidus-liquidus temperature interval of the metal matrix can be analyzed more precisely. Quenching of the foams after SHT can be done more rapidly in order to obtain supersaturated regions for fully hardened state.

A relation between foam density and Young's modulus can be investigated. In order to yield Young's modulus, compression tests have to be done as loading and unloading order, since it was seen that loading curves yielded inaccurate values. Effects of surface chemistry on interface reactions can also be investigated.

Various sizes of TiH_2 and aluminum powders can be used in order to assess the effects of powder sizes on foaming behaviour.

REFERENCES

1. U.S. Pat. 4,713,277 (December 15, 1987), Akiyama, S., U. Hidetoshi, K. Imagawa, A. Kitahara, S. Nagata, K. Morimoto, T. Nishikawa, and M. Itoh.

2. U.S. Pat. 5,151,246 (September 29, 1992), Baumeister, J. and H. Schrader.

3. U.S. Pat. 5,865,237 (February 2, 1999), Schorghuber, F., F. Simancik, and E. Hartl.

4. U.S. Pat. 6,391,250 (May 21, 2002), Wolfsgruber, E., H. Worz, and F. Simancik.

5. U.S. Pat. 6,464,933 (October 15, 2002), Popoola, O. O., R. Jahn, and R. C. McCune.

6. U.S. Pat. 6,524,522 (February 25, 2003), Vaidyanathan, K. R., J. L. Lombardi, J. Walish, and R. A. Cipriani.

7. U.S. Pat. 3,087,807 (April 30, 1963), Allen, B. C., M. W. Mote, and A. M. Sabroff.

8. Banhart, J., "Metal Foams: The Mystery of Stabilization", 2005 .

9. Banhart, J., "Manufacture, Characterization and Application of Cellular Metals and Metal Foams", *Progress in Materials Science*, Vol.46, pp.559-632, 2001.

10. Babcsan, N., J. Banhart, and D. Leitmelet, *Metal Foams – Manufacture and Physics of Foaming*, 2005.

11. Miyoshi, T., M. Itoh, S. Akiyama, and A. Kitahara, "ALPORAS Aluminium Foam: Production Process, Properties, and Applications", *Advanced Engineering Materials*, Vol.2, No.4, pp.179-184, 2000.

12. Kennedy, A. R., "The Effect of TiH_2 Heat Treatment on Gas Release and Foaming in Al-TiH_2 Preforms", *Scripta Materialia*, Vol.47, pp.763-767, 2002.

13. Zeppelin, F. v., M. Hirscher, H. Stanzick, and J. Banhart, "Desorption of Hydrogen from Blowing Agents Used for Foaming Metals", *Composite Science and Technology*, Vol.63, pp.2293-2300, 2003.

14. Duarte, I. and J. Banhart, "A Study of Aluminium Foam Formation - Kinetics and Microstructure", *Acta Materialia*, Vol.48, pp.2349-2362, 2000.

15. Fusheng, H., W. Jianning, C. Hefa, and G. Junchang, "Effects of Process Parameters and Alloy Compositions on Pore Structure of Foamed Aluminum", *Journal of Materials Processing Technology*, Vol.138, pp.505-507, 2003.

16. Matijasevic, B. and J. Banhart, "Improvement of Aluminium Foam Technology by Tailoring of Blowing Agent", *Scripta Materialia*, Vol.54, pp.503-508, 2006.

17. Kennedy, A. R., "Effect of Foaming Configuration on Expansion", *Journal of Materials Science*, Vol.39, pp.1143-1145, 2004.

18. Körner, C., F. Berger, M. Arnold, C. Stadelmann, and R. F. Singer, "Influence of Processing Conditions on Morphology of Metal Foams Produced from Metal Powder", *Materials Science and Technology*, Vol.16, No.7/8, pp.781-784, 2000.

19. Chen, S. P., K. M. Mussert, and S. V. D. Zwaag, "Precipitation Kinetics in Al6061 and in an Al6061-alumina Particle Composite", *Journal of Materials Science*, Vol.22, pp.4477-4483, 1998.

20. Lehmhus, D., J. Banhart, and M. A. Rodriguez-Perez, "Adaptation of Aluninum Foam Properties by Means of precipitation Hardening", *Materials Science and Technology*, Vol.18, pp.1-6, 2002.

21. Kitazono, K., E. Sato, and K. Kuribayashi, "Novel Manufacturing Process of Closed-Cell Aluminum Foam by Accumulative Roll-Bonding", *Scripta Materialia*, Vol.50, pp.495-498, 2004.

22. Claar, T. D., C.-J. Yu, I. Hall, J. Banhart, J. Baumeister, and W. Seeliger, "Ultra-Lightweight Aluminum Foam Materials for Automotive Applications", *SAE*, pp.1-9, 2000.

23. Matijasevic-Lux, B., A. Rack, A. Heibel, and J. Banhart, "Influence of Powder Pre-Treatments on Metal Foam Pore Structure", Cellular Metals and Polymers 2004, 2004.

24. Kennedy, A. R. and V. H. Lopez, "The Decomposition Behavior of As-Received and Oxidized TiH_2 Foaming-Agent Powder", *Materials Science and Engineering A*, Vol.357, pp.258-263, 2003.

25. Baumgartner, F., I. Duarte, and J. Banhart, "Industrialization of Powder Compact Foaming Process", *Advanced Engineering Materials*, Vol.2, No.4, pp.168-174, 2000.

26. Lehmhus, D. and J. Banhart, "Properties of Heat-treated Aluminium Foams", *Materials Science and Engineering A*, Vol.349, pp.98-110, 2003.

27. Ashby, M. F., A. G. Evans, N. A. Fleck, L. J. Gibson, J. W. Hutchinson, and H. N. G. Wadley, *Metal Foams: A Design Guide*. Butterworth-Heinemann, 2000.

28. U.S. Pat. 5,112,697 (May 12, 1992), Jin, I., L. D. Kenny, and H. Sang.

29. Simone, A. E. and L. J. Gibson, "Aluminum Foams Produced by Liquid-State Processes", *Acta Materialia*, Vol.46, No.9, pp.3109-3124, 1998.

30. Ma, L. and Z. Song, "Cellular Structure Control of Aluminium Foams During Foaming Process of Aluminium Melt", *Scripta Materialia*, Vol.39, No.11, pp.1523-1528, 1998.

31. Tzeng, S.-C. and W.-P. Ma, "A novel approach to manufacturing and experimental investigation of closed-cell Al foams", *International Journal of Advanced Manufacturing Technologies*, 2005.

32. Banhart, J., "Metallic Foams: Challenges and Opportunities", Eurofoam2000, Bremen, Germany, pp.13-20, 2000.

33. Yu, C.-J., H. H. Eifert, J. Banhart, and J. Baumeister, "Metal foaming by a powder metallurgy method: Production, properties and applications", *Materials Research Innovations*, Vol.2, No.3, pp.181-188, 1998.

34. Stanzick, H., M. Wichmann, J. Weise, L. Helfen, T. Baumbach, and J. Banhart, "Process Control in Aluminum Foam Production Using Real-Time X-Ray Radioscopy", *Advanced Engineering Materials*, Vol.4, No.10, pp.814-823, 2002.

35. Elbir, S., S. Yılmaz, A. K. Toksoy, M. Güden, and I. W. Hall, "SiC-particle Aluminum Composite Foams Produced by Powder Compacts: Foaming and Compression Behavior", *Journal of Materials Science*, Vol.38, pp.4745-4755, 2003.

36. Kennedy, A. R., "Effect of Compaction Density on Foamability of Al-TiH_2 Powder Compacts", *Powder Metallurgy*, Vol.45, No.1, pp.75-79, 2002.

37. Garcia-Moreno, F., N. Babcsan, J. Banhart, M. Haesche, and J. Weise, "Analysis of Metal Foaming Behaviour and Development of Foaming Processes", Cellular Metals and Polymers, 2004.

38. Garcia-Moreno, F., N. Babcsan, and J. Banhart, *The Role of the Gas Pressure on the Foaming of Metals Following the P/M-Route*, Hahn-Meitner Institute, 2005.

39. Helwig, H. M. and J. Banhart, "Heat Distribution During Metal Foaming", Cellular Metals and Metal Foaming Technology, Berlin, Germany, 2003.

40. Lehmhus, D. and G. Rausch, "Tailoring Titanium Hydride Decomposition Kinetics by Annealing in Various Atmospheres", *Advanced Engineering Materials*, Vol.6, No.5, pp.313-330, 2004.

41. Sandim, H. R. Z., B. V. Morente, and P. Atsushi, "Kinetics of thermal decomposition of titanium hydride powder using in situ high-temperature X-ray diffraction (HTXRD)", *Materials Research*, Vol.8, No.3, pp.293-297, 2005.

42. Fang, J., Z. Yang, H. Zhang, and B. Ding, "The Coating Process of Silica Film on TiH_2 Particles and Gas Release Characteristic", *Chemical Engineering Science*, Vol.60, pp.845-850, 2005.

43. Kennedy, A. R. and S. Asavavisithchai, "Effect of Ceramic Particle Additions on Foam Expansion and Stability in Compacted Al-TiH_2 Powder Precursors", *Advanced Engineering Materials*, Vol.6, No.6, pp.400-402, 2004.

44. Epler, M., *Structures by Precipitation from Solid Solution*, *ASM Handbook*, ASM International. p. 1-6. 2004.

45. Edwards, G. A., K. Stiller, G. L. Dunlop, and J. Couper, "The Precipitation Sequence in Al-Mg-Si Alloys", *Acta Materialia*, Vol.46, No.11, pp.3893-3904, 1998.

46. Zehn, L., W. D. Fei, S. B. Kang, and H. W. Kim, "Precipitation Behaviour of Al-Mg-Si Alloys with High Silicon Content", *Journal of Materials Science*, Vol.32, pp.1895-1902, 1997.

47. Bastawros, A.-F. and A. G. Evans, "Deformation Heterogeneity in Cellular Al Alloys", *Advanced Engineering Materials*, Vol.2, No.4, pp.210-214, 2000.

48. Papadopoulos, D. P., I. C. Konstantinidis, N. Papanastasiou, S. Skolianos, H. Lefakis, and D. N. Tsipas, "Mechanical Properties of Al Metal Foams", *Materials Letters*, Vol.58, pp.2574-2578, 2004.

49. Gibson, L. J. and M. F. Ashby, *Cellular Solids: Structure and Properties*. Cambridge University Press, NewYork, 1999.

50. Yang, Z., J. Fang, and B. Ding, "Effect of SiO_2 Coating Layer Morphology on TiH_2 Gas Release Characteristics", *Journal of Colloid and Interface Science*, Vol.209, pp.305-309, 2005.

51. Aluminum 6061-T6; 6061-T651, http://www.matweb.com/search/SpecificMaterial.asp?bassnum=MA6016, 2006.

52. Zhang, H. and E. H. Kisi, "Formation of Titanium Hydride at Room Temperature by Ball Milling", *Journal of Physics: Condensed Matter*, Vol.9, pp.185-190, 1997.

53. Cheng, Z.-H., G. R. MacKay, D. A. Small, and R. A. Dunlap, "Phase development in titanium by mechanical alloying under hydrogen atmosphere", *J. Phys. D: Appl. Phys*, Vol.32, pp.1934-1937, 1999.

54. Garcia-Moreno, F., N. Babcsan, and J. Banhart, "X-ray radioscopy of liquid metalfoams: influence of heating profile, atmosphere and pressure", *Colloids and Surfaces A: Physicochemical Engineering Aspects*, Vol.263, pp.290-294, 2005.

55. Matijasevic, B., S. Fiechter, I. Zizak, O. Görke, N. Wanderka, P. Schubert-Bischoff, and J. Banhart, *Decomposition Behaviour of As-Received and Oxidized TiH_2 Powder*, Institute of Materials Science and Technology, Technical University of Berlin

56. Gupta, A. K., D. J. Lloyd, and S. A. Court, "Precipitation Hardening in Al-Mg-Si Alloys with and without Excess Si", *Materials Science and Engineering A*, Vol.316, pp.11-17, 2001.

57. Bhosle, V., E. G. Baburaj, M. Miranova, and K. Salama, "Dehydrogenation of TiH_2", *Materials and Engineering A*, Vol.356, pp.190-199, 2003.